An Analysis of
Wireless High-speed Data Services for
Cellular CDMA Systems

by

Kevin Kwong-Hang Chan

A thesis
presented to the University of Waterloo
in fulfillment of the
thesis requirement for the degree of
Master of Applied Science
in
Electrical and Computer Engineering

Waterloo, Ontario, December 2002

AUTHOR'S DECLARATION FOR ELECTRONIC SUBMISSION OF A THESIS

I hereby declare that I am the sole author of this thesis. This is a true copy of the thesis, including any required final revisions, as accepted by my examiners.

I understand that my thesis may be made electronically available to the public.

Acknowledgements

Abstract

The interest in the development of wireless high-speed data services is in response to the strong market demand for high-speed wireless Internet access. Current standards aim at delivering a peak data rate greater than 2Mbps on the forward link. Since data services and voice services are fundamentally different, new concepts were introduced in the design of the forward data channel. In addition, methods of evaluating the performance of a cellular CDMA system have to be revisited. This thesis proposes a method which can be used to find the forward link peak and average data rates, throughput and coverage of a cellular CDMA system which is capable of delivering high-speed wireless data. A summary of changes in design philosophy and recent advances in technologies which enable high-speed wireless data delivery are presented. The proposed method takes into account major aspects commonly found in the forward data channel and applies the generalized Shannon capacity formula for multi-element antenna (MEA) systems. The analysis focuses on the physical layer and is flexible enough to be adapted to various propagation environments, antenna configurations, multicode allocations, user distributions and cell site configurations. Sample numerical results for various multicode allocations are shown using a system model with two-tier interfering cells with one transmit antenna and two receive antennas operating under a frequency selective slow fading channel with propagation environment described by the Recommendation ITU-R M.1225 indoor office, outdoor to indoor and pedestrian and vehicular test environments. Different transmit / receive antenna configurations and multicode allocations and their impact on the average data rate is also explored.

Contents

List of Tables

List of Figures

Chapter 1

Introduction

1.1 Introduction to High-speed Wireless Mobile Data

There is not much debate that wireless communication systems have a lot of advantages over wireline communication systems: (1) they provide instant communications between individuals located anywhere around the world; (2) they provide a mean of communication for individuals located in area which are underserved by wireline or wiring is impossible; (3) they allow information to be retrieved anytime and anywhere around the world.

In 1990, wireline data volume across the Internet in the United States averaged to around 1.0 terabytes per month. Few would have predicted that this number could reach an average of 27500 terabytes per month [19] in 2000. This dramatic increase was caused by the enhancement in usability and the introduction of "killer applications" from time to time. Inputs for early wireline applications were difficult to create and their outputs were limited to text and low-resolution graphics. Usability enhancements such as the introduction of graphical interfaces and the steady increase in available data transfer speeds were drivers for such dramatic growth. In addition, the emergence of "killer applications" from time to time is also found to have a major contribution to this growth rate. One study conducted by AT&T Research Labs [19] based on UC Berkeley's network statistics showed that Napster[1]'s traffic has grown to about 50% of the total traffic in 2000 since its

---

[1]Napster provides software that enables users connected to the Internet to exchange and/or download MP3 music files.

introduction in 1999.

Today's wireless data experience mirrors the wireline experience from the early 1990s. Current wireless data offerings such as Short Message Service (SMS), Wireless Application Protocol (WAP) and i-Mode all suffer from abbreviated interfaces with primarily text-only inputs and low-resolution graphics. Rich media applications typical of today's wireline experience are not yet widely available for wireless. It is predicted that wireless systems with enhanced usability and "killer applications" will most likely to follow the astronomical growth rate wireline systems have experienced. Wireless operators and equipment manufacturers are forecasting such a growth rate to occur and this motivates the joint development effort of third-generation (3G) wireless systems which can support high-speed wireless data.

In addition, in many markets around the world, the growth in wireless voice penetration rates begins to slow down as they reach 80% or higher. Although minutes of use are increasing, the price per minute of voice service continues to decline [35]. In this environment, revenue growth from voice services will likely slow over the next several years and data services will become increasing important to drive revenue growth.

As of late 2001, there are several offerings and proposals which promise to deliver wireless data at rates beyond the capabilities of second-generation (2G) systems. In this thesis, a system capable of delivering "high-speed wireless data" is defined as a system which is capable of delivering data stream wirelessly at a speed greater than 14.4kbps, the peak data rate supported by current IS-95 systems. Table 1.1 shows a snapshot of current high-speed wireless data offerings and proposals.

Table 1.1: High-speed wireless data technologies as of November 2001

Technologies	Gener-ation	Multiple Access Scheme	Carrier Bandwidth	Peak Data Rate	Modulation	Data / Voice Support
GPRS [35, 73]	2.5G	TDMA	0.2MHz	115kbps	GMSK	data
	Designed as overlay on GSM / TDMA Networks					
EDGE	2.5G	TDMA	2.4Mbps	384kbps	8PSK /	data

Table 1.1: High-speed wireless data technologies as of November 2001 (Continued)

Technologies	Gener-ation	Multiple Access Scheme	Carrier Bandwidth	Peak Data Rate	Modulation	Data / Voice Support
[61]					GMSK	
	Designed as overlay on GSM / TDMA Networks					
cdma2000 1x [15, 35]	3G	CDMA	1.25Mbps	625kbps	BPSK / QPSK	data + voice
cdma2000 1xEV-DO (HDR / IS-856) [3, 35]	3G+	CDMA / TDMA	1.25Mbps	2.458Mbps	QPSK / 8PSK / 16QAM	data
	Designed as high data rate extension to cdma2000 1x					
cdma2000 1xEV-DV (1XTREME) [52, 66]	3G+	CDMA / TDMA	1.25Mbps	4.838Mbps	8PSK / 16QAM / 64QAM	data + voice
	Designed as high data rate extension to cdma2000 1x with voice support					
cdma2000 1xEV-DV (L3NQS) [21]	3G+	CDMA	1.25Mbps	3.072Mbps	QPSK / 8PSK / 16QAM	data + voice
	Designed as high data rate extension to cdma2000 1x with voice support					
WCDMA [15, 35]	3G	CDMA	3.84MHz	2Mbps	BPSK / QPSK	data + voice
HSDPA [54] (in development)	3G+	CDMA	3.84MHz	8-10Mbps	16QAM / 64QAM	data
	Designed as high throughput, high peak data rate extension to WCDMA					

1.2   Implementation of High-speed Wireless Mobile Data

There are a lot of fundamental differences between voice oriented services and data oriented services. First of all, voice services are symmetrical, while data services are asymmetrical. The downlink demand for data services is likely to be several times greater than the uplink. In addition, data services can tolerate considerably more delay than voice. Latencies of several times more than voice are hardly noticeable for data services. Furthermore, the quality of service (QoS) requirements for data services are much tighter than voice services. According to an evaluation guideline released by International Telecommunication Union (ITU) regarding radio transmission technologies for 3G [62, Table 1], the maximum bit error rate (BER) allowed for data services is 10^{-6} while the maximum BER tolerated for voice services is just 10^{-3}. As a result, current system designs which are targeted towards voice services are incapable to deliver high-speed wireless data.

Since data services have higher QoS requirements than voice services, improving the signal quality at the mobile receiver is the key to implement high-speed wireless mobile data. Several new concepts have been proposed with this regard: (1) the base station devotes maximum power to only one user at a time regardless of its location in order to save resources on overheads and reduce intracell interference; (2) deploying multiple transmit antennas at the base station to exploit the rich nature of fading channels; (3) hard handoffs are being used instead of soft handoffs to save resources on synchronization overheads; (4) channel codes which exhibits very good error-correcting properties with possibly higher latencies are being used; (5) modulation and coding redundancy can adapt themselves according to channel conditions.

1.3   Motivation of this Research

As seen in Table 1.1, there are numerous proposals and standards for high-speed wireless data access. As a new proposal is being introduced, the peak data rate advertised in that proposal is always higher than previous introduced proposals. This makes the newly introduced proposal looks very good from a marketing point of view. The trick for this to

happen is to shorten the symbol duration for a symbol signalling time and go higher in modulation. For example, the highest modulation scheme supported in HDR is 16QAM. 1XTREME, which was introduced several months later than HDR, supports a modulation scheme of 64QAM. This results into a peak data rate of 4.838Mbps, which is several Mbps higher than HDR. In one extreme case, LAS-CDMA, which was introduced around the same time when 1XTREME was proposed, claims to support a mode of 256QAM and a peak data rate greater than 10Mbps [1], in a 1.25MHz bandwidth.

To judge whether the proposals made a fair statement, a good approach is to evaluate the channel capacity for a practical real world system. The highest error-free data rate supported in any communication system is well governed by the channel capacity formula. In a perfect noiseless environment where the signal to noise ratio (SNR) is infinite, the channel capacity will be infinite. However, in a real world system, it is not the case. By evaluating users' SNR at various location and applying the channel capacity formula, one is able to see if the peak data rate advertised in the proposal is supported and to what extend it is supported. In addition, the channel capacity "map" resulting from the operation described above is of great use in coverage analysis and throughput calculation as well. In summary, channel capacity, throughput and coverage are important figures of merit wireless system engineers require to evaluate the performance of a wireless high-speed data system, to understand the cost advantages and disadvantages of various technologies and to aid in frequency planning.

Peak data rate is the maximum transmission speed that an individual user may experience in ideal conditions. Since data traffic is bursty in nature, peak data rate affects an individual user's experience. It will be argued in upcoming session that peak data rate and channel capacity are equivalent terms in this analysis. Throughput is the average total capacity available to multiple users within a cell. As throughput increases, each cell site can handle higher volumes of data traffic, and the network requires less equipment and fewer cell sites, reducing operational expenses and capital investments. Throughput affects both the operator's cost to deliver service and the user's experience. Coverage is the area in which a certain grade of service is guaranteed. As position location technology is required by government regulatory bodies in future wireless operator licensing, it is important to make sure users located at cell boundaries are still covered with minimal grade of service.

Thesis Statement

This research will analyze through simulations the peak and average data rates, throughput and coverage of cellular CDMA systems proposed for high-speed wireless data delivery in 3G systems.

1.4   Thesis Organization

This thesis is organized as follows:

Chapter 2 provides descriptions of the channel model, propagation models and system model this research is based on. Specifically, the widely used channel model for evaluation of third generation systems — Recommendation ITU-R M.1225 Guidelines for Evaluation of Radio Transmission Technologies for IMT-2000 [62] will be introduced and its usage will be justified. In addition, channel fadings, ambient noise, distance path loss and the honeycomb system model will be reviewed and discussed.

Chapter 3 discusses the rationales behind the development of cellular CDMA systems that support wireless high-speed data. The "enablers" of wireless high-speed data: technological advances in recent years and changes in design philosophy when compared to second generation systems will be presented.

Chapter 4 presents an analytical model which let one to find out the peak and average data rates, throughput and coverage of a cellular CDMA systems which support high-speed data. The analytical model will take into account the "enablers" discussed in Chapter 3.

Chapter 5 devotes to the presentations of the results by applying the analytical model described in Chapter 4 on systems which support various mixtures of data and voice users, operating under various channels and antenna configurations.

Chapter 6 concludes the findings of this thesis.

Chapter 2

Channel, Propagation and System Modelling

In this chapter, the channel model, propagation model and system model which are applicable to this research will be described in details.

2.1 Backgrounds

2.1.1 Theories on Channel Modelling

Fading multipath channels are frequently used in the analysis and design of wireless communication systems [13]. A fading multipath channel is generally characterized as a linear, time-varying system having an equivalent lowpass impulse response $c(t; \tau)$ (or a time-varying frequency response $C(t; f)$) which is a wide-sense stationary random process in the t-variable. Time variations in the channel impulse response or frequency response result in frequency spreading, generally called Doppler spreading, of the signal transmitted through the channel. Multipath propagation results in spreading the transmitted signal in time. Consequently, a fading multipath channel may be generally characterized as a doubly spread channel in time and frequency.

Channel models under the wide-sense stationary uncorrelated scattering (WSSUS) assumption is recommended by the International Telecommunication Union (ITU) in Recom-

mendation ITU-R M.1225 [62] for evaluation of IMT-2000[1] radio transmission technologies. The statistics of a WSSUS channel are approximately stationary for time intervals that are sufficiently long (WSS assumption) and the multipath signals propagating through the channel at different delays are uncorrelated (US assumption). A doubly spread channel under the WSSUS assumption may be characterized by the scattering function $S(\tau; \lambda)$, which is a measure of the power spectrum of the channel at delay τ and frequency offset λ (relative to the carrier frequency). From the scattering function, the *delay power spectrum* $S_c(\tau)$ of the channel (also called the *multipath intensity profile*) may be obtained by simply averaging $S(\tau; \lambda)$ over λ, i.e.,

$$S_c(\tau) = \int_{-\infty}^{\infty} S(\tau; \lambda) d\lambda. \tag{2.1}$$

Similarly, the Doppler power spectrum $S_c(\lambda)$ is

$$S_c(\lambda) = \int_{0}^{\infty} S(\tau; \lambda) d\tau. \tag{2.2}$$

The range of values over which the delay power spectrum $S_c(\tau)$ is nonzero is defined as the multipath spread T_m of the channel. Similarly, the range of values over which the Doppler power spectrum $S_c(\lambda)$ is nonzero is defined as the Doppler spread B_d of the channel.

The value of the Doppler spread B_d provides a measure of how rapidly the channel impulse response varies in time. The larger the value of B_d, the more rapidly the channel impulse response is changing with time. Another way to measure how rapidly the channel impulse response changes with time is the *channel coherence time* T_{coh} and it is defined [58, Equation 14-1-19] as:

$$T_{coh} = \frac{1}{B_d}. \tag{2.3}$$

Channel coherence time provides a measure of the time duration in which the channel fading statistics are highly correlated. If two signals are transmitted within the channel coherence time, they are affected by similar channel response. In a similar manner, the

---

[1]International Mobile Telecommunications-2000, which is an industry standard for the third generation of wireless technology. It encompasses three different CDMA operating modes, cdma2000, WCDMA and TD-SCDMA[36].

channel coherence bandwidth B_{coh} is defined as the reciprocal of the multipath spread [58, Equation 14-1-16]:

$$B_{coh} = \frac{1}{T_m}. \tag{2.4}$$

Channel coherence bandwidth provides a measure of the width of the frequency band in which fading is highly correlated.

Channel coherence bandwidth B_{coh} and the channel coherence time T_{coh}, along with the transmitted signal symbol duration T and bandwidth W determine which type of channel model to use. If the transmitted signal's bandwidth W is smaller than the channel coherence bandwidth B_{coh}, i.e., $W < B_{coh}$, then all the frequency components will undergo the same attenuation and phase shift in transmission through the channel. This implies that within the bandwidth W occupied by the transmitted signal, the time-varying frequency response $C(t; f)$ of the channel is constant in the frequency variable. Such a channel is called *frequency nonselective*. On the other hand, if $W > B_{coh}$, *frequency selective* channel results. Similarly, if the symbol duration of the transmitted signal T is much smaller than the channel coherence time T_{coh}, i.e., $T << T_{coh}$, then the channel is said to be *slowly fading*. Otherwise, the channel is said to be *rapid fading*. Table 2.1 summarizes the decision criteria of which type of channel model to use.

Table 2.1: Decision criteria for the types of channel model to use

	$T > T_{coh}$	$T << T_{coh}$
$W > B_{coh}$	Frequency Selective Rapidly Fading	Frequency Selective Slowly Fading
$W << B_{coh}$	Frequency Non-selective Rapidly Fading	Frequency Non-selective Slowly Fading

2.1.2 Propagation Model

To accurately model the mobile user's ability to receive the transmitted signal, in addition to selecting a suitable channel model, several more factors which are related to the behaviour of the mobile user and its operating environment should be considered. They are

the mobility of the user, the location in which the mobile user is located, the mobile user's operating frequency, the geometric path loss governed by the terrestrial environment, the statistical variation of shadow fading (large scale fading) and the statistical variability for the envelope of the channels (small scale fading). An accurate propagation model should taken into account the above factors.

Since the mobile user may operate under any possible environment, instead of constructing for all possible operating environments, ITU-R M.1225 Recommendation [62] suggests a smaller set of test environments which adequately span the overall range of possible operating environments and user's mobilities. Possible operating environments include large and small cities, tropical, rural and desert areas. Two extremes of user's mobilities include fixed and mobile wireless applications. These test environments may not correspond to the actual mobile user's operating environment, but they should give a very good idea on how the mobile user performs under different environments.

Specifically, ITU-R M.1225 Recommendation [62] suggests three test environments for evaluations of the performance of third generation systems. They are: (1) indoor office test environment; (2) outdoor to indoor and pedestrian test environment and (3) vehicular test environment. Indoor office test environment is characterized by small cells and low transmit power. Both base stations and pedestrian users are located indoors. Outdoor to indoor and pedestrian test environment is described by small cells and low transmit power. Base stations with low antenna heights are located indoor while pedestrian users are located on streets and inside buildings. Vehicular test environment is characterized by large cells, high transmit power and fast moving terminals. Detailed mathematical descriptions of these models will be presented in the next section, after the usage of frequency-selective, slowly-fading channel model is justified.

2.1.3   Frequency Selective Slowly-fading Channel Model

Third generation system is characterized by its wide bandwidth requirement (spread spectrum) and its capabilities to deliver high rate data. As discussed in Section 2.1.1, these characteristics affect the channel model of choice.

The channel coherence time T_{coh} and the coherence bandwidth B_{coh} determine the type of channel model to use. The channel impulse response $c(t; \tau)$ is required to determine T_{coh}

and B_{coh}. However, measurement of the channel impulse response is extremely difficult and unreliable, if not possible, especially for spread spectrum systems with a *spread factor* $T_m B_d$ usually greater than one [13, Section II].

Fortunately, the channel coherence time T_{coh} and the channel coherence bandwidth B_{coh} can also be found using some empirical formulas. To be able to apply those empirical formulas, the r.m.s. delay spread σ_τ of the channel and the maximum Doppler spread f_d are required. The r.m.s. delay spread of the channel is defined as [59]:

$$\sigma_\tau = \sqrt{\overline{\tau^2} - (\overline{\tau})^2} \tag{2.5}$$

where $\overline{\tau}$ is the mean excess delay, $(\overline{\tau})^2$ is the mean squared excess delay and $\overline{\tau^2}$ is the second moment of excess delay. Sousa et. al. in [65] outlined a method to measure the r.m.s. delay spread of urban Toronto channels empirically.

The maximum Doppler spread f_d is defined as [64, Equation 17]:

$$f_d = \frac{v}{\lambda} \tag{2.6}$$

where v is the velocity of the mobile user and λ is the signal wavelength.

Once the r.m.s. delay spread σ_τ is obtained, the channel coherence bandwidth B_{coh} can be found using the following equation [64, Equation 11]:

$$B_{coh} = \frac{0.276}{\sigma_\tau}. \tag{2.7}$$

Equation (2.7) is based on the *dense-scatter* channel model in which the bandwidth interval over which the channel's complex frequency transfer function has a correlation of at least 0.5. A dense-scatter channel model is unlikely to overestimate the channel coherence bandwidth.

Similarly, when the channel coherence time T_{coh} is defined as the time duration over which the channel's response to a sinusoid has a correlation greater than 0.5, the relationship between T_{coh} and f_d is approximately given by [64, Equation 19]:

$$T_{coh} = \frac{9}{16\pi f_d}. \tag{2.8}$$

There are other empirical formulas which allow one to estimate B_{coh} and T_{coh}. It is beyond the scope of this thesis to describe all of them since Equations (2.7) and (2.8) are sufficient to justify the channel model of choice.

Third generation systems are all spread spectrum based with a bandwidth requirement ranging from 1.25MHZ to 3.84MHz (see Table 1.1). On the other hand, the three test environments as described in ITU-R M.1225 Recommendation have a r.m.s. delay spread σ_τ ranging from 35ns to 4000ns [62, Table 2]. Using Equation (2.7), Table 2.2 shows the channel coherence bandwidth B_{coh} for each respective test environment.

Table 2.2: R.M.S. delay spread and channel coherence bandwidth of ITU-R M.1225 Test Channels [62, Table 2]

Test	Channel A		Channel B	
Environment	σ_τ (ns)	B_{coh} (MHz)	σ_τ (ns)	B_{coh} (MHz)
Indoor Office	35	7.89	100	2.76
Outdoor to Indoor and Pedestrian	45	6.13	750	0.368
Vehicular	370	0.746	4000	0.069

As seen from Table 2.2, the vehicular test channel has a channel coherence bandwidth B_{coh} much smaller than the signal bandwidth. As a result, frequently selective channel model is the appropriate choice. On the other hand, the usage of frequency selective channel model is in doubt for indoor office environment and it is sometimes in doubt for outdoor to indoor and pedestrian test environment.

Although frequency non-selective channel model seems to be a more reasonable choice for indoor office environment and sometimes for outdoor to indoor and pedestrian test environment, it can be shown [64, Figure 8] that systems with $B_{coh} > W$ can still manifest frequency selective fading on occasions. This happens when the null of channel frequency-transfer function occurs at the centre of the signal band. Whenever this occurs, the base-band pulse will be especially mutilated by deprivation of its DC component. One consequence of the loss of DC is the absence of a reliable pulse peak on which to establish the timing synchronization, or from which to sample the carrier phase carried by the pulse. These will result into frequency selective fading. Figure 2.1 approximates such condition.

As a result, it is fair to say that channel which is classified as frequency non-selective cannot exhibit frequency non-selective fadings all the time. By means of that, frequency selective channel models will be used in this research.

Another distinct feature of third generation systems is that they all support high speed
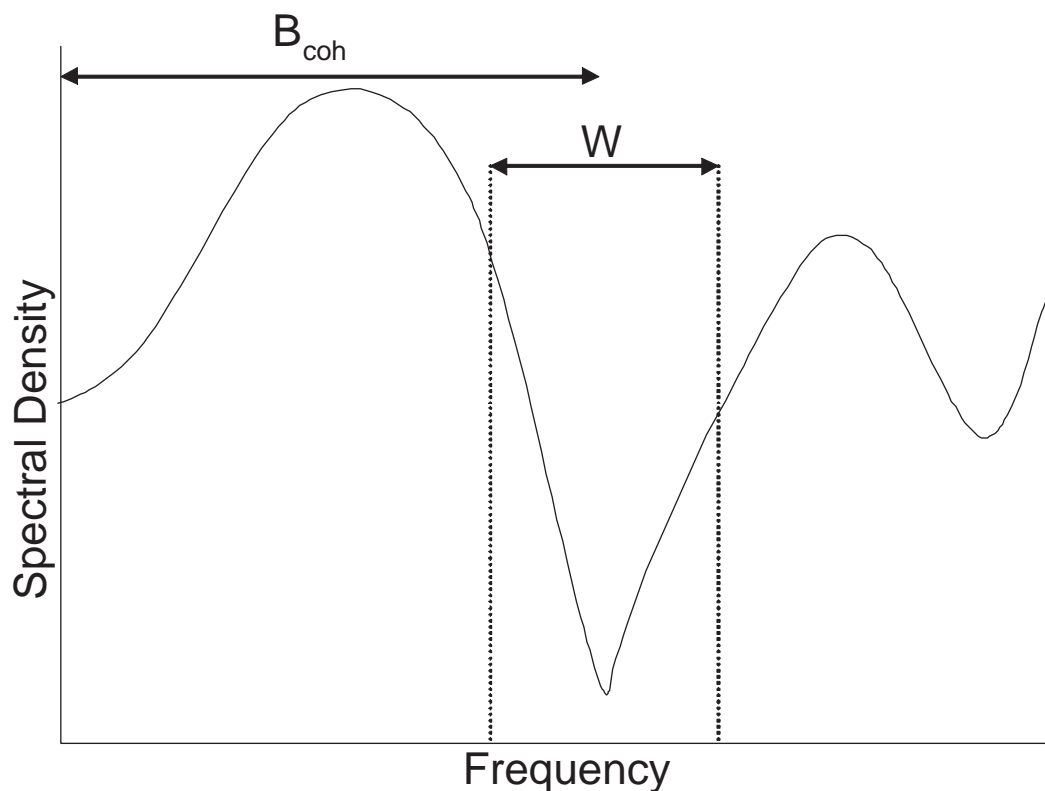
Figure 2.1: Null of channel frequency response occurs at signal band centre, resulting into a frequency selective channel with $B_{coh} > W$

data with a data rate greater than 14.4kbps. To determine whether a slow fading channel model or rapid fading channel model should be used, the symbol duration T and the channel coherence time T_{coh} are required. Assuming 64QAM modulation is being used to support a data rate of 14.4kbps, the symbol duration under this arbitrary configuration is 0.417ms. Note that higher data rate or simpler modulation will not result into a longer symbol duration. On the other hand, the channel coherence time can be found by applying Equations (2.6) and (2.8). Assuming a modulation frequency of 1.9GHz and the mobile user moves at a speed of 120km/h, by applying Equation (2.6), the maximum Doppler spread f_d is found to be 211Hz. Substituting $f_d = 211$Hz into Equation (2.8) gives a

channel coherence time T_{coh} of 0.849ms. A simple comparison of the symbol duration and the channel coherence time T_{coh} shows that slow fading channel models are appropriate. Note that a mobile user moving at a slower speed will result into a longer channel coherence time and the slow fading channel models are still applicable.

In conclusion, frequency selective slow fading channel models are appropriate choices for theoretical analysis of third generation systems.

2.1.4   System Model

System modelling refers to the modelling of the surrounding terrestrial characteristics of the transmitter. The size of the cell which the transmitter is operating in (the target cell), the size of the neighbouring cells, the number of interfering cells surrounding the target cell (or the number of "tier" of cells taken into account for interference), the terrain of the the target cell and its neighbouring cells, the shape of the target cell and its neighbouring cells, sectorization of the target cell, the antenna pattern of the transmitter are examples of what might be taken into account when deriving a system model.

2.2   Channel Model Descriptions

As discussed in the previous section, a frequency selective fading channel is appropriate to model the propagation environments of third generation systems. Frequency selective fading channels can be modelled as a tapped delay line (transversal) filter with time-variant tap coefficients [58, p.772, pp.795-797]. Multipath components in the channel (the taps in the tapped delay line) are resolvable when they are separated by at least $1/W$, where W is the bandwidth of the bandpass signal. By applying the sampling theorem, frequency selective fading channel can be represented by its time-varying channel impulse response

$$c(t; \tau) = \sum_{n=1}^{L} \sqrt{p_n} c_n(t) \delta(\tau - \frac{n}{W})$$

(2.9)

and the corresponding time-varying frequency response

$$C(t; f) = \sum_{n=1}^{L} \sqrt{p_n} c_n(t) e^{\frac{j2\pi f n}{w}}$$

(2.10)

where p_n is the strength of the n-th multipath component; $c_n(t)$ is the complex random process describing the tap gain of the n-th multipath component and L is the number of resolvable multipath components. Since the multipath spread is T_m and the time resolution of the multipath is $\frac{1}{W}$, it follows that

$$L = \lfloor T_m W \rfloor + 1. \tag{2.11}$$

Note that the path strengths have the following relationship:

$$\sum_{n=1}^{L} p_n \approx 1. \tag{2.12}$$

If the input signal is represented by its complex lowpass representation $z(t)$ and the additive white Gaussian noise is represented by $n(t)$, with the uncorrelated scattering assumption, the lowpass representation of the channel output signal $w(t)$ is given by:

$$w(t) = \int_{-\infty}^{\infty} c(t; \tau) z(t - \tau) d\tau + n(t) \tag{2.13}$$

$$w(t) = \sum_{n=1}^{L} \sqrt{p_n} c_n(t) z(t - \frac{n}{W}) + n(t). \tag{2.14}$$

Figure 2.2 represents the input-output relationship of the frequency selective fading channel.

2.2.1   Channel Parameters

Three parameters are needed to be specified in order to completely define the tapped-delay line channel model described in the previous section. They are the Doppler spectra of the tap weights $P_n(v), n = 1, ..., L$; the tap delays $\tau_n; n = 1, ..., L$ and the tap weight strengths $p_n, n = 1, ..., L$. This section is devoted to the descriptions of the three parameters and additive white Gaussian noise.
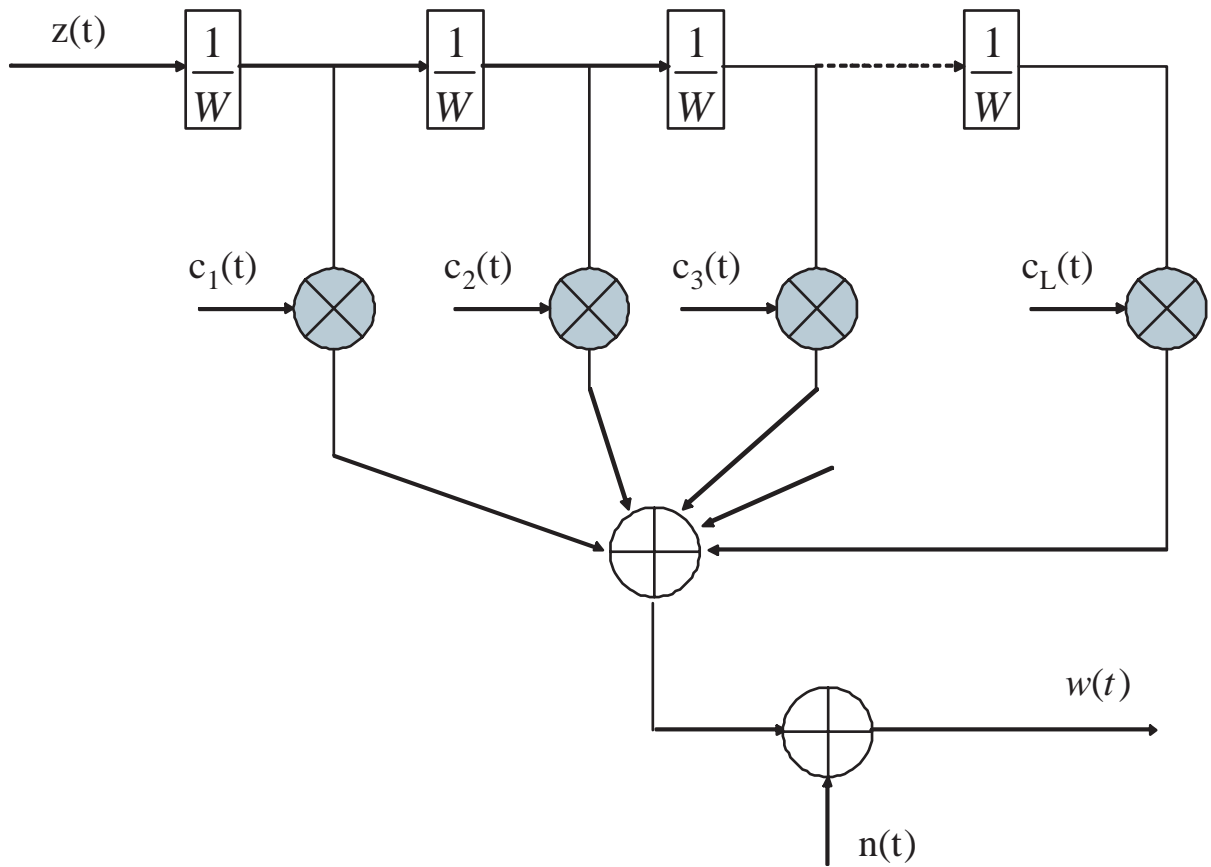
Figure 2.2: Tapped-delay line channel model for frequency selective channel

Doppler Spectra

The random process tap gain for the n-th multipath component $c_n(t)$ is to be interpreted as modelling the superposition of unresolved multipath components arriving from different angles and in the vicinity of the delay interval:

$$\tau_n - \frac{1}{2W} < \tau < \tau + \frac{1}{2W}. \tag{2.15}$$

Each ray, in general, has a different Doppler shift corresponding to a different value of the cosine of the angle between the ray direction and the velocity vector. For outdoor channels, a very large number of receive rays will arrive uniformly distributed in azimuth at the mobile station and at zero elevation for each delay interval. Assuming a uniform antenna pattern in the azimuth direction, the Doppler spectrum as seen by the mobile station is described by [62]:

$$P_n(v) = \frac{1}{\pi} \frac{1}{\sqrt{(\frac{V}{\lambda})^2 - v^2}} \tag{2.16}$$

for which

$$|v| < \frac{V}{\lambda}$$

where V is the velocity of the mobile and λ is the wavelength of the carrier frequency. This Doppler spectrum is called the classical Doppler spectrum or the Jakes' Doppler spectrum.

For indoor channels, the Doppler spectrum is described by the the flat spectrum [62]:

$$P_n(v) = \frac{\lambda}{2V} \tag{2.17}$$

for which

$$|v| < \frac{V}{\lambda}.$$

This fluctuation of carrier frequency, collectively called the Doppler effect and characterized by Doppler spectra, yields an irreducible error rate that cannot be overcome by simply increasing the signal energy [7]. However, for small values of Doppler shifts less than $0.01 \times W$, the coherent demodulators that lock onto and track the information signal can practically suppress the effect of frequency fluctuations due to Doppler shift and thus cancel the impact of Doppler effect on the signal quality [64]. A simple comparison of

the maximum Doppler shift found in Section 2.1.3 and $0.01 \times W$ shows that the Doppler effect can be safely ignored. As a result, the effect of Doppler shift will not be modelled in subsequent analyses.

For interested readers who strive for accuracy, [55] shows several methods on how to take Doppler effect into account in modelling channels.

Tap Delays and Tap Weight Strengths

Equations (2.11) and (2.14) show the number of resolvable multipath components in the channel model and their respective time delays. However, from the point of view of the receiver, it is unrealistic to track all the multipath components and unwise to put the receiver fingers at fixed delay intervals. As a result, Equation (2.14) has to be redefined, taking into consideration of the design of the receiver.

Specifically, the number of taps L, the tap delays $\tau_n, n = 1, ..., L$ and the tap weight strengths $p_n, n = 1, ..., L$ have to be specified from the point of view of the receiver. The number of taps (or the number of multipath components) tracked by the receiver is limited by the number of RAKE fingers the receiver has. In addition, some multipath components may be too weak to meaningfully be tracked at all. As a result, a new parameter has to be defined to replace L in order to take into account realistic design constrains and propagation phenomenon.

Effective number of taps L' is defined as the number of meaningful paths tracked by the RAKE fingers of the receiver. L' is strictly less than or equal to the number of RAKE fingers implemented in the receiver.

The ITU-R M.1225 Recommendation [62] specifies the tap delays $\tau_n, n = 1, ..., L'$ relative to the first tap and the tap weight strengths $p_n, n = 1, ..., L'$ relative to the strongest tap for the three test environments, namely the indoor office test environment, the outdoor to indoor and pedestrian test environment and the vehicular test environment. Since these values are measured empirically, it is hard to characterize a particular test environment with only one set of tap delays and tap weight strengths. It is due to the fact that in some "worst case" scenario, the r.m.s. delay spread can be an order of magnitude higher than the average case scenario, as shown in Table 2.2. As a result, two sets of channel parameters are given for a particular test environment, where each set of parameters is

associated with a fixed probability. Table 2.3 shows the probabilities of the two sets of parameters for each of the test environment.

Table 2.3: Channel probabilities for ITU-R M.1225 test channels [62, Table 2]

Test Environment	Channel A Probabilities (%)	Channel B Probabilities (%)
Indoor Office	50	45
Outdoor to Indoor and Pedestrian	40	55
Vehicular	40	55

Note that since the sum of the channel probabilities for each test environment do not add up to 100%, the probabilities will be normalized to 1 in subsequent analyses.

Table 2.4 shows the tap delays $\tau_n, n = 1, ..., L'$ relative to the first tap and the tap weight strengths $p_n, n = 1, ..., L'$ relative to the strongest tap for the indoor office test environment [62, Table 3].

Table 2.4: Indoor office test environment tapped-delay-line parameters

Tap	Channel A ($L' = 6$)		Channel B ($L' = 6$)	
	Relative Delay (ns)	Average Power (dB)	Relative Delay (ns)	Average Power (dB)
1	0	0	0	0
2	50	-3.0	100	-3.6
3	110	-10.0	200	-7.2
4	170	-18.0	300	-10.8
5	290	-26.0	500	-18.0
6	310	-32.0	700	-25.2

Table 2.5 shows the tap delays $\tau_n, n = 1, ..., L'$ relative to the first tap and the tap weight strengths $p_n, n = 1, ..., L'$ relative to the strongest tap for the outdoor to indoor and pedestrian test environment [62, Table 3].

Table 2.6 shows the tap delays $\tau_n; n = 1, ..., L'$ relative to the first tap and the tap weight strengths $p_n, n = 1, ..., L'$ relative to the strongest tap for the outdoor to indoor

Table 2.5: Outdoor to indoor and pedestrian test environment tapped-delay-line parameters

Tap	Channel A ($L' = 4$)		Channel B ($L' = 6$)	
	Relative Delay (ns)	Average Power (dB)	Relative Delay (ns)	Average Power (dB)
1	0	0	0	0
2	110	-9.7	200	-0.9
3	190	-19.2	800	-4.9
4	410	-22.8	1200	-8.0
5	-	-	2300	-7.8
6	-	-	3700	-23.9

and pedestrian test environment [62, Table 3].

Table 2.6: Vehicular test environment tapped-delay-line parameters

Tap	Channel A ($L' = 6$)		Channel B ($L' = 6$)	
	Relative Delay (ns)	Average Power (dB)	Relative Delay (ns)	Average Power (dB)
1	0	0	0	-2.5
2	310	-1.0	300	0
3	710	-9.0	8900	-12.8
4	1090	-10.0	12900	-10.0
5	1730	-15.0	17100	-25.2
6	2510	-20.0	20000	-16.0

In order to apply Table 2.4 - Table 2.6 to Equation (2.14), several assumptions have to be made. First of all, it is assumed that the RAKE fingers of the receiver are perfectly tracking each of the taps. Secondly, it is assumed that the only mean for energy propagation from the transmitter to the receiver is through the L' tap channels. Mathematically speaking,

it is assumed that

$$\sum_{n=1}^{L'} p_n = 1. \tag{2.18}$$

$p_n, n = 1, ..., L'$ can be calculated by dividing each of the tap power by the sum of all tap powers.

By applying Table 2.4 - Table 2.6, Equation (2.14) can be expressed as:

$$w(t) = \sum_{n=1}^{L'} \sqrt{p_n} c_n(t) z(t - \tau_n). \tag{2.19}$$

Additive White Gaussian Noise

The power of additive white Gaussian noise, represented by N_o, is calculated using the following equation [59, p.566]:

$$N_o = kTB \tag{2.20}$$

where k is the Boltzmann's constant $1.380622 \times 10^{-23} J/K$, B is the bandwidth of the communication system and T is the noise temperature in Kelvin. By substituting $T = 297K$, Equation (2.20) defines the noise power transferred by a simple passive load at room temperature.

To conclude this section, the input / output relationship of the three test environments has been described. In the next section, propagation models will be used to describe the complex random process $c_n(t), n = 1, ..., L'$.

2.3 Propagation Models Descriptions

As discussed in Section 2.1.2, there are a lot of factors to be considered in modelling the mobile user's ability to receive the transmitted signal. These factors are collectively called propagation effects and they are described by propagation models detailed below. The propagation effects can be categorized into three different types. They are mean path loss

due to distance separation, slow variation about the mean due to shadowing and scattering, and the rapid variation in the signal strength due to multipath effects [62, Section 1.2]. Equations are given for the mean path loss for each of the three test environments. Slow variation and fast variations are described probabilistically. Slow variation is described by a log-normal distributed random variable while rapid variation is described by Rayleigh distributed random variable.

It is important to point out that the slow variation and rapid variation of the propagation effects are about the mean path loss. The mean path loss can be calculated by using the mean path loss equation which corresponds to the propagation environment and the distance between the transmitter-receiver pair. As a result, the log-normal distributed and Rayleigh distributed random variables both have an amplitude mean of zero dB and assumed a mean power of one.

In addition to the signal strength loss due to physical separation and the signal strength variation around the mean, the channel will induce phase ϕ distortion to the transmitted signal. Taking into account all the above effects, the complex random process $c_n(t), n = 1, ..., L^{'}$ can be described mathematically as follows:

$$c_n(t) = 10^{\frac{-L_{50}}{20}} 10^{\frac{-\xi}{20}} \alpha e^{-j\phi} \qquad (2.21)$$

where L_{50} is the mean path loss in dB given by the corresponding mean path loss equation for that particular propagation environment; ξ is the Gaussian distributed random variable with zero mean and standard deviation of σ_ξ listed in Table 2.7; α is the Rayleigh distributed random variable (or Rician distributed random variable if line-of-sight component exists); and ϕ represents the phase distortion caused by the channel.

It should be noted that Equation (2.21) is a combined random variable which describes the randomness of the signal amplitude. In terms of signal power, it is described by the total path loss equation $L_n^t(t), n = 1, ..., L^{'}$ [39, Equation 1]:

$$L_n^t(t) = 10^{\frac{-L_{50}}{10}} 10^{\frac{-\xi}{10}} \alpha^2. \qquad (2.22)$$

Note that the phase distortion term equals to one due to Euler's rule.

2.3.1 Mean Path Loss

Mean path loss for the three test environments are all based on the PCS extension (COST-231) [33] of the Hata model [30]. Mean path loss is a function of distance and the terrestrial environments. ITU-R M.1225 Recommendation [62] provides the mean path loss equations for the three test environments under worst case propagation.

The mean path loss equation for indoor test environment is given by [62, Section 1.2.1.1]:

$$L_{50} = 37 + 30 \log_{10} R + 18.3 n^{\frac{n+2}{n+1}-0.46} \, dB \tag{2.23}$$

where R is the transmitter-receiver separation in metres and n is the number of floors in the propagation path.

The mean path loss equation for the outdoor to indoor and pedestrian test environment is given by [62, Section 1.2.1.2]:

$$L_{50} = 40 \log_{10} R + 30 \log_{10} f + 49 \, dB \tag{2.24}$$

where R is the base station-mobile station separation in kilometres and f is carrier frequency in MHz.

The mean path loss equation for the vehicular test environment is given by [62, Section 1.2.1.3]:

$$L_{50} = 40(1 - 4 \times 10^{-3} \Delta h_b) \log_{10} R - 18 \log_{10} \Delta h_b + 21 \log_{10} f + 80 \, dB \tag{2.25}$$

where R is the base station-mobile station separation in kilometres; f is the carrier frequency in MHz and Δh_b is the base station antenna height measured from the average rooftop in metres. The valid range for Δh_b is from 0 to 50m.

It should be noted that the mean path losses given by Equations (2.23) - (2.25) in no circumstances be less than free space path loss. Free space path loss is given by:

$$L = 10 \log_{10}(R^{-4}) \, dB \tag{2.26}$$

where R is the transmitter-receiver separation in metres.

2.3.2   Log-Normal Shadowing

Mean path loss is an average signal degradation caused by distance separation between the transmitter-receiver (T-R) pair. However, it is not adequate to describe any particular setting or signal path since the surrounding environment clutter may be vastly different at two different locations having the same T-R separation. Measurements have shown that at any given T-R separation, the path loss is random and log-normally distributed (normal in dB) about the mean distance-dependent value [59, p.104].

The log-normal distribution describes the random shadowing effects which occur over a large number of measurement locations having the same T-R separation, but having different levels of clutter on the propagation path. This phenomenon is referred to as log-normal shadowing. Log-normal shadowing is also called slow fading or large-scale fading since the rate of change is much slower than that caused by the multipath effects described by the Rayleigh distribution.

Log-normal shadowing is characterized by the standard deviation σ_ξ which can be obtained by measurements. Mathematically speaking, $\xi_{(dB)} \approx N(0, \sigma_\xi^2)$ and in linear scale is said to follow a lognormal distribution with pdf given by:

$$f_\xi(x) = \frac{20/\ln 10}{\sqrt{2\pi}x\sigma_\xi}exp[-\frac{(20\log_{10}x)^2}{2\sigma_\xi^2}].$$ (2.27)

Note that $\xi_{(dB)} = 20\log_{10}\xi$.

ITU-R M.1225 Recommendation [62] specifies the standard deviations σ_ξ for the three test environments and it is presented in Table 2.7.

2.3.3   Rayleigh Fading

When signals are transmitted through mobile radio channels, small changes in position of the objects within the channel, such as a moving receive antenna, will affect the amplitude of the received signal envelope. In addition, due to the multipath nature of the propagation channel, the transmitted signal will propagate to the receiver through multiple reflective paths of possibly different time delays. These two effects cause the received signal envelope to be varying with time.

Table 2.7: Standard deviations of log-normal distributed random variables for the three test environments

Test Environment	Standard Deviation σ_ξ dB
Indoor	12
Outdoor to indoor and pedestrian (Users located outdoor)	10
Outdoor to indoor and pedestrian (Users located indoor)	12
Vehicular	10

Rayleigh distribution is commonly used to describe the statistical time varying nature of the received envelope of an individual multipath component [59, p.172]. It is well known that the envelope of the sum of two quadrature Gaussian noise signals obeys a Rayleigh distribution. Rayleigh fading is also called small-scale fading or fast fading. Equation (2.28) shows the Rayleigh pdf:

$$f_\alpha(r) = \begin{cases} \frac{r}{\sigma^2} exp[-\frac{r^2}{2\sigma^2}] & r \geq 0 \\ 0 & r < 0 \end{cases} \tag{2.28}$$

where r is the envelope amplitude of the received signal, and $2\sigma^2$ is the pre-detection mean power of the multipath signal [64]. Since it is assumed in Section 2.3 that the Rayleigh distributed random variable has a mean power of one, $\sigma = \sqrt{1/2}$. This assumption is justified when the channel capacity bound for multi-element antennas is discussed in the next chapter.

2.4   System Model Descriptions

The system model used in this analysis is a cellular system consisting of identical shaped hexagonal cells. The model will take into account interferences generated by two-tier of neighbouring cells. Therefore, there are 18 interfering cells. The system is located on a flat terrain and all the cells are identical in size. The system is fully loaded: all base station transmitters are transmitting at the maximum allowable power permitted by regulations.

This also means that all base stations are transmitting at the same amount of power. In the event that more than on transmit antennas are deployed at each cell site, the total amount of power transmitted remains at the same level as in the case with only one transmit antenna. Cells are not sectorized and omni-directional antennas are being used. Figure 2.3 shows the system model mapped into a coordinate system. Note that the shaded cell is the target cell of the system model.
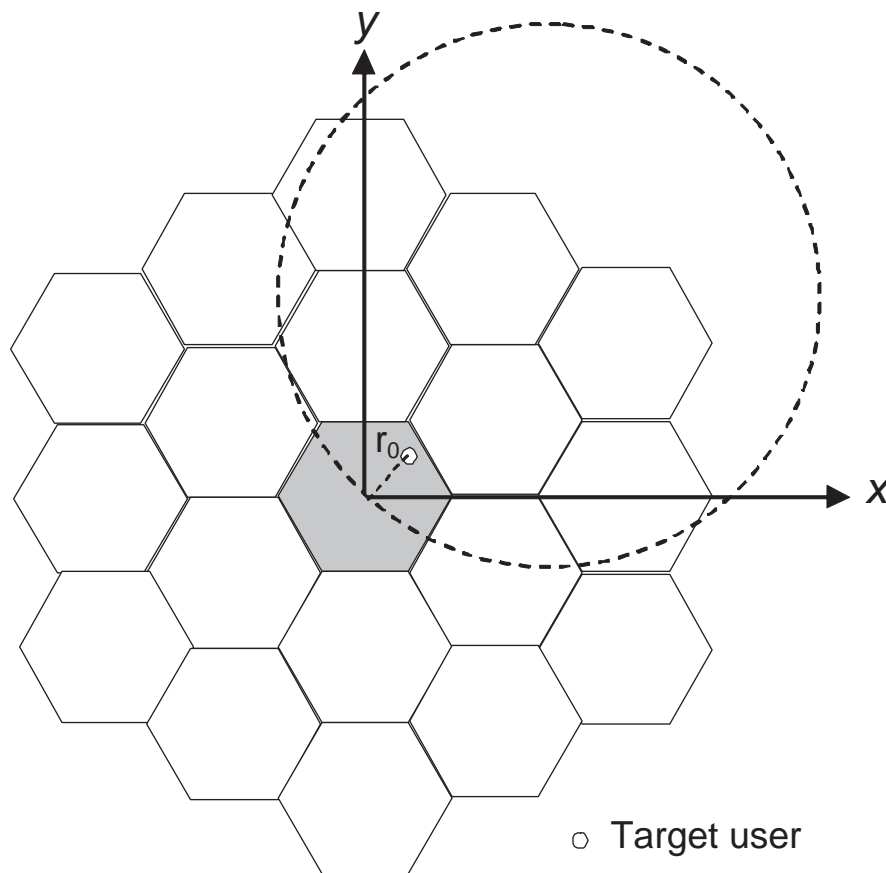
Figure 2.3: System model

The distance between the transmitter-receiver pair is of importance when calculating the path loss caused by distance separation, as shown in Section 2.3.1. The distance

between the base station and the user in the target cell can be easily calculated by using the following equation:

$$r_o = \sqrt{(x^2 + y^2)}. \tag{2.29}$$

To compute the distance between an interfering cell's base station and a user in the target cell, a new coordinate system is needed in order to simplify the task. The new coordinate system will consist of the two axes, namely the i-axis and the j-axis. The i-axis and the j axis form a 60° degree angle between them. Let R be the radius of the hexagonal cells, Figure 2.4 shows the circled area in Figure 2.3:

Two distances are needed in order to compute the distance between any interfering base station and a user in the target cell. They are the distance between the interfering base station and the target cell base station and the distance between the target cell base station and the user. If the interfering base station is located on either the i-axis or the j-axis, the distance between the interfering base station and the target cell base station is simply $iR\sqrt{3}$ or $jR\sqrt{3}$, for $i, j = 0, 1, 2$. If the interfering base station is not on any of the axes, the distance can still be found by noting that the i-axis and the x-axis form a 30° angle.

Let $r_n, n = 1...18$ denotes the distance between the n-th interfering base station and the target cell base station and $\theta_n, n = 1...18$ be the angle formed between the line connecting the n-th interfering base station with the target cell base station and the line connecting the target cell base station with the target user, as shown in Figure 2.4. With r_n, r_o and θ_n, the distance between the n-th interfering base station and a user in the target cell can be obtained using cosine law. Table 2.8 shows various θ_n and r_n values for all the 18 interfering cells. Figure 2.5 shows the enumeration on the 18 interfering cells. The distance between the interfering base station and a user in target cell is given by:

$$r(x, y|n) = (x^2 + y^2 + r_n^2 - 2(\sqrt{x^2 + y^2})r_n \cos \theta_n)^{1/2}. \tag{2.30}$$

To conclude this section, the application of frequency selective slowly-fading channel model in this research is justified. Channel models and propagation models for various propagation environments are presented. Additive white Gaussian noise is mathematically

Table 2.8: Parameters used to calculate the distance between interfering base station and the target user

Cell Number	θ_n	r_n
1	$\tan^{-1}(x/y) + 120^o$	$R\sqrt{3}$
2	$\tan^{-1}(x/y) + 60^o$	$R\sqrt{3}$
3	$\tan^{-1}(x/y)$	$R\sqrt{3}$
4	$\tan^{-1}(y/x) - 30^o$	$R\sqrt{3}$
5	$\tan^{-1}(y/x) + 30^o$	$R\sqrt{3}$
6	$\tan^{-1}(y/x) + 90^o$	$R\sqrt{3}$
7	$\tan^{-1}(x/y) + 120^o$	$2R\sqrt{3}$
8	$\tan^{-1}(x/y) + 90^o$	$3R$
9	$\tan^{-1}(x/y) + 60^o$	$2R\sqrt{3}$
10	$\tan^{-1}(x/y) + 30^o$	$3R$
11	$\tan^{-1}(x/y)$	$2R\sqrt{3}$
12	$30^o - \tan^{-1}(x/y)$	$3R$
13	$\tan^{-1}(y/x) - 30^o$	$2R\sqrt{3}$
14	$\tan^{-1}(y/x)$	$3R$
15	$\tan^{-1}(y/x) + 30^o$	$2R\sqrt{3}$
16	$\tan^{-1}(y/x) + 60^o$	$3R$
17	$\tan^{-1}(y/x) + 90^o$	$2R\sqrt{3}$
18	$\tan^{-1}(x/y) + 150^o$	$3R$

tracked. The honeycomb system model is also described. These models will be used in subsequent analyses.
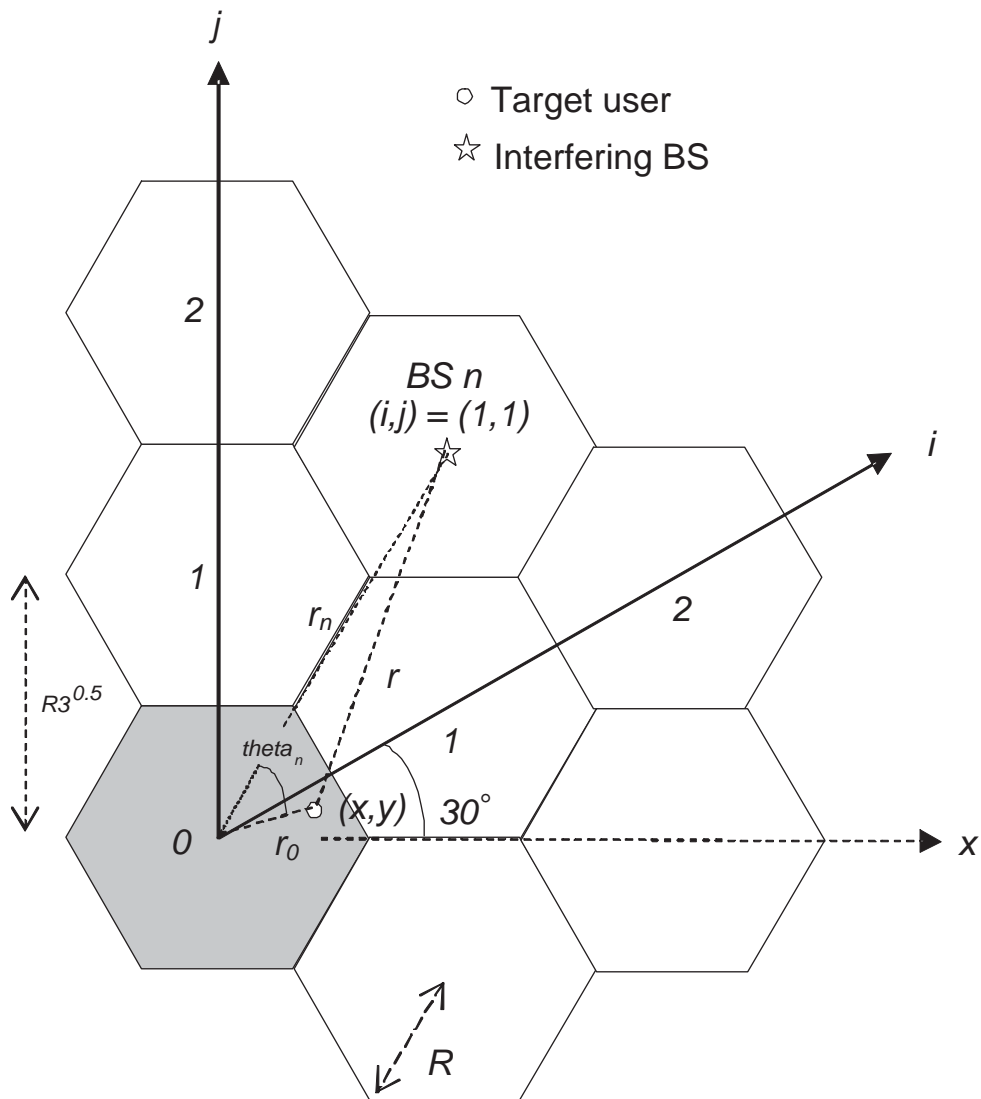
Figure 2.4: System model with the i-axis and the j-axis
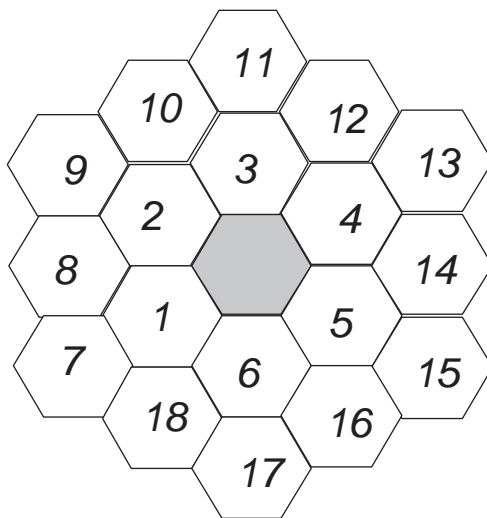
Figure 2.5: Interfering cells numbering

Chapter 3

A Synopsis of Cellular CDMA Systems that support Wireless High-speed Data

This chapter is devoted to the discussion of cellular CDMA systems that support wireless high-speed data. Specifically, the rationales behind the development of cellular CDMA systems that support wireless high-speed data, from a system design point of view and from a communication theory point of view, will be followed by the technological advances which enable the development of such system. Then noticeable changes in design philosophy in third generation systems which enables the support of high-speed wireless data, when compared to second generation systems, will be presented.

3.1   Rationales Behind the Development

There is not much debate that consumer demands triggered the development of wireless systems that support high-speed data. However, one may ask why current offerings are inadequate to provide such services. Before this question can be answered, the differences between voice services and data services should be reviewed.

Most data applications differ fundamentally from speech requirements in two respects: traffic asymmetry and tolerance to latency. Two-way conversational speech requires strict

adherence to symmetry. However, this is not the case for data traffic. The nature of data traffic is decidedly asymmetric. A much higher downlink rate is required from the base station than that generated by the mobile terminal in the uplink direction. In addition, conversational speech requires real-time handling by the system. Latencies above 100ms are intolerable (this corresponds to about 1kb of data for most speech vocoders). However, latencies of 10s are hardly noticeable for data services. For example, for a 1Mb/s data link, a 100ms delay represents only 12.5kbytes of data.

In addition to traffic asymmetry and tolerance to latency, voice services and data services differ in terms of BER requirement and traffic burstiness. The BER requirement for data services is tighter than voice services. Also, data traffic tends to appear in burst while voice traffic tends to be more continuous. In simple terms, voice services and data services are fundamentally different.

Current second generation systems were designed to handle low-rate voice services and limited data services only. In the IS-95 downlink, a multitude of low-data-rate channels are multiplexed together (with transmissions made orthogonal in the code domain) and share the available base station transmitted power with some form of power control. This is in fact an optimal choice for many low-rate channels sharing a common bandwidth [8]. However, the situation will become less optimal when a low number of high-rate users share the channel since the system is not optimized for bursty high-data rate traffic. Users who require high-rate traffic will suffer from bad user experiences. The inefficiencies increase further when the same bandwidth is shared between low-rate voice and high-rate data users, since their requirements are vastly different, as discussed previously. As a result, from a system design point of view, it would be unwise to use current systems to handle high-data rate services. In fact, the first fundamental design choice made by QUALCOMM Incorporated in the IS-856 HDR system [3] is to separate low-rate data from high-rate data services by using adjacent but non-overlapping spectrum allocation.

Next generation high-data rate systems aim to provide a data speed up to 4.838Mbps in a 1.25MHz spectrum (see Table 1.1). This equates to a spectral efficiency around 4bps/Hz. A SNR per bit (E_b/N_o) of 15dB [59, p.272] is required for unencoded communication through AWGN channel using 16QAM to achieve this spectral efficiency with symbol error probability P_M of 10^{-5}. On the other hand, coded communication is expected to lower the

SNR requirement. It is shown [20, Fig. 15] that a SNR per bit (E_b/N_o) of 7.4dB is required to support a symbol error probability P_M around 10^{-5} when the signals are encoded with parallel concatenated trellis-coded modulation under 64QAM with code rate of $r = 2/3$[1] and decoded with 10 iterations. Parallel concatenated trellis-coded modulation is one of the most advanced coding techniques which can lower the SNR requirement to achieve a certain spectral efficiency. Its BER performance is even better than turbo codes.

According to noisy channel coding theorem [58, p.386], there exist channel codes (and decoders) that make it possible to achieve reliable communication, with as small an error probability as desired, if the transmission rate $R < C$, where C is the channel capacity. If $R > C$, it is not possible to make the probability of error tend toward zero with any code. The capacity C of the band-limited AWGN waveform channel with a band-limited and average power-limited input is given as [58, Eq. 7-1-34]:

$$\frac{C}{W} = \log_2(1 + \frac{C}{W}\frac{E_b}{N_o}).$$ (3.1)

Equation (3.1) is also called the Shannon capacity bound since it depicts the theoretical maximum allowable transmission rate.

Figure 3.1 is a plot of Equation (3.1) on a plane with SNR per bit (E_b/N_o) on the x-axis and spectral efficiency R/W [bps/Hz] on the y-axis. In addition, the minimum SNR per bit (E_b/N_o) requirement for unencoded communication using 16QAM and coded communication using parallel concatenated trellis-coded modulation are included. A close investigation of Figure 3.1 reveals the following:

First of all, coded communication greatly lowers the SNR per bit (E_b/N_o) requirement to achieve a certain error probability. Secondly, parallel concatenated trellis-coded modulation can achieve near capacity performance. Thirdly, reliable communication can only be achieved when SNR per bit (E_b/N_o) is greater than 5.7403dB. If the SNR per bit (E_b/N_o) of a user is less than 5.7403dB, there is no way to achieve a spectral efficiency of 4bps/Hz, i.e., it is impossible to deliver a data rate of 5Mbps in a 1.25MHz spectrum!

The last observation indeed is the greatest challenge wireless system engineers face when they design a wireless system which supports high-data rates. No matter how good the encoding technique is, without the minimum SNR governed by the Shannon capacity

---

[1]This equates to a spectral efficiency of 4bps/Hz.
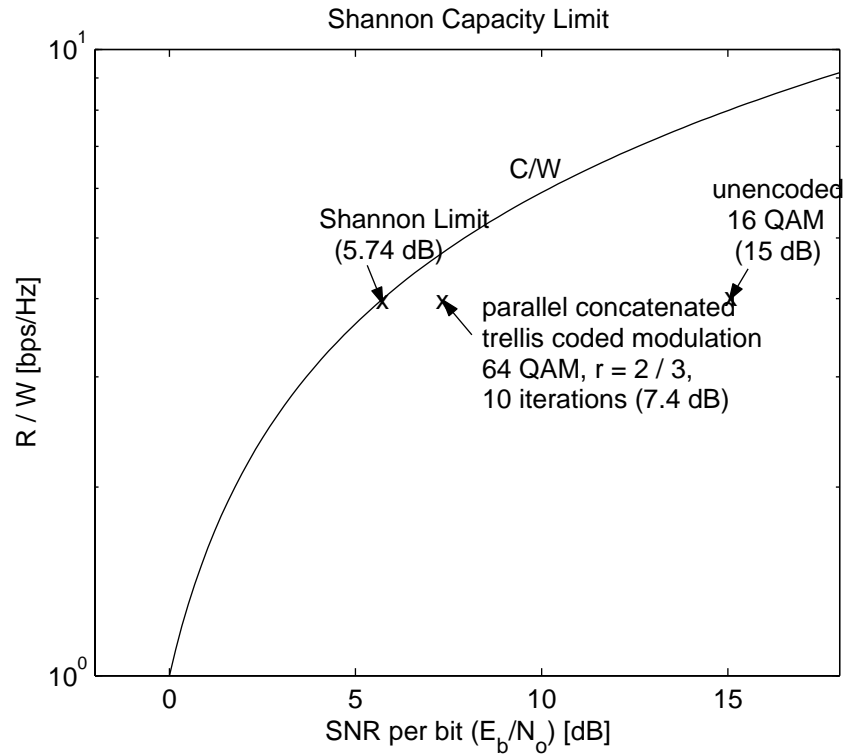
Figure 3.1: Shannon capacity bound

bound, delivering a certain high-rate data service over a wireless link is impossible. From the fact that one of the most advanced coding techniques currently available is very close to the Shannon limit, there is not much room for improvement. Fortunately, recent advances in communication system design and communication theory relief that problem and they will be discussed in the next section.

3.2   Advances in Technologies

Between the time second generation systems were introduced and third generation systems are drafted, there are a lot of advances in wireless technologies, both theoretical and practical, which enable the delivery of high-rate data over a wireless link. This subsection is

devoted to the discussion of these advances.

3.2.1 Multi-Element Antenna (MEA) Systems

As discussed in the previous section, the future breakthroughs in wireless communications will be driven largely by high data rate applications. Sending video rather than speech, for example, increases the data rate by two or three orders of magnitude. Increasing the link or channel bandwidth is a simple but costly – and ultimately unsatisfactory – remedy. As a result, in a continuing effort to find ways to improve system capacity and enhance throughput, researchers around the world have been looking into ways to improve the signal quality under a scattering propagation environment, thus enhancing the data rate that a user experiences. The classic approach is to employ antenna diversity, in which antenna diversity is believed to be a practical and effective technique for reducing the effect of multipath fading [37].

The traditional approach towards antenna diversity is to use multiple antennas at the receiver and perform combining or selection and switching in order to improve the quality of the received signal. This is the basis of CDMA RAKE receivers, in which each RAKE finger independently tracks a replica of the transmitted signal conveyed by the scattering channel. However, due to space constraint, it is difficult to deploy substantial number of antennas at a mobile handset. In addition, the economy of scale makes it unreasonable to have a large number of antennas on each mobile handset. As a result, researchers came up with an idea to deploy multiple antennas at the base station.

Fading is traditionally regarded as a nuisance by the designers of wireless communication systems. Its effect is often mitigated by some combination of different phase modulation, interleaving, or the transmission of pilot or training signals [13]. However, paradoxically, fading channels can be beneficial for a multi-antenna communication link. Foschini and Gans [24] pioneered[2] the development of communication theories and architecture for multi-element antenna (MEA) wireless systems. As discussed in the previous section, current technology offerings are very close to the Shannon limit. It will be shown in the following section that by deploying multiple transmit and receive antennas, the

---

[2]The paper by Foschini and Gans is the first published article the author could find which discusses the enormous capacity increase promised by a MEA system.

spectral efficiency is dramatically increased for a given received SNR when compared to a system with one transmit antenna and one receive antenna. This has the same effect as moving the C/W curve shown in Figure 3.1 higher along the R/W axis and it ultimately reliefs the challenge that current offerings are very close to the Shannon limit. In addition, the spectral efficiency for MEA systems scale more favourably for any increase in SNR than single antenna systems. For example, for a single antenna system, the classical Shannon formula scales as one more bps/Hz[3] for every 3dB of SNR increase. Remarkably, MEA systems with n transmit and n receive antennas, the scaling is almost like n bps/Hz for each 3dB increase in SNR. In the following subsection, the capacity formula for MEA system will be presented.

Generalized Shannon Capacity and its Application to MEA Systems

The standard formula for the Shannon capacity expressed in bps/Hz is [23, Equation 3] is:

$$C = \log_2(1 + \rho|H|^2) \tag{3.2}$$

where $|H|^2$ is the normalized channel power transfer characteristic and ρ is the expected SNR at the receiver's antenna. Note that this capacity bound applies to any channel defined by $|H|^2$, while the capacity bound given in Equation (3.1) applies only to AWGN channel.

  Since data communication occurs in packets (bursts), and with the slow fading channel assumption given in Section 2.1.3, it is reasonable to assume the channel is essentially fixed during a burst and behave differently from burst to burst. Under this *quasi-static* scenario, the channel transfer function is piecewise-constant over time and channel coding can be performed over many such independent intervals. Let the multi-element antenna system consists of n_t transmit antennas and n_r receive antennas. Since the transmitter does not know the channel, the transmitted signal power is simply distributed equally over the n_t transmitting antennas[4]. It is assumed that the receiver is provided with a noise-free measurement of the propagation channel. This can be done by sending training data from

---

[3]at high SNR

[4]It has been reported that "water-pouring" algorithm for allocating power among transmitting antennas can maximize the capacity of a MEA system [63, 31].

which the receiver can estimate the propagation coefficients. Subjecting to the average power constraint given in Equation (3.4) and limited bandwidth, the capacity expression in bps/Hz becomes [23, Equation 4]:

$$C = \log_2(|I_{n_r} + (\frac{\rho}{n_t}) \cdot \overline{H}\overline{H^\dagger}|) \tag{3.3}$$

where $\overline{H}$ is the channel transfer function matrix; $|\cdot|$ denotes the determinant operator; † denotes the operation of taking transpose conjugate on the matrix; I_{n_r} is a $n_r \times n_r$ identity matrix and ρ is the average SNRs at the receive antennas[5].

The average power constraint is [50, Equation 2]:

$$\frac{1}{n_t} \sum_{i=1}^{n_t} E|s_i|^2 = 1 \tag{3.4}$$

where E is the expectation operator, $s_i, i = 1 \dots n_t$ are the signals transmitted on the i-th transmitting antenna. An average power constraint of one means that the transmitting signals across multiple transmit antennas are normalized. The SNR term ρ will take care of the actual power being transmitted.

The capacity bound given in Equation (3.3) is called the *perfect-knowledge* upper bound [50, 51]. When $\overline{H}$ is known to the receiver, the perfect-knowledge capacity bound is achieved when the transmitted signal is a circularly symmetric complex Gaussian with zero mean and unit variance [69]. This coincides with the fact that from an information theory point of view, Gaussian distributed inputs are entropy maximizers under additive Gaussian noise channel with constrained input energy [26, p.335].

A closer look at Equation (3.3) reveals that the channel transfer function and the SNRs of the antennas are needed to compute the capacity. The following section is devoted to the discussion of the MEA channel and application of the channel transfer function matrix $\overline{H}$ in the capacity expression.

MEA Channel

As discussed in the previous section, there are n_t transmit antennas and n_r receive antennas in the MEA system. As a result, the channel transfer function matrix $\overline{H}$ will have a

---

[5]Discussions on how to obtain average SNRs of the receive antennas will be followed.

dimension of $n_t \times n_r$.

$$\overline{H} = \begin{bmatrix} h_{11} & h_{12} & \dots & h_{1n_r} \\ h_{21} & h_{22} & \dots & h_{2n_r} \\ \vdots & \vdots & \vdots & \vdots \\ h_{n_t 1} & h_{n_t 2} & \dots & h_{n_t n_r} \end{bmatrix}. \tag{3.5}$$

Let the signal transmitted on the i-th transmitting antenna be s_i, the signal received on the j-th receiving antenna be r_j and the additive noise which appears on the j-th receiving antenna be n_j, Figure 3.2 shows the complete MEA system under investigation.
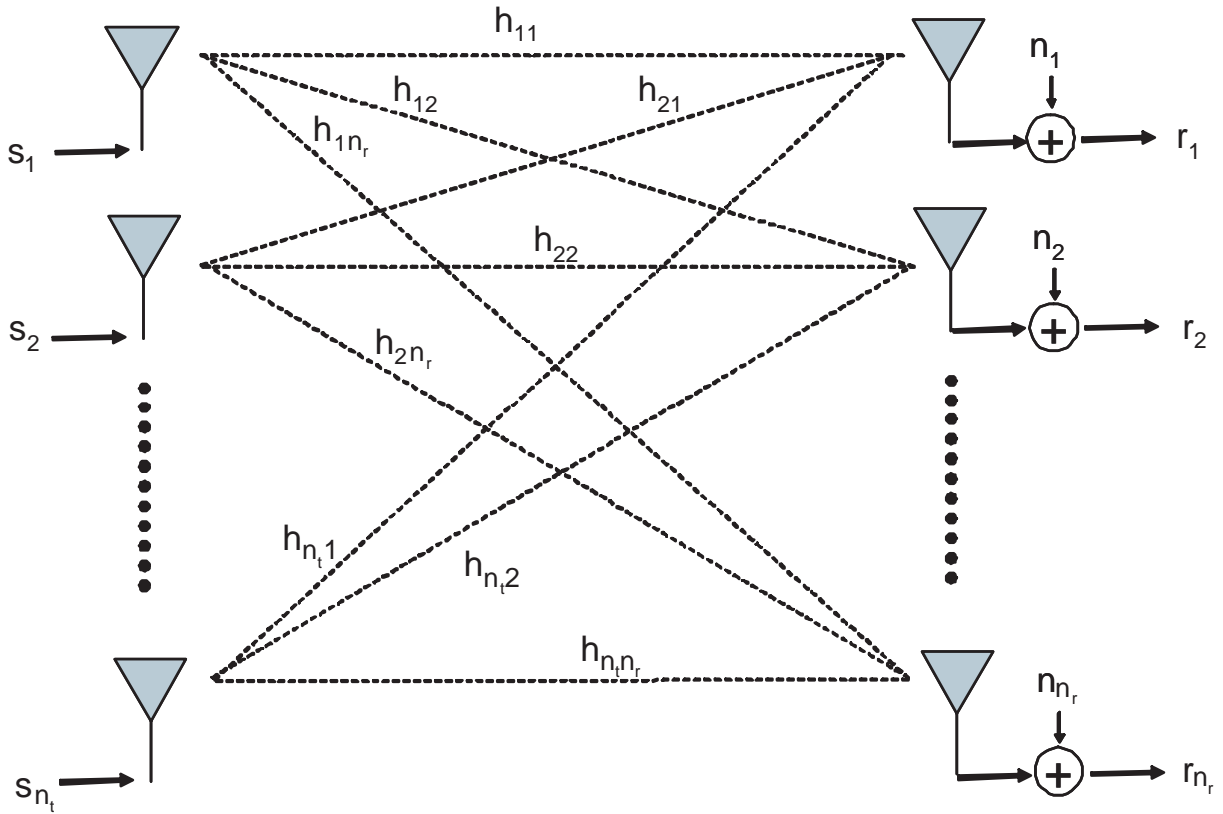
Figure 3.2: A multi-element antenna system with n_t transmit antennas and n_r receive antennas

As discussed in the previous section, each element of the channel transfer function matrix $\overline{H}$ is piecewise-constant over time. To evaluate each element of the channel transfer function matrix $\overline{H}$, the complex random process which describes the propagation effects given in Equation (2.21) can be used. The equation is repeated here:

$$c_n(t) = 10^{\frac{-L_{50}}{20}} 10^{\frac{-\xi}{20}} \alpha e^{-j\phi}. \tag{3.6}$$

To simplify the numerical computation of the MEA capacity, several subtle observations have to be made. First of all, from the insight that the SNRs of each receiving antennas are needed, any power related terms from Equation (3.6) can be taken into account when computing the SNR. Therefore, the term associated with the mean path loss ($10^{\frac{-L_{50}}{20}}$), as well as the term associated with phase attenuation ($e^{-j\phi}$) can be considered later. Secondly, only Rayleigh fading will be taken in account in the application of MEA channel capacity equation. There are several reasons behind this decision. Since the signal power is required when computing capacity, the gain associated with Rayleigh fading has to be squared, as shown in the term α^2 in Equation (2.22). It is well known that the square of a Rayleigh fading random variable gives the chi-square distribution [58, p.41] and addition of chi-square distributed random variables gives the *chi-square pdf with* n *degree of freedom*. The chi-square random variable, as well as the first two moments of chi-square pdf with n degree of freedom are well defined. These will simplify the computation of capacity, as it will be shown later. By means of that, the remaining log-normal shadowing term ($10^{\frac{-\xi}{20}}$) will also be taken into account when computing SNR in subsequent sections. On the other hand, for readers who want to aggregate all fading characteristics in one equation, the proposed method does allow readers to include log-normal shadowing, or any other fading characteristics in computing capacity. For example, the Suzuki process, which is obtained by the multiplication of a Rayleigh process with a log-normal process [55] can be used in the channel transfer function. However, it should be noted that the square of the random variable is required, which may not be easily constructed or mathematically trackable.

According to the uncorrelated scattering assumption described in Section 2.1.1, elements of the channel transfer function matrix are independent of each other[6]. Since the MEA system operates under one physical channel, it is reasonable to assume that all el-

---

[6]For the effect of correlated fading and its effect on the capacity of a MEA system, refer to [63].

ements in the channel transfer function matrix are identically distributed. Taking into account the above observation and assumption, each element of the channel transfer function matrix is defined as follows:

$$h_{mn} = \alpha_{mn} \tag{3.7}$$

where α_{mn} is the i.i.d. Rayleigh random variable, $m = 1 \ldots n_t$ and $n = 1 \ldots n_r$. Note that the only term which is left from Equation (3.6) is the Rayleigh random variable.

As discussed in Section 2.3.3, the Rayleigh random variable is the envelope of the sum of two quadrature Gaussian noise signals. In addition, it is assumed the Rayleigh random variable has a mean power of one. Therefore,

$$\alpha_{mn} = |\mathcal{N}(0, \frac{1}{\sqrt{2}}) + j \cdot \mathcal{N}(0, \frac{1}{\sqrt{2}})| \tag{3.8}$$

where $\mathcal{N}$ is the Gaussian distributed random variable, $m = 1 \ldots n_t$ and $n = 1 \ldots n_r$. With Equation (3.7) and (3.8), the elements of the channel transfer functions matrix, $h_{mn}, m = 1 \ldots n_t, n = 1 \ldots n_r$ has i.i.d., complex, zero mean, unit variance entries [23, Equation 8]:

$$h_{mn} = \alpha_{mn} = |\mathcal{N}(0, \frac{1}{\sqrt{2}}) + j \cdot \mathcal{N}(0, \frac{1}{\sqrt{2}})|. \tag{3.9}$$

Consider the case that there is only one transmit antenna and one receive antenna. Direct evaluation of Equation (3.3) with Equation (3.9) gives the following:

$$C = \log_2(1 + \rho \cdot |\alpha|^2). \tag{3.10}$$

Note that the term $|\alpha|^2$ is a random variable with the central chi-square pdf with 2 degrees of freedom distribution. Since extensive use of central chi-square pdf with various degree of freedom will be used, a new notation is needed for better clarity. Let χ_{2k}^2 denotes the central chi-square pdf with $2k$ degrees of freedom, Equation (3.10) becomes:

$$C = \log_2(1 + \rho \cdot \chi_2^2). \tag{3.11}$$

It is worthwhile to discuss the random variable χ_2^2. According to Equation (3.9), h_{mn} has unit variance entry. Therefore, the variance of the random variable χ_2^2 equals to one.

On the other hand, the variance of any central chi-square random variable with n degrees of freedom is given as follows [58, Equation 2-1-112]:

$$var(\chi_n^2) = 2n\sigma^4. \tag{3.12}$$

Substituting $var(\chi_2^2) = 1$ into Equation (3.12) gives $\sigma^2 = 1/2$. This agrees with the assumption given in Section 2.3 that the Rayleigh distributed random variable has a mean power of one.

The capacity expression given in Equation (3.3) is a very powerful expression. For a system with receive diversity only (i.e.: $n_t = 1$), Equation (3.3) becomes:

$$C = \log_2(1 + \rho \sum_{n=1}^{n_r} h_{1n}^2). \tag{3.13}$$

Note that the terms $h_{1n}^2, n = 1 \ldots n_r$ are i.i.d. central chi-square random variables with 2 degrees of freedom. The subscript $1n$ denotes the subchannel between first transmit antenna and the n-th receive antenna. Since $h_{1n}^2, n = 1 \ldots n_r$ are i.i.d. central chi-square random variables with 2 degrees of freedom, using the notation χ^2, Equation (3.13) becomes:

$$C = \log_2(1 + \rho \sum_{n=1}^{n_r} \chi_{2,n}^2). \tag{3.14}$$

Addition of central chi-square random variables will simply increase the degree of freedom, in contrast to sum of other random variables such as log-normal random variable which requires complex mathematical analysis [14]. This is a very important characteristic of chi-square random variables. Since chi-square random variable with any degrees of freedom is simple and well defined, this characteristic will simplify the calculation. Suppose the random variable Y is defined as:

$$Y = \sum_{i=1}^{n/2} \chi_2^2 \tag{3.15}$$

then Y becomes a chi-square random variable with n degrees of freedom, with pdf given by [58, Equation 2-1-110]:

$$p_Y(y) = \frac{1}{\sigma^n 2^{n/2} \Gamma(n/2)} y^{n/2-1} e^{-y/2\sigma^2} \tag{3.16}$$

where $\Gamma(\cdot)$ is the gamma function.

Applying the same concept, Equation (3.14) becomes:

$$C = \log_2(1 + \rho \chi_{2n_r}^2). \tag{3.17}$$

A closer look at Equation (3.14) reveals some interesting facts. Assuming there is only one RAKE finger at each of the receive antenna and all the antennas have the same SNR, Equation (3.14) follows a similar pattern that under maximal ratio combining, the average SNR of the whole system is simply equal to the sum of the individual average SNR from each finger of the receiver [59, p.328].

For a system with transmit diversity only (i.e.: $n_r = 1$), by following the steps described throughout this section and using Equation (3.3) and the notation χ^2, the MEA system capacity for such system is:

$$C = \log_2[1 + (\rho/n_t)\chi_{2n_t}^2]. \tag{3.18}$$

MEA System Capacity Lower Bound

Before presenting the capacity formula for a system with combined transmit and receive diversity, it is worthwhile to discuss the *capacity lower bound* for an MEA system. The perfect knowledge upper bound is based on receiver's perfect knowledge of the channel and inputs which follow the Gaussian distribution. It is possible for a receiver to estimate the channel accurately, especially under a slow fading channel. However, it is unrealistic to assume all possible inputs to conform to the Gaussian distribution. As a result, capacity lower bound is derived to conservatively estimate the channel capacity. Currently, there are two approaches in estimating the capacity lower bound. The first approach (Foschini and Gans) is to use an *unitarily equivalent* of the channel transfer function matrix $\overline{H}$ [23, Section 4.11]. The other approach (Hochwald and Marzetta) is to assume an input

distribution which will minimize the mutual information between the inputs and the outputs [50, Section V-B]. The capacity lower bound given by Foschini and Gans is more mathematically trackable and easier to understand. The capacity lower bound given by Hochwald and Marzetta requires the understanding of *sphere-hardening* phenomenon of Gaussian channel [72, p.323], which is an important, but very abstract concept in information theory. There is no comparison between the results obtained by the two different approaches or discussion about which method is preferred over the other. It will be an interesting subject to investigate in the future. Since the capacity bound given by Foschini and Gans is simpler than the one given by Hochwald and Marzetta, the former is chosen in subsequent analysis.

The capacity lower bound given by Foschini and Gans for a combined transmit and receive diversity MEA system is given as follow [23, Equation 12]:

$$C > \sum_{k=n_t-(n_r-1)}^{n_t} \log_2[1 + (\rho/n_t) \cdot \chi_{2k}^2]. \tag{3.19}$$

Equation (3.19) can be interpreted as follows: since there are multiple transmit and receive antennas, there are multiple subchannels between the transmitter and the receiver. With the uncorrelated scattering assumption, the total MEA system capacity will be the sum of capacities of the subchannels. The number of subchannels available between the transmitter and receiver is determined by the number of transmit and receive antennas, as indicated in the summation indices in Equation (3.19). In addition, each of the subchannel provides *two* or *multiple of two degrees of diversity*, as given by the chi-square random variable with two or multiple of two degrees of freedom. The two degrees of diversity come from the fact that there are real and quadrature components in the elements of the channel transfer function matrix. Next section will discuss the degrees of diversity of each subchannel when the receiver structure is being presented. Since the total capacity is the sum of individual subchannel capacity, an MEA system can deliver an increase in capacity when compared to system with only one transmit and one receive antenna.

There are certain conditions in which deploying multiple antennas does not enhance the overall system capacity. First noticeable condition from Equation (3.19) is the effect of the term $\frac{1}{n_t}$. Although there are more channels between the transmitter and receiver,

if the SNR of each channel for an MEA system is not as high as the case with only one transmit and one receive antenna, there may not be any enhancement by deploying multiple antennas. This will be further investigated when simulation results are presented in Chapter 5.

It is worthwhile to note that the difference between the mean values of the perfect-knowledge upper bound and the lower bound is proven to be *no greater* than n_t bps/Hz [63, Section III-B]. Application of the perfect knowledge upper bound may provide an overly optimistic estimate.

Here is an example on the application of the capacity lower bound. Assume there are two transmit antennas and two receive antennas and the average SNRs at the two receive antennas are ρ, Equation (3.19) becomes:

$$C > \log_2[1 + (\rho/2)\chi_2^2] + \log_2[1 + (\rho/2)\chi_4^2]. \qquad (3.20)$$

The second term on the right hand side of Equation (3.20) means that the second receiver has two subchannels to choose from (as shown by the chi-square random variable with 4 degrees of freedom) while the first receiver only has one. It is obvious that the second receiver has two subchannels since there are two propagation paths, one from the first transmitter and one from the second transmitter. However, the fact that the first receiver only has one subchannel requires an indepth understanding of the receiver architecture.

Layered Space-Time Processing Architecture for MEA Systems

The Bell LAbs LAyered Space-Time (BLAST) architecture has been proposed [24] to exploit the enormous capacity increase promised by MEA communication theory. Figure 3.3 shows the coded layered space-time architecture, with n_r receive antennas and n_t transmit antennas.

Assuming $n_r = n_t$[7], a top level view on how the architecture detects the n_t transmitted signals is as follow: in the first layer, the receiver detects a first transmitted signal by nulling out interference from $n_t - 1$ other transmitted signals through array processing. It is shown that with the "zero forcing" constraint, one receive antenna tracking one subchannel is

---

[7]Next section will discuss the case when $n_r > n_t$. The case when $n_t > n_r$ is not allowed in BLAST architecture.
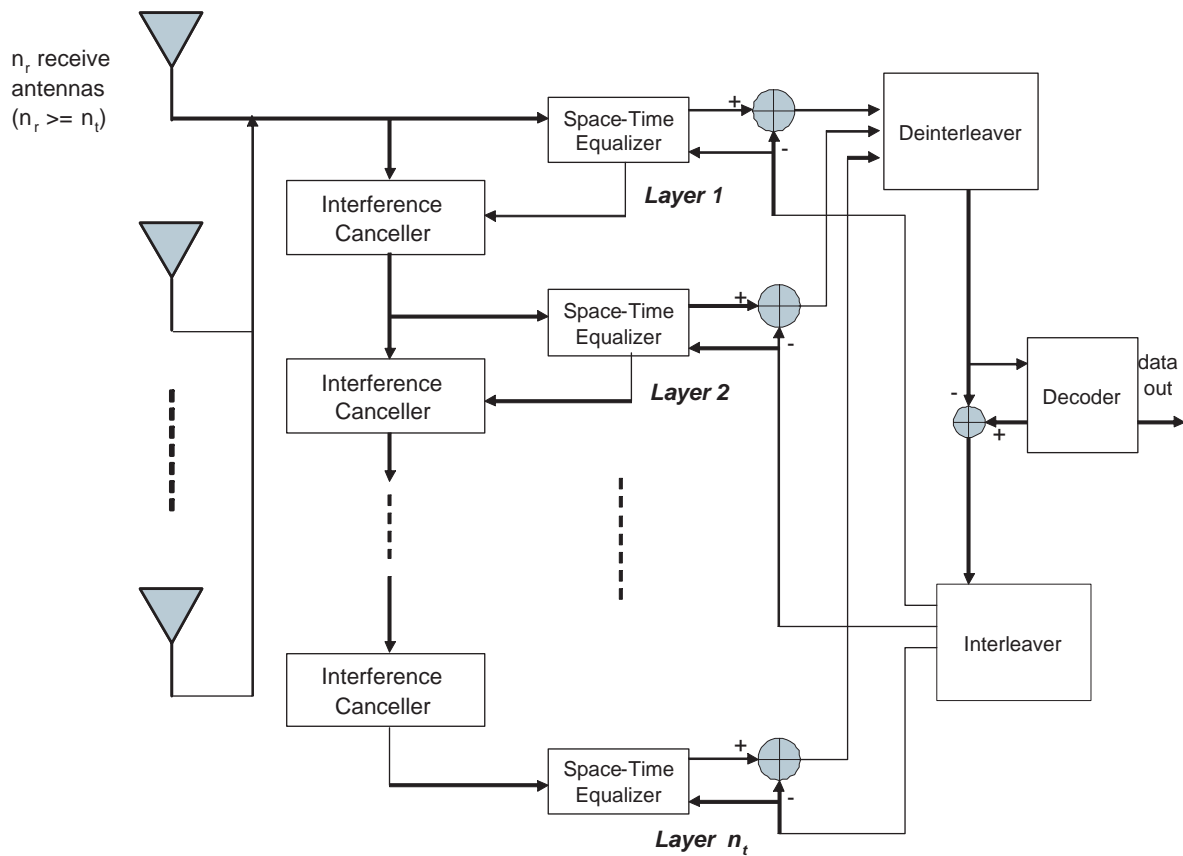
Figure 3.3: Coded layered space-time architecture with n_t receive antennas and n_r transmit antennas [4, Figure 1]

needed to completely correlate and subtract each interference [71]. As a result, the overall process of nulling out $n_t - 1$ interferences leaves the first layer with $n_t - (n_t - 1) = 1$ subchannel practically. Due to the fact that each subchannel has real and quadrature components, a subchannel can provide a diversity order of 2 [4]. This diversity order will be reflected in the chi-square random variable with 2 degrees of freedom in the capacity expression. With all the above observations, the first layer will afford a diversity order of 2. This agrees with what is shown in the first term on the right hand side of Equation (3.20). Once detected, the first signal is subtracted from the remaining undetected signals. The remaining undetected signals will then be fed to the subsequent layers.

In the second layer, the receiver performs similar interference nulling to detect a second transmitted signal. This time, the first transmitted signal is no longer interference to the second layer because it is completely detected by the first layer. As a result, there are only $n_t - 2$ remaining interferences. Applying the same "zero forcing" constraint, the process of nulling out $n_t - 2$ interferences will leave the receiver with practically $n_t - (n_t - 2) = 2$ subchannels to provide diversity for the second signal. Since each subchannel has real and quadrature components and provides a diversity order of 2, having 2 subchannels will therefore allow the receiver to have a diversity order of 4. This agrees with what is shown in the second term on the right hand side of Equation (3.20). The second detected signals is then subtracted from the received signals provided by the first layer and then be fed to subsequent layers.

Repeating the above interference nulling/cancelling step through n_t layers, the receiver affords an increasing order of diversity from 2 to $2n_t$. If the capacities achieved in individual layers can be combined in some manner, then the layered space-time approach will achieve the capacity expression given in Equation (3.19). For the discussion of capacities combining techniques, consult [4, 71] and the references herein.

It is worthwhile to mention that the layered space-time processing architecture represents only part of the solution to achieve the great capacity promised by information theory for an MEA system. The missing part of the solution includes the design of a transmitter architecture, as well as the design of the channel encoder/decoder pair which utilize such a transmitter-receiver architecture. As shown in Figure 3.1, with the advances of technology, it is possible for a transmitter-receiver pair with a strong channel code to achieve within a

certain percentage of capacity. Channel codec technology for 1-D system is a highly developed field. It has been shown that channel codes such as turbo code (parallel concatenated convolution code) [12] and serial concatenated convolutional code [10] can greatly reduce the SNR requirement to achieve a certain BER. Deploying multiple transmit antennas introduces a new area of channel codec design. Instead of transmitting the coded bits in time domain, it is now possible to transmit the coded bits in the spatial domain. It should be noted that the layered space-time processing architecture described above detects the transmitted signal by decoupling. By using such architecture, signals from different transmit antennas are decoupled, rather than joint detection. Such decoupling process requires the transmitted signal to contain some orthogonal structure. In addition, the encoding structure which ensure orthogonality among different transmit antennas must be able to scale to any arbitrary number of transmit antennas. This leads to the design of space-time block code [68] - the codec scheme which aids multi-user detection, as well as exploiting the maximum number of diversity order in both time and spatial domain. Examples of space-time block codes are orthogonal transmit diversity (OTD) and space-time transmit diversity (STTD). Both OTD and STTD have been adopted by third generation CDMA systems as an optional mode of operation. In [40], the authors did an excellent but easy to understand comparison between different space-time block coding schemes. Furthermore, since space-time block codes are not designed to achieve additional coding gain, researchers come up with an idea to combine space-time block codes with some highly developed 1-D channel codec such as convolutional code, turbo convolutional codes, and turbo BCH codes [48]. Moreover, turbo trellis modulation, a modulation scheme which is designed to maximize the effective Euclidean distance between signalling points as well as providing coding gain has been proposed to work with space-time block coding [6]. In summary, the BLAST architecture described above is only part of the solutions which enables the huge capacity increase promised by MEA capacity theories. There are a lot of work to be done at the transmitter side and codec design as well.

Notes on Applying the MEA System Capacity Lower Bound

Since the capacity bound given in Equation (3.19) does not impose any restrictions on the number of transmit and receive antennas, there are several cases in which the upper

and lower limits of the summation have to be modified. In general, there are four possible cases for the number of transmit and receive antennas. They are systems with receive diversity only ($n_r = 1$); systems with transmit diversity only ($n_t = 1$); systems in which the number of transmit antennas is greater than or equal to the number of receive antennas ($n_t \geq n_r$) and systems in which the number of receive antennas is greater than the number of transmit antennas ($n_r > n_t$). A closer look at Equation (3.19) shows that in some cases, especially the case when $n_r > n_t$, will result into a chi-square random variable with zero or negative degree of freedom. The upper bound and/or the lower bound have to be modified for these cases.

Shiu, Foschini, Gans and Kahn in [63] have shown that an n_t-input n_r-output multiple antenna system consists of $n = min(n_t, n_r)$ subchannels and the channel capacity is the sum of individual subchannel capacities. One may doubt the practicability of deploying systems with $n_r > n_t$ or $n_t > n_r$, since the number of subchannels will be limited by n. Although the number of subchannels is limited by n, the degree of diversity of each subchannel (as seen in the degree of freedom of the chi-square random variable) is not.

Consider the case when $n_r > n_t$, there are only n_t subchannels under this configuration. Modification of the lower summation index of Equation (3.19) to one will properly capture the number of subchannels available. However, the diversity order of each of the subchannels is not properly captured. The total capacity given by direct application of Equation (3.17) after the modification of the lower bound is the sum of capacities of n subchannels with degree of diversity from 2 and $2n$. Although the extra $n_r - n_t$ antennas do not increase the number of subchannels, it does increase the diversity order of each subchannel. It has been shown by Shiu and et. al. [63, Section III-B] that each extra $n_r - n_t$ antenna effectively provides a new subchannel on each of the receiving antenna. In other words, each extra $n_r - n_t$ antenna increases the degree of diversity of each of the receiving antenna by two. In short, the MEA capacity is lower-bounded by the sum of capacities of n subchannels with degree of freedom $2 + 2(n_r - n_t)$, $4 + 2(n_r - n_t)$, ..., $2n_t - 2 + 2(n_r - n_t)$, $2n_t + 2(n_r - n_t)$, or simply $2(n_r - n_t + 1)$, $2(n_r - n_t + 2)$, ..., $2n_r - 2$, $2n_r$.

Consider the case when $n_t \geq n_r$, no modification of the bounds is needed and the degree of diversity of each subchannel is properly captured.

The case $n_t = 1$ is the case when there is receive diversity only. Equation (3.17) shows the capacity bound of a receive diversity only system. Note that the capacity upper bound and the capacity lower bound are the same. It is because the channel transfer function matrix $\overline{H}$ is just a row matrix and application of unitarily equivalent on such row matrix will not result into a different bound.

The case $n_r = 1$ is the case when there is transmit diversity only. Equation (3.18) is the capacity bound of a transmit diversity only system. Only one bound exists for a transmit diversity system.

The application of MEA channel capacity equations shown in Equation (3.3) and (3.19) require the average SNRs ρ at the receive antennas. This discussion is devoted to obtaining the average SNRs. Foschini and et.al. in [25] discusses that the average SNR should be measured by a probe receive antenna element. The probe receive antenna, as well as a test transmit antenna are independently moved over their respective volumes and a spatial average is taken across different antenna positions. Alternatively, if the propagation environment changes substantially from packet to packet, ρ could be defined as the SNR seen by a single receive antenna averaged over a large number of packets from a single transmitter. The first method will result into one ρ value and the value is averaged spatially at the receiving end. The second method assumes the receive antennas are placed substantially close to each other so that the channel characteristics will be the same across multiple antennas. Note that in general, if antennas are placed at a distance greater than half wavelength of the signal, their channel characteristics are considered uncorrelated.

Third generation systems and their high data rate extensions are all operating at a carrier frequency greater or equal to 1.9GHz. This equates to a signal wavelength of 0.16m or smaller. If all the receive antennas are placed within 8cm of each other, with the quasi-static channel assumption, the second method of obtaining average SNR is appropriate and only one ρ value results. However, if a receiver ever deploys multiple antennas, it will be ridiculous to placed them so closely.

Assuming receive antennas are placed at least half wavelength from each other or any other distance that makes them uncorrelated, the multipath channels will be uncorrelated to each other. Therefore, it will be more appropriate to obtain an average SNR value for each of the receive antenna, rather than one spatial average or temporal average. By means

of that, let $\rho_k, k = 1 \ldots n_r$ be the SNR value seen by the k-th receive antenna averaged over time and Equation (3.19) becomes:

$$C > \sum_{k=n_t-(n_r-1)}^{n_t} \log_2[1 + (\rho_k/n_t) \cdot \chi_{2k}^2]. \tag{3.21}$$

For the case where there is only one transmit antenna, Equation (3.14) becomes:

$$C = \log_2(1 + \sum_{k=1}^{n_r} \rho_k \chi_2^2). \tag{3.22}$$

It is clear from Equation (3.19) that the capacity lower bound consists of random variables which are related to the channel propagation effects. As a result, the capacity expression is not deterministic and therefore the capacity should be treated as a random variable. To apply capacity which is a random variable, the complementary cumulative distribution function (ccdf) can be used. The ccdf of capacity shows the probability of the channel capacity which exceeds a certain bps/Hz. For the trivial case, the random varying channel capacity will exceed 0 bps/Hz with a probability of one. A threshold percentage of 99% is often used [23, Section 1] as a figure of merit. It is because capacity expressions are intended to give the maximum achievable error free bit rate promised by information theory and a 99% threshold is believed to be suffice for this purpose. Other suggestions include mean plus one or two standard deviations.

A random varying capacity expression thresholded at 99% means that the capacity value is guaranteed 99% of the time. For example, if the channel capacity thresholded at 99% gives a value of 3bps/Hz, this means that for 99% of the time, a user of the channel will find himself / herself with a data rate less than 3bps/Hz. In addition, since current technologies as shown in Figure 3.1, although very close, is still 1-2 bps/Hz away from channel capacity, it is safe to assume that the random varying channel capacity thresholded at 99% is the maximum error free bit rate a user can experience. The capacity value obtained by thresholding a random varying capacity expression is also called *outage capacity*. The capacity value obtained by thresholding at 99% is called the 1% outage capacity.

It has been explained in the above paragraphs that the MEA system capacity lower bound is the sum of individual subchannel capacities. To be able to calculate individual

subchannel capacities, the SNRs ρ_k at each of the receiving antennas are needed, as shown in Equation (3.21). The SNR of each receiving antenna can be calculated by taking into account the receiver structure and other factors such as the distance between the user and the transmitting base station, intercell interferences, the number of multicodes the user is assigned, etc. Section 4.1 will discuss receiver structure and Section 4.2 will detail the methods to calculate SNR at each receiving antenna.

To conclude this section, multiple transmit and receive antennas deployed under multipath fading channels with the uncorrelated scattering assumption creates a certain number of independent subchannels. By using the BLAST architecture, the capacities of each subchannel can be combined and this delivers an increase in spectral efficiency. To generate graphs similar to Figure 3.1, the SNRs at each receiver are required. Before the discussion on computing the SNRs at each of the receiver, it is worthwhile to discuss several other common characteristics found on high-speed wireless data systems, in addition to multiple transmit and receive antennas. These characteristics may affect the SNR of each receiver.

3.2.2   Concatenated Codes

In addition to MEA systems, another noticeable breakthrough in wireless systems design after the introduction of second generation systems is the use of concatenated codes as the choice of channel encoding scheme. Concatenated coding technique is not new. It had been reported in literature since 1966 [22]. However, with the introduction of *turbo code* by Berrou [11] in 1993, it has caught the research community a lot of attention. The great interest in turbo codes is motivated by the fact that they perform near the Shannon limit, as shown in Figure 3.1.

Turbo codes are a sophisticated continuation of concatenated codes. They consist of parallel-concatenated recursive convolutional codes connected by an interleaver, and the overall code rate can be adjusted by puncturing the redundancy bits of each constituent code [44]. By means of that, turbo code is also called parallel-concatenated convolutional code (PCCC). Figure 3.4 shows a turbo encoder with two constituent codes with code rate 1/3.

The superior performance of turbo code is the combination of the works of the constituent codes and the interleaver. Since the constituent codes are recursive convolutional
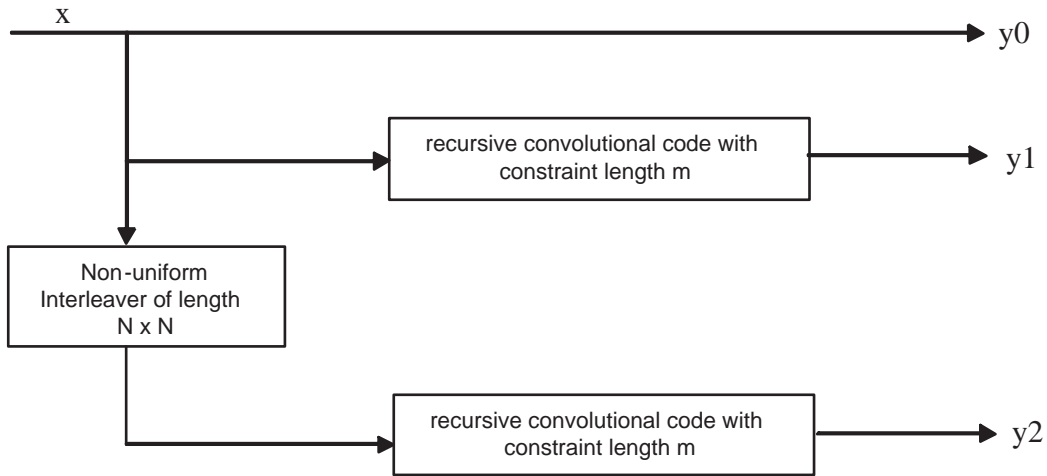
Figure 3.4: A turbo encoder with code rate 1/3

codes, a low-weight input sequence may generate a high-weight codeword and vice versa [67]. A good interleaver matches low-weight codewords from one constituent code with high-weight codewords from the other constituent code with high probability. The result of this process is called weight spectral thinning [56]. As a result, the turbo encoder structure will generate codewords which are close to an average weight. Codewords with weights close to an average weight will have more predictable error correcting property and therefore results into superior coding performance to other coding schemes.

When concatenating convolutional encoders in parallel perform so great, a logical investigation is to concatenate convolutional encoders in series. Serial concatenated convolutional code (SCCC), as its name suggested, is a channel coding technique obtained by serially concatenating two convolutional codes separated by an interleaver.

Concatenating codes serially is not a new concept. The most widely employed serial concatenated coding scheme before the introduction of SCCC was to make use of a Reed Solomon code as an outer code and of a convolutional code as an inner code [10]. The concept of putting an interleaver in between two convolutional codes emerged after the introduction of turbo code, forming a powerful integrated coding scheme. Before that, it was believed that the sole purpose of the interleaver is to randomize errors produced by

the inner encoder. Figure 3.5 shows a serial concatenated convolutional coder.
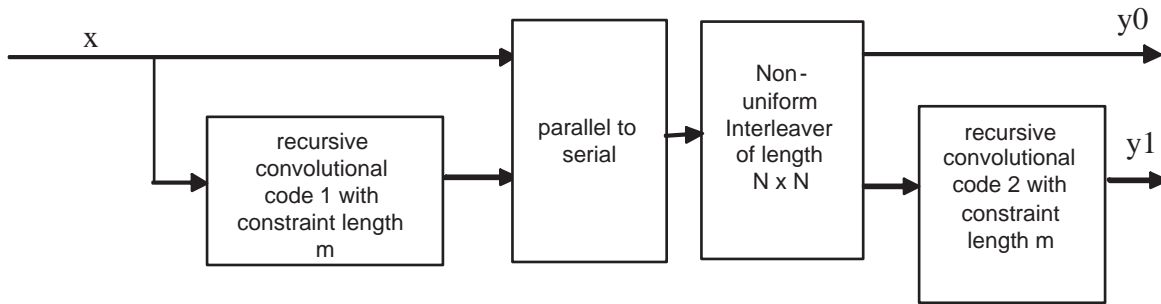
Figure 3.5: A serial concatenated convolutional coder with code rate 1/4

Turbo code has been adopted by the cdma2000 standard [2] as one of the channel coding schemes. Quasi-Complementary Turbo Codes (QCTC) has been proposed in the L3NQS 1xEV-DV standard [21]. QCTC is a class of variable rate turbo codes and it is used to form the incremental redundancy sub-packets. Although serial concatenated convolutional code is shown to be superior for low BER applications to turbo code [9], it has been withdrawn from the final IS-856 standard [3] due to compatibility issues with other cdma2000 systems.

Analysis of turbo code is not trivial. It is because the performance of a turbo code depends on a lot of issues. To name a few: the performance of turbo codes depends on the choice of constituent codes, the memory of constituent codes, the puncturing rate, interleaver size and interleaving algorithm, the number of iterations in the decoding process, etc. Luckily, the capacity model proposed in this research does not need an indepth analysis of turbo code. It is because the goal of any channel coding scheme is to deliver a higher spectral efficiency for a given SNR and BER when compared to uncoded communication. The highest spectral efficiency theoretically possible for a given SNR is given by the capacity expression. This value is independent of any channel coding scheme, therefore, no indepth analysis of turbo code is needed in this research. One may ask the question that by using the capacity expression, an overly optimistic estimate will result. This is true for current technologies. However, it is expected that as time progresses, a channel code which can achieve a spectral efficiency which is very close to the channel capacity will be invented. A very good example was the invention of turbo code. On the other hand, since a threshold

percentage is needed for the random varying MEA channel capacity and a 99% threshold is used in this research, a lower threshold percentage can probably be used if one wants to properly capture the lack of channel code which can achieve channel capacity.

The above two breakthroughs in wireless technologies after the introduction of second generation systems have been identified. To enable support for high-speed wireless data, changes in wireless system design philosophy are necessary. The following section is devoted to the discussion of noticeable changes in wireless systems design philosophy in third generation systems.

3.3   Changes in Design Philosophy

When one takes a careful look at how the forward link of high-data rate extensions of cdma2000 is implemented, he / she will identify a lot of differences when compared to second generation systems' forward link. This section is devoted to the discussion of the noticeable and significant changes in the forward link design philosophy of third generation systems.

3.3.1   Adaptive Modulation and Coding

Fixed modulation such as QPSK and a fixed channel code rate are being used in second generation systems. In high-speed data extensions of third generation systems, adaptive modulation and coding (AMC) is being used. AMC means that the signal constellation and channel code rate will vary from packet to packet, resulting into different data rate from packet to packet. As a result, wireless systems which support AMC will have *dynamic data rates*.

AMC is realized with the cooperation between the base station and the mobile station. The base station punctures pilots in pre-determined intervals on its forward data traffic channel, or delivers its pilots on a separate forward pilot channel. The mobile station measures the pilot strength and then reports its measured C/I (carrier-to-interference ratio) back to the base station, as well as its desired data rate. The base station then encodes the forward link at exactly the highest rate that the wireless channel can support at that instant. For example, if the channel condition is good, the base station can use 16QAM

rather than QPSK and a turbo code rate of 1/3 rather than 1/5. By doing this, a larger portion of channel capacity can be realized when compared to fixed modulation and coding. The adjustment of modulation scheme and code rate according to channel condition is called *link adaptation.*

Since AMC is a joint effort of the base station and the mobile station, a table with all the different combinations of modulation and channel code rate (and hence data rate) should be available to both base station and mobile station. This table is called the *M*odulation and *C*oding *S*cheme (MCS). In addition, the base station should be able to decide what modulation and code rate to use when it receives C/I feedback from the mobile station.

All the high-data rate extensions to cdma2000, i.e. IS-856 [3], L3NQS [21] and 1XTREME [52] support AMC based on channel condition feedbacks. The MCS can be found in the references mentioned above.

Since AMC is a method to utilize a larger portion of channel capacity and it does not affect the SNR of a user, by using the capacity expression, indepth analysis of AMC is not required.

3.3.2 Hybrid Automatic Repeat Request (ARQ) and Incremental Redundancy (IR)

Hybrid automatic repeat request (ARQ) and incremental redundancy (IR) are not new. They have been around for about two decades [41]. However, second generation systems do not employ ARQ or IR, probably due to the fact that sufficient computing power were not available when second generation systems were defined. In an effort to increase the data rate a wireless link can provide, hybrid ARQ and/or IR are introduced recently in 2.5G and 3G standards, noticeably GPRS, EDGE [53] and all the high-data rate extensions of cdma2000 [52, 3, 21].

In a basic hybrid ARQ scheme, a code that is designed for simultaneous error correction and error detection is used. When a received codeword is detected in error, the receiver first attempts to correct the errors. If the number of errors is within the designed error-correcting capabilities of the code, the errors are corrected. If, on the other hand, an uncorrectable error pattern is detected, the receiver rejects the packet in error and requests

its retransmission via a return channel. This ARQ strategy is known as type I hybrid ARQ strategy. The disadvantage of type I hybrid ARQ scheme is that once the code rate is fixed, all the parity bits for error correction are transmitted even if they are not all needed. This will reduce the channel use efficiency.

Type II hybrid ARQ is slightly differ from type I hybrid ARQ. Parity bits for error correction are sent to the receiver only when they are needed. A parity bits puncturing scheme is needed. Note that type II hybrid ARQ forms the basis for incremental redundancy (IR), since parity bits are only sent on demand.

Chase combining, as suggested by Chase in [16], is the application of code combining to hybrid ARQ schemes. Packets in error that must be retransmitted are not discarded as in conventional ARQ schemes, but are combined with their repeated copies in an optimum manner to yield a higher throughput.

Application of Chase combining on type II hybrid ARQ requires a special channel coding scheme: a coding scheme in which successful decoding of codewords can be done on any number of parity bits. Punctured convolutional coding [41] and quasi-complementary turbo code (QCTC) [21] are examples of them. QCTC is being proposed in the L3NQS proposal.

Note that an uplink handshaking channel is required for hybrid ARQ to work. For the case of successful decoding of codewords by the receiver, the receiver will send an ACK signal to the base station through an uplink handshaking channel. On the other hand, for the case of unsuccessful decoding, the receiver will send a NAK signal. In addition, a timeout period has to be defined in order to prevent the base station to wait indefinitely for lost ACK/NAK signals.

It has been shown in GPRS-136 system simulation [53] that incremental redundancy provides an approximately 11 percent higher throughput than fixed rate coding.

Similar to AMC, the goal of IR and hybrid ARQ schemes is to utilize a higher portion of channel capacity. In addition, both IR and hybrid ARQ schemes do not affect a user's SNR. As a result, by using the capacity expression, an indepth analysis of IR and ARQ schemes are not required.

3.3.3   Multiple Access Scheme

There are significant changes in the design of the forward traffic channel of high-data rate extensions of cdma2000, when compared to the design of forward traffic channel of second generation systems. The most noticeable change is the design of multiple access scheme.

In second generation CDMA systems, i.e. IS-95, the traffic for each user, after vocoding, channel encoding and scrambling, are being exclusive-ORed with a row of a dimension-64 Hadamard matrix [57, p.539]. This process is known as *Walsh Covering*. It ensures that each user within a given cell or sector is orthogonal to every other user within the cell or sector, provided that each user is assigned with a different row of the Hadamard matrix or Walsh cover. Different user in a given cell or sector possess different Walsh covers are being multiplexed together, forming the complete forward traffic channel. Since voice services are meant to be handled continuously, an active user will always possess a Walsh cover. To summarize, multiuser support in second generation CDMA system is realized through the orthogonality property of Walsh covers, and hence the name *C*ode *D*ivision *M*ultiple *A*ccess.

As discussed in Section 3.1, data services differ fundamentally from voice services, noticeably with its bursty nature and high system resource requirement for the short burst duration. In addition, data traffic is most likely to appear in the form of a packet. Since packet has a finite packet size (or packet duration), a time-division multiplexing (TDM) multiple access scheme fits perfectly in a packet based system.

Although a TDM based multiple access scheme serves packet based services adequately, wireless system designers still employ Walsh Covering as part of the forward traffic channel. There are several reasons behind this. First of all, not all packet traffic requires full system resources. It would be beneficial from utilization point of view to have a flexible structure so that the system can decide how much resources to be allocated to a user. Secondly, it is still expensive to deploy a carrier for data services only. It would be ideal for a system to be able to support both high-speed data services and legacy voice services. By employing Walsh Covering in the forward traffic channel, a very flexible system results. Figure 3.6 is a simplified block diagram of a high-speed wireless data system's forward traffic channel.

Walsh covering, originally designed to ensure orthogonality among different users in second generation systems, can be used to provide a *bandwidth on demand* platform for
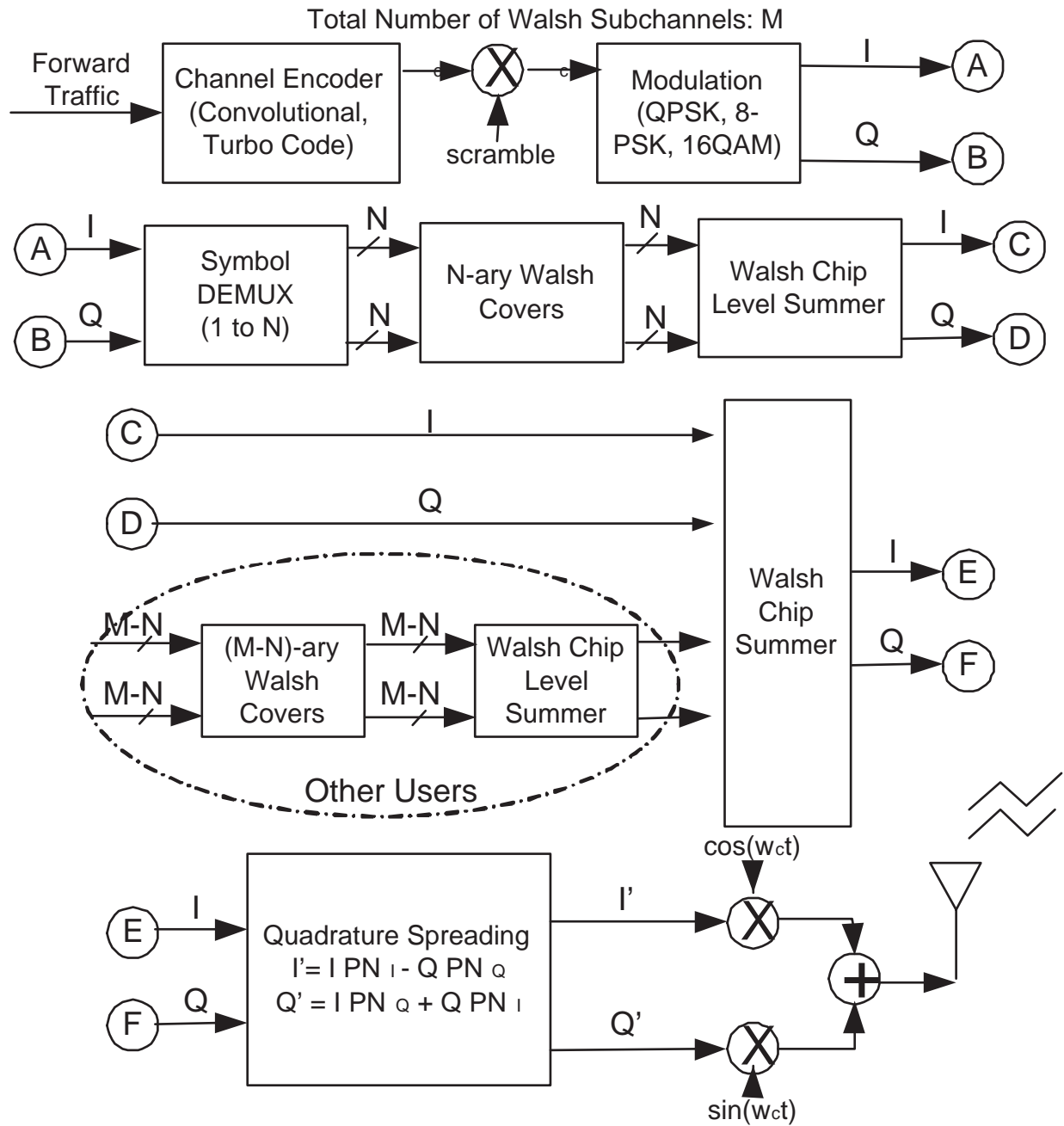
Figure 3.6: Simplified forward data channel structure of a wireless system which support high-speed data

flexible allocation of system resources among users. This is the basis of *multicode CDMA* [32]. Assume each Walsh subchannel[8] can deliver data at a certain data rate, by aggregating more than one Walsh subchannel, higher data rate results. The forward traffic shown in Figure 3.6 possesses N Walsh subchannels out of a total of M subchannels. The rest of the M-N subchannels can be assigned to different users. The number of Walsh subchannels assigned to a user can be adjusted according to the user's QoS requirement and system utilization. The action of assigning more than one Walsh code to a user is called *code aggregation*. Since the system can support various data rates, such a system is also called *multirate CDMA*.

It is worthwhile to note that voice services will most likely to be assigned with one Walsh subchannel. If a Walsh subchannel can support a data rate higher than the vocoder rate, a Walsh subchannel can be further time-multiplexed to support more than one voice user. However, this can only be realized when voice services are packetized.

There are 16 Walsh subchannels in the IS-856 standard [3, Figure 9.3.1.3.1-1], 14 Walsh subchannels in the 1XTREME proposal [52, p.2-151] and 28 Walsh subchannels in the L3NQS proposal [21, Figure 3.2.1-2].

With such an architecture depicted in Figure 3.6, the system can support both data users of various data rates and voice users at the same time. If all the Walsh subchannels are assigned to a single user, a time-division multiplexing downlink results. Such a downlink has a lot of benefits: First of all, since the base station only actively serves a user at a time, there will be no intracell interference. Secondly, since there is only one user, a lot of synchronization overhead can be saved. Thirdly, non-data signals such as pilots, control bits can be sent to the target user in advance, resulting into 100% of base station power devoted to data delivery. These benefits result into a very good signal quality and this translates to a very high data rate. This is exactly the case for IS-856's forward traffic channel. IS-856's forward traffic channel is a TDM based downlink and the base station is always transmtting at full power serving one user at a time. On the other hand, if all the codes are assigned to different users, the system can support the maximum number of simultaneously "on" users. This is ideal if all the users are of voice grades. A mixture

---

[8]Note that the concept of Walsh subchannel has nothing to do with the concept of subchannel in calculating the MEA system capacity

of data and voice users can also be supported simultaneously by carefully assigning the number of Walsh subchannels to any particular user.

To summarize, Walsh covering, originally used in IS-95 to enable multiple access, is extended in third generation systems to enable a flexible resource sharing platform. Such a platform can be tuned so that the multiple access scheme can range from a TDM fashion to a CDM fashion.

As discussed above, the level of intracell interference a user experience depends on the number of remaining Walsh subchannels not assigned to that particular user. Further discussion on this topic is left in Section 4.2.5.

3.3.4   Modulation Scheme

Second generation systems mostly use BPSK modulation[9]. However, higher order modulations are being used in third generation systems. As discussed in Section 3.2.1, multiple transmit and receive antennas realize a huge increase in achievable channel capacity, in terms of bps/Hz. Given a fixed bandwidth and a finite signalling interval, the modulation scheme should deliver an adequate number of bits per signalling interval to utilize a higher percentage of the channel capacity given by information theory. BPSK, a modulation scheme which can only deliver one bit of information per signalling interval, will not suffice in this purpose. As a result, higher order modulations such as QPSK, 8-PSK, 16QAM [3, 21] and even 64QAM [52] are being proposed.

Higher order modulations require a much higher SNR to achieve a certain BER, as discussed in Section 3.1. With the multiple access scheme described in the above section, a user's SNR can be at a very good level and this warrants the use of higher order modulations.

The goal of using higher order modulation is to achieve a higher percentage of channel capacity. It does not affect a user's SNR. By using the capacity expression, the effect of different modulation schemes can be ignored.

---

[9]Note that modulation differs from spreading. Indeed, QPSK spreading is used in both second and third generation systems.

3.3.5   Handoff Scheme

Since mobile stations move from cell to cell, handoff is essential for seamless communication. Handoff can be generally categorized into two types: soft handoff and hard handoff. Hard handoff is a "break-before-make" method, where a new channel is setup after the release of the old channel. On the other hand, soft handoff is a "make-before-break" method. When the pilot signal from a new base station is stronger than a threshold value T_{ADD}, a new link to the base station is established while maintaining the existing link. When the pilot signal from either the old base station or the new base station weakens to below T_{DROP}, the bad connection is released and only a good connection is maintained after that time [43]. *Softer* handoff is a soft handoff scheme in which handoff occurs between sectors within the same cell. CDMA systems support both soft handoff and hard handoff.

Soft handoff works well in interference limited systems such as IS-95. It is because mobile users at cell boundaries will get better signal quality with proper combining techniques, thus reducing the amount of power required. On the other hand, soft handoff increases handoff traffic by using multiple channels and also increases signalling traffic, network processing, and the amount of radio equipment required at the base station.

As described in Section 3.3.3, the forward traffic channel for high-data rate extension of cdma2000 systems can vary from a TDM fashion to a CDM fashion. When the forward traffic channel is operating at a TDM fashion, soft handoff will be very costly to the whole wireless network. It is because two base stations can only serve one user at a time and this also prevents any other mobile stations handing off to the two base stations. On the other hand, since packets are being served, hard handoff can occur in between packets seamlessly. From the above observations, hard handoff fits perfectly with high-data rate extension of cdma2000 systems.

All the high-data rate extensions to cdma2000, i.e. IS-856 [3], L3NQS [21] and 1XTREME [52] use hard handoff with fast cell site selection as the handoff scheme, in contrasting to second generation CDMA system in which soft handoff is being used. Each mobile station keeps an active set of possible serving base stations based on the strength of the received pilots and it requests service from the best base station in the active set. Selection of the best base station is done very frequently, typically at a rate of the length of a frame.

Since a mobile station can only be served by one base station at any instant, the signals

transmitted by all other base stations have to be treated as interferences. This fact will be taken into account in Section 4.2.4 when the intercell interference is being discussed.

3.3.6   Power Control Scheme

In the early days of CDMA cellular systems, it was widely believed that the IS-95 uplink, with its asynchronous transmission, would be the bottleneck in system capacity. However, experience has shown that the downlink is typically the system bottleneck. In the uplink, power control for each mobile user ensures that, at the base station, each user has approximately the same signal level. However, in the downlink there are a smaller number of unequally-powered signals, not conforming well to the assumption that each signal should look like AWGN to all other signals, arriving at a particular mobile station from the neighbouring base stations. This effects, combined with the lack of sufficient channel diversity in slow fading, non-handoff scenarios, has caused lower capacities to be experienced in the downlink [60]. Third generation CDMA networks mitigates this problem by adding fast power control to the forward link.

Power control can be categorized into two categories: open loop and close loop. Close loop refers to when feedback between the mobile and base station is used to make power adjustments. Open loop refers to when a transmitter make adjustments without explicit feedback from the receiver. cdma2000 uses close loop power control in both forward and reverse directions. In addition, close loop power control can be further divided into two sub-categories: inner loop and outer loop. Outer loop power control is used to dramatically adjust thresholds used in inner loop power control. Once a threshold is established, inner loop kicks in to make fine adjustment. cdma2000 uses outer loop power control to aid the forward closed inner loop power control.

cdma2000's forward link closed inner loop power control is done as follows: After the base station has transmitted its signal, the mobile station estimates the received power and compares it with the threshold. Based on the comparison, the mobile provides feedback to the base station by sending *power control bits* on the reverse pilot channel [2, Figure 3.1.3.1.10-1]. The transmission of power control bits is done every 1.25ms or at a rate of 800Hz. Upon receiving the power control bits, the base station responds accordingly.

Adding fast power control reduces the variability of the received signal strength in slow

to moderate fading conditions. When the received signal strength is more predictable, less power is required to sustain a certain signal quality for a particular user. This in return allows more users to be served at the same time since the overall transmit power is used more efficiently. Fast power control can also reduce intercell interferences in some cases.

The effect of fast power control on the capacity is hard to measure. The adjustment of transmitter power at a rate of 800Hz will affect the target user's received signal strength. In addition, the intercell interference on the target user will also be affected by other cell's transmitter power adjustments. All these factors affect the instantaneous SNR a user experiences at any point of time. However, with the fully loaded system assumption described in Section 2.4, it is assumed that all the base stations will transmit at their maximum allowable power all the time, regardless of the power control scheme. In addition, when AMC is done frequently, the base station in most of the time is required to transmit at its full power. As a matter of fact, the effect of fast power control on the channel capacity can only be taken into account by system simulation. Capacity estimate obtained by system simulation is not the original intent of this work. As a result, the effect of fast power control is ignored.

3.3.7 Opportunistic Scheduling

Although this research focuses on the physical layer of high-speed wireless data system, without mentioning opportunistic scheduling, a capture of all the changes in design philosophy will not be complete.

In wireless networks, the channel conditions for mobile users are time-varying. Users therefore receive time-varying service quality and/or quantity. For voice users, better channel conditions may result in better audio quality. For packet data service, better channel condition can be used to provide higher data rates. Good scheduling schemes should be able to exploit the time-varying channel conditions of users to achieve higher utilization of wireless resources, resulting into higher cell / sector throughout. Scheduling scheme which takes advantage of favourable channel conditions is generalized as opportunistic scheduling.

An opportunistic scheduling scheme which is designed only to maximize the overall throughput could be very unfair among users. For example, devoting full system resources to users close to the base station may result into very high cell throughput, but is very

unfair to other users. The dilemma between maximizing system resource utilization and fairness among users motivates the development of scheduling schemes [49] which balance the two goals.

It is worthwhile to mention that the application of opportunistic scheduling is only possible when users are requesting non-realtime services such as data transfers. Opportunistic scheduling gives priority to users with favourable channel conditions and, at the same time, delays access requests from users with unfavourable channel conditions. If users with unfavourable channel conditions are requesting real-time service, he / she should still be given immediate service. This is the reason why opportunistic scheduling was not introduced in voice oriented second generation systems. In addition, opportunistic scheduling relies on the adaptive modulation and coding and channel condition feedback from the mobile station to the base station, which are not available in second generation systems.

IS-856 uses a scheduling algorithm which satisfies the *proportional fairness* property [8]. Proportional fairness property states that if another scheduling algorithm is used to increase the throughput of a specific user by x% over what the user receives under the IS-856 scheduling algorithm, the sum of all the precentage decreases suffered by the throughputs of all the other users under the new algorithm will be more than x% [42].

Since this research focuses on the physical layer aspects of a high-speed wireless data system, scheduling algorithm will not be taken into account in computing throughputs.

To conclude this section, there are numerous changes in the forward link design philosophy of third generation systems, when compared to second generation systems. They are the introduction of link adaptation, opportunistic scheduling, hybrid ARQ, incremental redundancy, multicode, higher order signal modulation, hard handoff and fast power control. Some of the changes result from the lessons learnt from second generation systems. Some of the changes are implemented in order to utilize a higher portion of channel capacity. Some of the changes result from the fact that data traffic is fundamentally different from voice traffic. Since the MEA channel capacity requires the SNR of each receiving antenna, only changes which directly affect a user's SNR will be taken into consideration.

Chapter 4

Peak / Average Data Rate, Throughput and Coverage Analyses

This section is devoted to the mathematical analysis of cellular CDMA systems that support high-speed wireless data. The goal is to find out the peak and average data rates, throughput and coverage of such a system.

As discussed in Section 1.3, peak data rate is the maximum transmission speed an individual user may experience in ideal conditions. Peak data rate is an important figure of merit for wireless network operators. It is because with the bursty nature of data traffic, the higher the peak data rate, the shorter the time is required to serve an individual user. A lot of factors can affect the peak data rate a user experiences. To name a few: the physical separation between the transmitter and receiver, the wireless channel the connection depends on, the amount of interferences the user experiences, the transmitter power can all affect the peak data rate a user can achieve. Ultimately, these factors can be aggregated into one figure: the ratio of signal power to noise power, or simply SNR.

With the SNR available, by applying the Shannon Capacity bound given in Equation (3.1), one can obtain the theoretical maximum transmission rate. For wireless system which has multiple transmit and receive antennas, one can apply the MEA system capacity lower bound given in Equation (3.19) to obtain the theoretical maximum transmission rate.

It is reasonable to equate the peak data rate with the theoretical maximum transmission rate given by the channel capacity expression. First of all, as seen in Figure 3.1, as

technology advances, a channel code which can achieve a transmission rate which is very close to the theoretical maximum transmission rate for a given bandwidth will be invented. In addition, technologies such as adaptive modulation and coding, hybrid automatic repeat request, incremental redundancy are assisting the channel coding scheme to achieve the theoretical maximum transmission rate. As a result, the channel capacity is a good value to use when one wants to find out the peak data rate a user can achieve.

Average data rate is the data rate a user can achieve on the average case. Since the MEA capacity expression is a random varying, the average data rate can be easily obtained by taking the 50 percentile of the random varying capacity.

Throughput of a cell is the total amount of data available to multiple users within a cell for a give period of time. From a physical layer point of view, cell throughput can be obtained by integrating the peak data rate distribution across the cell coverage area, scaled by the user distribution. Using the coordinate system described in Section 2.4, for a peak or average data rate value at location (x,y) $f_d(x,y)$ and a geographical user distribution pdf $f_c(x,y)$, the average cell throughput tp_{avg} can be obtained using the following equation:

$$tp_{avg} = \frac{4}{2.598R^2}\left(\int_0^{\frac{R\sqrt{3}}{2}}\int_0^{R/2} f_d(x,y)f_c(x,y)dxdy + \int_{R/2}^{R}\int_0^{\sqrt{3}(R-x)} f_d(x,y)f_c(x,y)dydx\right)$$

(4.1)

where the first set of integrals takes care of the unshaded area in Figure 4.1 and the second set of integrals takes care of the shaded area. The radius of the hexagonal cell is R. The factor 4 takes care of the fact that the integration is only over one quarter of a hexagonal cell. The throughput is averaged over a hexagonal cell with area $2.598R^2$.

Note that the throughput figure obtained by Equation (4.1) does not assume any particular scheduling algorithm. Scheduling algorithm plays an important role in the overall cell throughtput figure. For example, if the scheduler allocates more resources to users with favourable SNRs, the overall throughput figure will be higher than the figure obtained by fair scheduling. Since this study focuses on the physical layer aspects of a wireless system, the effect of scheduling algorithm on the cell throughput will be ignored. In fact, the throughtput figure obtained by Equation (4.1) can be viewed as modelling round-robin scheduling.
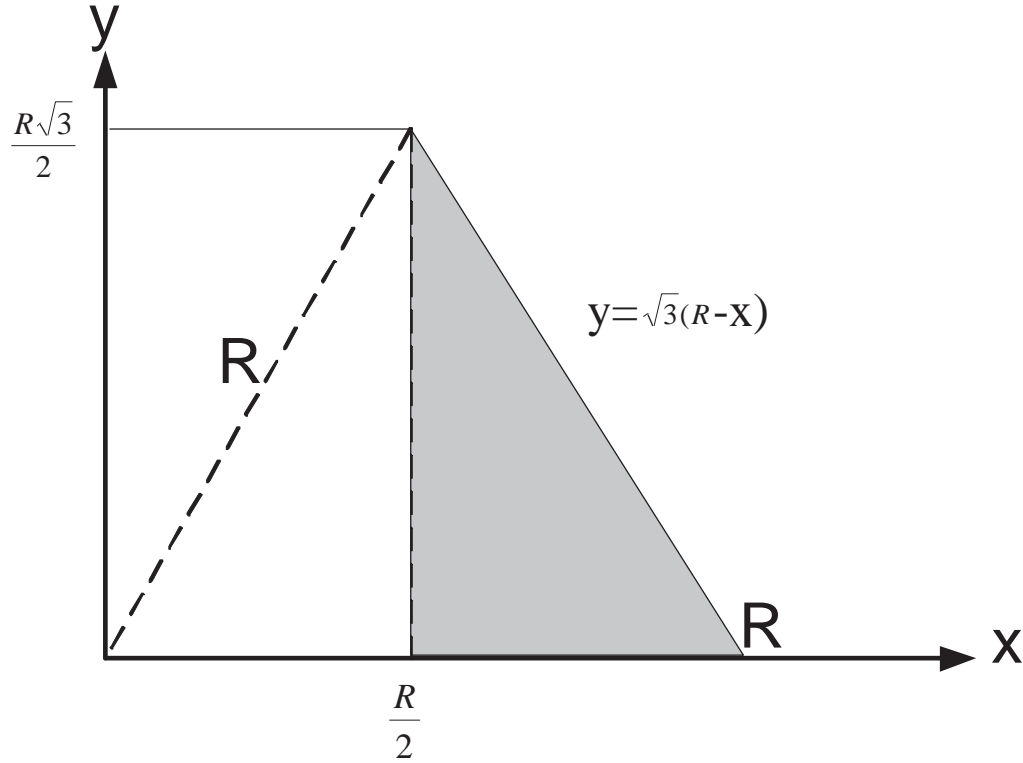
Figure 4.1: One quarter of a hexagonal cell

Geographical user distribution plays an important role in the overall cell throughput. Since user distribution can vary from time to time and from cell to cell, a general user distribution pdf, which allows one to fine tune the distribution from a centre-focused distribution to an edge-focused distribution should be used. Equation (4.2) described such a pdf [47]:

$$f_c(x, y) = \beta \frac{exp(-\beta[x^2 + y^2])}{\pi[1 - exp(-\beta R^2)]} \tag{4.2}$$

where β is the distribution index with range $-\infty < \beta < \infty$; (x,y) are the coordinates with ranges $-R \leq (x, y) \leq R$. Equation (4.2) is a rotationally-symmetrical two-dimensional pdf describing user location distribution across a circular cell coverage area.

By varying the distribution index β, an optimistic cell throughput to an pessimistic cell throughput can be obtained. A centre-focused user distribution, obtained when β is positive, will generate an optimistic cell throughput value. It is because the data rate when users are located near the cell centre is higher than users located at cell boundaries. Similarly, an edge-focused user distribution, obtained when β is negative, will generate a pessimistic cell throughput value. When β equals 0, an uniform distribution results.

Cell throughput is another important figure of merit for wireless engineers. As throughput increases, each cell site can handle higher volumes of data traffic. Such a network requires less equipment and fewer cell sites, resulting into reduction of operational expenses and capital investments.

Coverage is the area in which a certain grade of service is guaranteed. A cell is said to be covered when a pre-defined minimal grade of service is guaranteed throughout the whole cell, especially area which is close to cell boundaries. Wireless network operators want their cells to be fully covered always. In addition, wireless network operators may also want to find out the percentage of area in which a certain grade of service can be provided. The coverage map is of great use here. Using the average data rate is more appropriate in evaluating coverage than using the peak data rate.

To be able to apply the MEA system capacity formula, the SNR of each receiving antenna is needed. The SNR of each receiving antenna can be found by taking into account the percentage of total power captured by the receive antenna, the physical separation between the base station and mobile station, fading, transmitter power, intracell interference, ambient noise, intercell interference, interpath interference, interchip interference and the receiver's antenna structure. More discussion on these will be followed.

In general, there are two ways to calculate the SNR for any communication system. The first method uses a timed expression of the signal and noise components. The SNR is then expressed as a fraction with numerator equals to the square of the signal component and denominator equals to the variance of noise components [58, p.240]. The second method computes the SNR from a pure power perspective. The SNR is expressed as a fraction with numerator equals to the average power received by the user and denominator equals to the sum of average interference power experienced by the user [58, p.845].

This is no guideline on which method should be used: both methods will produce

the required SNR value. This research will use the second method. There are several reasons behind this decision. First of all, the first method requires the variance of noise components. In most cases, considerably amount of mathematical manipulation is required to find the variance of a timed signal expression. Secondly, initial papers on CDMA system capacity, such as paper written by Gilhousen and et.al [28, Section VI] computes the SNR of a forward link user from a power perspective. It would be beneficial for this work to follow an approach which is simple and proven. As a result, the SNR of each antenna will be computed from a power perspective. The remainder of this chapter is devoted to the discussion on how to compute the downlink signal energy received by the user and interference energy experienced by the user.

4.1   Receiver Structure and Combining Strategy

As discussed in Section 3.2.1, the receiver structure plays an important role in the calculation of the SNR. In addition to the receiver structure, the combining strategy can also affect the output SNR of the receiver. This section is devoted to the discussion of these two factors.

The RAKE receiver is the most commonly used receiver structure in CDMA systems. A RAKE receiver attempts to collect time-shifted versions of the original transmitted signals by providing a separate correlation receiver for each of the multipath signals. Figure 4.2 shows an M-finger RAKE receiver.

A RAKE receiver utilizes multiple correlators to separately detect the M strongest multipath components. The outputs of each correlator are weighted to provide a better estimate of the transmitted signal than is provided by a single component. In Figure 4.2, $\beta_n, n = 1 \ldots M$, are the weights assigned to each of the finger. The strategy which assigns weights to the fingers is called combining strategy. Demodulation and bit decisions are then based on the weighted outputs of the M correlators.

There are several combining strategies available, namely selective diversity combining, maximal ratio combining (MRC), and equal gain combining. Maximal ratio combining assigns weights to each of the finger by its corresponding channel gain. By doing this, a stronger signal carries a larger weight than a weak signal. Maximal ratio combining is
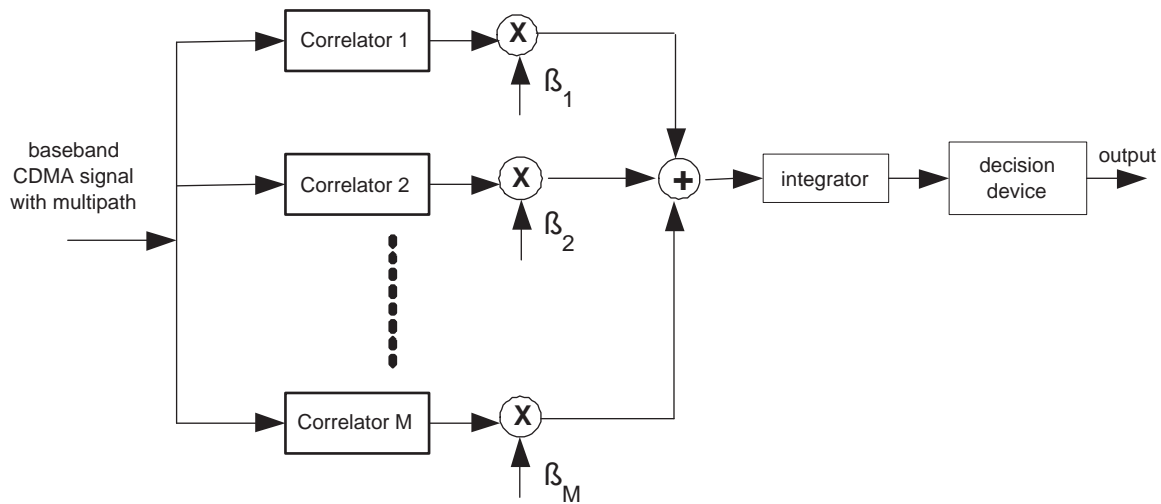
Figure 4.2: An M-finger RAKE receiver

proven to achieve the highest SNR at the receiver at all times [59, p.328]. By means of that, RAKE receiver employing MRC will be assumed to be the receiver structure in this analysis.

It is proven that for a RAKE receiver which employs maximal ratio combining, the average SNR at the output of the receiver structure is simply equal to the sum of the individual average SNR from each finger of the receiver [59, p.328]. Next section is devoted to the discussion on how to calculate the SNR of each finger.

For systems which deploy multiple receive antennas, it is assumed that each of the receive antenna will have its own RAKE receiver employing MRC. By means of that, each receiver will have its own output SNR and the output SNR of each of the receive antenna will be used in Equation (3.21) or (3.22) to compute the channel capacity lower bound.

4.2   Downlink Signal Power to Noise Power Ratio (SNR)

With the system model described in Section 2.4, there are several interference sources which can be readily identified. In this research, the following interference sources will be considered: intercell interference, intracell interference, interchip interference (ICI),

interpath interference (IPI) and ambient noise. Before the discussion on how to capture all the interferences and the desired signal mathematically, it is necessary to discuss the effect of multicode CDMA and code aggregation on signal and noise power.

4.2.1   Multicode CDMA

As discussed in Section 3.3.3, multicode CDMA provides a bandwidth on demand platform for flexible resources allocation to different users within a cell. By aggregation more Walsh subchannels to a user, he/she will get more system resources and a higher data rate. On the other hand, the level of intracell interference a user experiences depends on the number of remaining Walsh subchannels not assigned to that particular user. For a multi-user power limited wireless communication systems, allocating more Walsh subchannels to a user is equivalent to allocating more power to that particular user [5, Section III-B]. Assume the total transmitted power is S_T and there are M Walsh subchannels available, each of the Walsh subchannel will therefore deliver a power of $\frac{S_T}{M}$. This is based on the assumption that the transmitter power is distributed equally among all the identical Walsh subchannels.

Without considering all the propagation and fading effects, a user who possesses N out of M Walsh subchannels will be allocated a total power of $N\frac{S_T}{M}$. The remaining power $\frac{(M-N)S_T}{M}$ will become interference to that particular user.

The primary purpose of multicode CDMA is to create orthogonal subchannels so that data can be delivered to the intended user in parallel, resulting into an overall increase in the data rate achievable by the user. If the user is allocated with N multicode subchannels, it should be viewed as having N separate and independent subchannels for data delivery. Each of the subchannel still has a power of $\frac{S_T}{M}$. The overall data rate is N times the data rate of each of the subchannel with power $\frac{S_T}{M}$. In other words, although the user is allocated with a total power of $N\frac{S_T}{M}$, it should be viewed as having N subchannels. Each of the subchannel has a power of $\frac{S_T}{M}$. The way to capture the above observations is to calculate the capacity of each of the multicode subchannel. The overall capacity with N multicode subchannels is simply N times the capacity of an individual subchannel because the channel characteristics of the multicode subchannels are equivalent. The above observations will be taken into account when numerical results are presented in Section 5.

It is assumed that a user who possesses more than one Walsh subchannel will not incur

self interference. Self interference occurs when the Walsh subchannels assigned to a user are not orthogonal to each other. Since the user's Walsh subchannels are created from the same codebook and they are delivered through the same physical medium, they are orthogonal to each other by default. As a result, there will not be any self interference. On the other hand, self interference can also be eliminated by a technique called *subcode concatenation* [32, Section 2]. Subcode concatenation ensures orthogonality among subchannels by exclusive-ORing the subchannel covers with a codebook with orthogonal entries.

Since all the subchannels of a cell are created from the same codebook, one may question why subchannels assigned to a user do not incur self interference and subchannels assigned to other users incur intracell interference to the intended user. The difference between the two cases is the physical medium used. In the former case, the subchannels are using the same physical medium with the same propagation characteristics. In the latter case, the propagation characteristics of the channels for the two users are different. Orthogonality cannot be enforced. More discussion on how to characterize intracell interference will be discussed later.

4.2.2   Signal Power

To compute the received signal power at any location within a cell, the total path loss equation $L_n^t(t)$ described in Equation (2.22) can be used. Since the effect of Rayleigh fading has been taken care by the MEA system capacity given in Equation (3.21), the components left in the total path loss equation is the mean path loss $10^{\frac{-L_{50}(r_o,f)}{10}}$ and log-normal fading $10^{\frac{-\xi_1}{10}}$. It will be explained later the reason why the notation ξ_1 is used instead of ξ. Section 2.3.1 describes the mean path loss equations which are applicable to indoor, outdoor to indoor pedestrian and vehicular test environments. Note that the mean path loss Equations (2.23) - (2.25) are all functions of distance r_o and frequency f. Therefore, the notation $L_{50}(r_o, f)$ is introduced. r_o is given in Equation (2.29). Also note that the total path loss equation is independent of time due to the quasi-static assumption, i.e. $L_n^t(t) \equiv L_n^t$.

Assume the transmitter power is S_T and a total of M Walsh subchannels, a user located at a distance r_o from the base station operating at a frequency f will received a signal power

equals to:

$$S'_T = \frac{S_T 10^{\frac{-L_{50}(r_o,f)}{10}} 10^{\frac{-\xi_1}{10}}}{M} \qquad (4.3)$$

where $L_{50}(r_o, f)$ are given in Equations (2.23) - (2.25).

Note that S'_T in Equation (4.3) is a random variable due to the log-normal fading term. Since the rest of the expression is constant for a given carrier frequency, distance and number of Walsh subchannels, the user's signal power can be obtained by multiplying the constant terms with a random number generated according to the log-normal distribution described in Equation (2.27). A statistical average can then be taken on the set of random numbers generated in this manner as the average signal power.

Since the output SNR of a RAKE receiver is the sum of SNR on each of the RAKE finger, a power weight can be introduced to Equation (4.3) to describe the signal power received on a particular RAKE finger. The power weights of all the fingers are given in the channel profile of the operating environment. Let the power weight of the i-th RAKE finger be p_i, the power received on the i-th RAKE finger is therefore:

$$S''_T = \frac{p_i S_T 10^{\frac{-L_{50}(r_o,f)}{10}} 10^{\frac{-\xi_1}{10}}}{M}. \qquad (4.4)$$

4.2.3 Interpath Interference (IPI)

Baseband waveshaping filtering, also referred to as chip pulse shaping, has significant impact on interpath interference (IPI) and interchip interference (ICI). Before IPI power is mathematically captured in this section, it is worthwhile to devote sometime to discuss chip pulse shaping.

IS-95, cdma2000 and all high data rate extensions of cdma2000 use baseband waveshaping filters designed to meet a bandwidth constraint while minimizing intersymbol interference or interchip interference. It is beyond the scope of this research to discuss how to design such a filter. However, a figure of merit which has impact on IPI is the total duration of the waveshaping filter's impulse response. With a chip rate of 1.2288Mcps, a IS-95 waveshaping filter is time-limited to a duration of $12T_c$ [46, p.60], where T_c is the chip duration $813ns$.

With the IS-95 waveshaping filter, assuming the l-th RAKE finger is placed at time τ_l and the i-th multipath appears at time τ_p, if $|\tau_l - \tau_p| < 6T_c{}^1$, then the l-th RAKE finger will capture power from the i-th multipath. Otherwise, the i-th multipath will not contribute any signal power to the RAKE finger and the power delivered through that multipath will become interference. This type of interference is generalized as interpath interference (IPI) [38, Section III].

A quick inspection of the channel profiles shown in Tables 2.4 - 2.6 reveals that the time separation between different multipaths, in most of the cases, is smaller than $6T_c$. This leads to an interesting result: a RAKE finger, with its power capture window which spans across 12 chip durations, will receive power from more than one multipath. Signals from the unintended multipaths will spill into the power capture window of the intended multipath. Although the unintended multipaths are delivering the same information bits as the intended multipath, the power delivered through these unintended multipaths is treated as interferences. There are several reasons behind this decision. First of all, channel estimation done by the receive antenna is only for the intended multipath. With the uncorrelated scattering assumption, the channel estimate for the intended multipath will most likely not useful for other multipaths. Secondly, SNR maximizing receiver, such as the matched filter receiver, relies on accurate channel estimation. With inaccurate channel estimates, the contribution of signal power from the unintended multipaths will be little. Thirdly, most of the power of an IS-95 pulse can be found from $-T_c$ to T_c [46, Figure 1.50]. There are negligible power from the unintended multipaths which is spilled to the power capture window of the intended multipath anyway. As a result, power delivered through these unintended multipaths will be wholly treated as interference to the intended multipath. This will accomplish a worst case analysis.

Since the power weight of the i-th multipath is p_i, with Equation (2.18), the sum of IPI power which appears on the i-th multipath will therefore has a weight of $1 - p_i$. With the transmitter power S_T and a total of M Walsh subchannels, a user located at a distance r_o from the base station operating at a frequency f will received an IPI power equals to:

$$\mathcal{I}_{IPI} = \frac{(1 - p_i)S_T 10^{\frac{-L_{50}(r_o, f)}{10}} 10^{\frac{-\xi_1}{10}}}{M}. \tag{4.5}$$

---

[1]The waveshaping filter impulse response spans from $-6T_c + \tau_p$ to $6T_c + \tau_p$

4.2.4   Intercell Interference

One of the distinctive features of cellular CDMA system is universal frequency reuse. All the cells within the coverage area are operating at the same carrier frequency. As a result, technically all the neighbouring cells will introduce interference to the target user. This type of interference is generalized as intercell interference.

According to the system model described in Section 2.4, only two-tier of neighbouring cells will be taken into account for intercell interference. Since the power transmitted by neighbouring cells is not intended for the target user, it will be considered as interference completely. The interference power the target user experiences is the sum of transmitter power of the two-tier of neighbouring cells. Log-normal fading is ignored in this case for simplicity reason. If log-normal fading was taken into account, the sum of 18 log-normal random variables is required and [14] describes the procedure of obtaining such sum. Equation (4.6) describes intercell interference mathematically:

$$\mathcal{J}_{inter} = \sum_{n=1}^{18} S_T 10^{\frac{-L_{50}(r(x,y|n),f)}{10}} \tag{4.6}$$

where $r(x,y|n)$ is the distance between the n-th interfering base station and the target user and it is given in Equation (2.30); (x,y) is the target user's coordinates; f is the operating frequency; S_T is the neighbouring cells transmitter power and $L_{50}(r,f)$ is the one of the mean path loss equations described in Section 2.3.1. Note that there are 18 neighbouring cells in the two-tier system model and the system model assumes all the cells are transmitting at the same power level.

4.2.5   Intracell Interference

Another distinctive feature of cellular CDMA system is that users do not need to be assigned with specific time slot or frequency slot. Multiuser support is accomplished through the use of Walsh subchannels. Each Walsh subchannel is designed to be orthogonal to each others. In the ideal case in which the propagation characteristics of wireless channels used by different users are the same, there will be no intracell interference. It is because interference will be completely eliminated by orthogonal Walsh covers.

In reality, users request services at different time. If the time between services is greater than the channel coherence time T_{coh}, the users will experience different propagation characteristics on their wireless channels. By means of that, the Walsh covers will no longer be orthogonal to each others and users will experience interferences from their neighbours. This type of interference is generalized as intracell interference.

With the fully loaded assumption described in Section 2.4, if the target user is assigned with N Walsh subchannels out of a total of M subchannels, the rest of the $(M - N)$ Walsh subchannels will be assigned to other users. With a total transmitted power of S_T and an operating frequency of f, a user who is located at r_o from the base station will experience a intracell interference power of:

$$\mathcal{J}_{intra} = \frac{\zeta(M - N)S_T 10^{\frac{-L_{50}(r_o,f)}{10}} 10^{\frac{-\xi_2}{10}}}{M}. \tag{4.7}$$

Note that a different log-normal random variable term ξ_2 is used in Equation (4.7). It is because the wireless channel used by intracell interferers are different than the one used by the target user. A new realization of the random variable is needed.

In some literatures [17, 75], an orthogonal factor $\zeta, 0 \leq \zeta \leq 1$, is introduced in the intracell interference expression. This factor is used to capture the fact that Walsh coverings, in some cases, may be orthogonal to each other. For example, for LOS communication with no multipath, an orthogonal factor of zero can be used. For a worst case analysis, an orthogonal factor equals to 1 can be used. This research will adopt a worst case analysis, i.e., an orthogonal factor of 1 will be used.

4.2.6   Interchip Interference (ICI)

As shown in Figure 3.6, signals on the forward link will go through a quadrature spreading block. The quadrature spreading block will apply a pseudo random spreading sequence to the incoming signal, as well as a waveshaping pulse designed to meet a bandwidth constrain and minimize interference to other signals[2]. In some cases described below, the receiver's current chip window will unintentionally capture power from the previous chips and future

---

[2]the waveshaping pulse is not shown in Figure 3.6

chips. Interchip interference (ICI) refers to the power spilled from the previous chips and future chips into the current chip.

Obviously, the design of the waveshaping pulse has direct relationship with interchip interference. If the autocorrelation function of the waveshaping pulse does not satisfy the Nyquist criterion, interchip interference will occur [74]. Autocorrelation function is used here because SNR maximizing receivers such as the matched filter receiver use the same waveshaping pulse as the transmitter to derive their output statistics. The other scenario in which ICI will occur is the receiver's imperfectness of the incoming paths tracking.

First, the autocorrelation function of the chip waveforms is required. Let $g(t)$ be the time domain representation of the chip waveform satisfying $\int_{-\infty}^{\infty} |g(t)|^2 dt = 1$, the autocorrelation function of the chip waveform $\hat{g}(t)$ is as follow:

$$\hat{g}(t) \equiv g(t) * g^*(-t) \equiv \int_{-\infty}^{\infty} g(t+\tau)g(\tau)d\tau \tag{4.8}$$

where $*$ is the convolution operator and * is the complex conjugate operator.

It is interesting to note that $\hat{g}(0) = 1$. Since any autocorrelation function is maximum at its origin, $\hat{g}(t) \leq 1$.

Considering only the waveshaping pulse and neglecting any propagation effect, if the receiver perfectly tracks the incoming path, the average power of the receiver's output equals to $|\hat{g}(0)|^2$ [27].

Consider the case where the autocorrelation function of the waveshaping pulse does not satisfy the Nyquist criterion, the user will receive an interference power $\mathcal{J}_{ICI_1}$ described by:

$$\mathcal{J}_{ICI_1} = S_T'' \sum_{l=-\infty, l\neq 0}^{\infty} |\hat{g}(lT_c)|^2 \tag{4.9}$$

where S_T'' is given in Equation (4.4).

Consider the case where there is a difference of τ_o between the time the receiver places its receiving finger and the time the incoming multipath appears, the interference power $\mathcal{J}_{ICI_2}$ can be described by:

$$\mathcal{J}_{ICI_2} = S_T''(1 - |\hat{g}(\tau_o)|^2) \tag{4.10}$$

and a factor of $|\hat{g}(\tau_o)|^2$ has to be introduced to Equation (4.4) in order to correctly reflect the fact that the receiver receives less signal power than the perfect tracking case.

For the case where the waveshaping pulse does not satisfy Nyquist criterion and there exists incoming paths tracking errors, Equation (4.9) becomes:

$$\mathcal{J}'_{ICI_1} = S''_T \sum_{l=-\infty, l\neq 0}^{\infty} |\hat{g}(lT_c + \tau_o)|^2. \tag{4.11}$$

The total ICI power the user receives in this case is the sum of $\mathcal{J}'_{ICI_1}$ and $\mathcal{J}_{ICI_2}$.

The tracking error τ_o can be described as a random variable which is uniformly distributed from $[0, T_c]$. The average ICI power in the presence of tracking errors is therefore:

$$\mathcal{J}_{ICI_{avg}} = E[\mathcal{J}'_{ICI_1}|\tau_o] + E[\mathcal{J}_{ICI_2}|\tau_o] \tag{4.12}$$

where $E[\cdot]$ is the expectation operator.

There are several interesting things which worth to point out. First of all, in addition to tracking errors in timing, there exists tracking errors in the signal phase as well. Phase tracking errors do not have any influence on the signal and interference powers. It is because the power of any phase errors $e^{-j\theta_n}$ equals to 1. Secondly, intersymbol interference (ISI) is a special case of ICI. Similar to the definition of ICI, ISI refers to the power spilled from the previous symbols and future symbols into the current symbol interval. It is easy to picture that Equation (4.12) takes care of ISI. Thirdly, as discussed in Section 4.2.3, an IS-95 chip waveform is time-limited to $12T_c$. By means of that, the summation range of $-\infty$ to ∞ used in Equations (4.9) and (4.11) can be changed to a range of $-11T_c$ to $11T_c$.

For the calculation of data rates, coverage and throughput, this work does not intend to include ICI. It is because neglecting ICI can greatly improve the simplicity of the mathematical analyses. Secondly, for systems with large spreading factor, it is shown [45, pp. 339-342] that ICI is dwarfed in comparison to that of intracell interference. The above equations are presented for readers who strive for accuracy and for those who want to solely analyze the effect of ICI on system capacities.

4.2.7 Ambient Noise

Ambient noise is modelled as additive white Gaussian noise. It is represented by N_o and is given in Equation (2.20). This noise power will be taken into account when computing SNR in subsequent sections.

Taking into account all the interference sources, given the user is located at coordinate (x,y), which is at distance r_o from the serving base station, with N out of a total of M Walsh subchannels and operating at frequency f with transmitter power S_T, the signal power to noise power ratio of i-th RAKE finger, ρ_i, for that particular user is:

$$\rho_i = \frac{S_T''}{\mathcal{I}_{IPI} + \mathcal{J}_{inter} + \mathcal{J}_{intra} + \mathcal{J}_{ICI_{avg}} + N_o} \tag{4.13}$$

where S_T'', $\mathcal{I}_{IPI}$, $\mathcal{J}_{inter}$, $\mathcal{J}_{intra}$, $\mathcal{J}_{ICI_{avg}}$ and N_o are given in Equations (4.4), (4.5), (4.6), (4.7), (4.12) and (2.20) respectively.

Assume there are q fingers in the RAKE receiver, by summing $\rho_i, i = 1 \ldots q$, the output SNR of the antenna can be obtained. By substituting output SNRs of the receive antennas into Equation (3.21), the peak and average data rates at any location within a cell can be found. Once the peak data rate is found for any location, average cell throughput tp_{avg} can be found using Equation (4.1). Coverage of a cell can be found by observing the peak data rate distribution throughout the cell. The next chapter is devoted to the presentations of sample numerical results.

Chapter 5

Numerical Results

This chapter is devoted to the presentation of numerical results by applying the mathematical model described in Chapter 4 and simulation results available in open literatures.

5.1   Methodologies

Numerical results for the downlink is obtained through the application of MEA system lower bound described in Equation (3.21) and the SNR expression described in Equation (4.13). There are several random variables in the overall capacity expression, namely the k chi-square random variables with $2k$ degrees of freedom in Equation (3.21), the log-normal random variable ξ_1 in Equations (4.4) and (4.5), and the log-normal random variable ξ_2 in Equation (4.7). Each of the random variable is instantiated 100000 times according to its corresponding distribution. There are 100000 SNR and capacity samples for each location. The 99 percentile capacity is taken as the peak data rate and the 50 percentile capacity is taken as the average data rate. Peak and average spectral efficiency are calculated by dividing the peak or average data rate by the bandwidth respectively. A uniform user distribution is assumed, i.e. $\beta = 0$ is used in Equation (4.2). Interchip (intersymbol) interference is ignored. A noise temperature of 297K is used in Equation (2.20). System model described in Section 2.4 is used. The radius of a cell is assumed to be 5km for the vehicular and outdoor to indoor pedestrian channels while the radius of a cell is assumed to be 50m for the indoor channel. For the vehicular and outdoor to indoor pedestrian

channels, a new SNR and capacity value is computed for every 100m along the x-axis and y-axis and these two values are assumed to remain the same for the $100m \times 100m$ area. In order to accomplish a worst case analysis and be conservative, the lowest data rate within the $100m \times 100m$ area as indicated by the black dot in Figure 5.1 is used in Equation (4.1) to compute the peak and average throughputs. For the indoor channel, a new SNR and capacity value is computed for every 1m along the x-axis and y-axis and these two values are assumed to be constant for the $1m \times 1m$ area. The lowest data rate within the $1m \times 1m$ area is used. An orthogonal factor $\zeta = 1$ is used in Equation (4.7). The RAKE receiver is assumed to have 3 fingers tracking the three strongest paths from the multipath channel. Bandwidth is 1.25MHz.
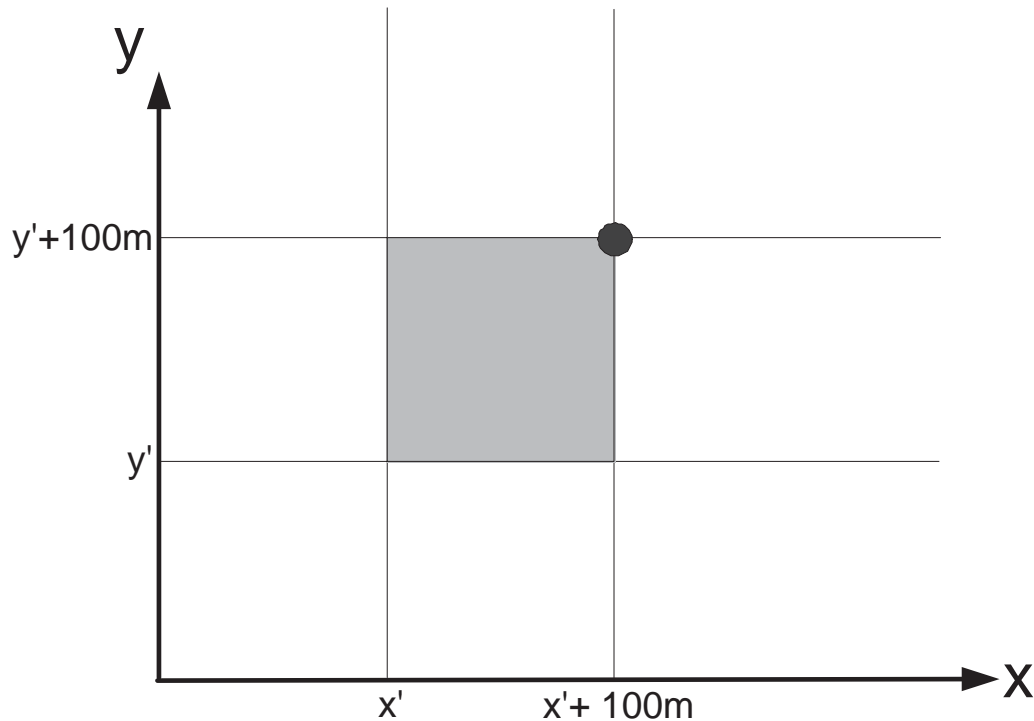

Figure 5.1: The lowest data rate of the shaded area as indicated by the black dot is used in computing throughputs

5.2   Result 1: System Supporting Data User in a TDM Fashion

The first numerical result presented here is for systems which are designed to support only data users in a TDM fashion. At any given time, the system will allocate resources to only one user. The system does so by allocating all its multicode channels to that particular user for a specific duration. Multiuser support is accomplished in a TDM fashion. Since there is only one user at a time, there is no power sharing among users and no overhead power required for synchronization. In addition, there is no intracell interference. As a result, the best possible signal quality is provided to the user. Such a system will achieve the highest peak data rate and cell throughput and provide the best coverage. This configuration is good for finding the optimal operating performance of a wireless systems optimized for data.

Vehicular Channel

For $n_t = 1$ and $n_r = 2$, Figure 5.2 is a surface plot of the 50 percentile capacity over one quarter of the hexagonal cell. Figure 5.3 is the coverage map for the same portion. Figure 5.4 shows the peak and average data rates along the x-axis for the vehicular channel. Table 5.1 summarizes several key parameters for the vehicular channel. The operating frequency is assumed to be 2GHz and the base station antenna is assumed to have a height of 15m.

Table 5.1: Downlink performance of a high-speed wireless data system supporting data user only operating under the ITU-R M.1225 vehicular channel model, $n_t = 1, n_r = 2$

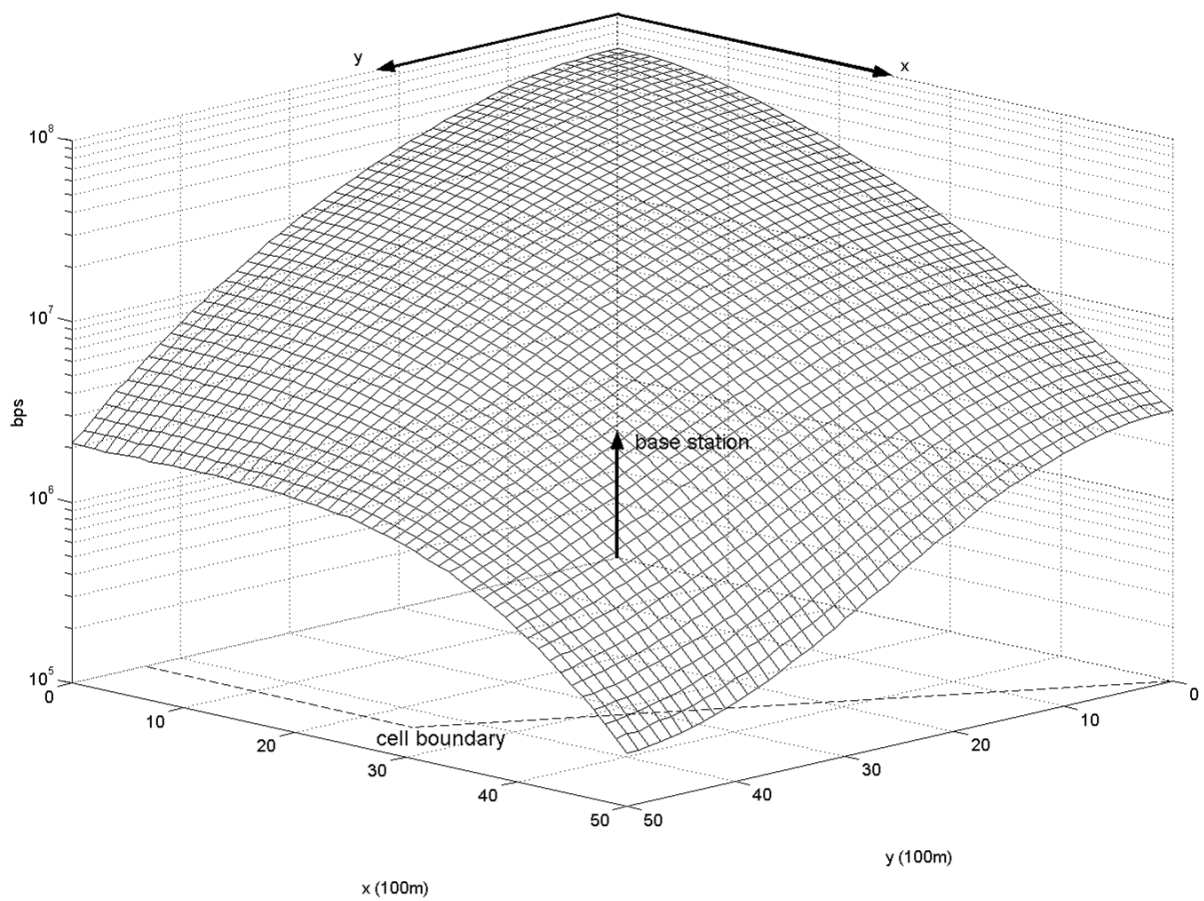| Peak data rate (Mbps)	Peak throughput (Mbps)	Average throughput (Mbps)	Peak spectral efficiency (bps/Hz)	Average spectral efficiency (bps/Hz)
128.51	74.850	20.807	35.936 - 102.808	2.2328 - 55.59

Figure 5.2: Downlink average data rate of a data user operating under ITU-R M.1225 vehicular channel model, $n_t = 1, n_r = 2$, user is assigned with M/M multicode channels
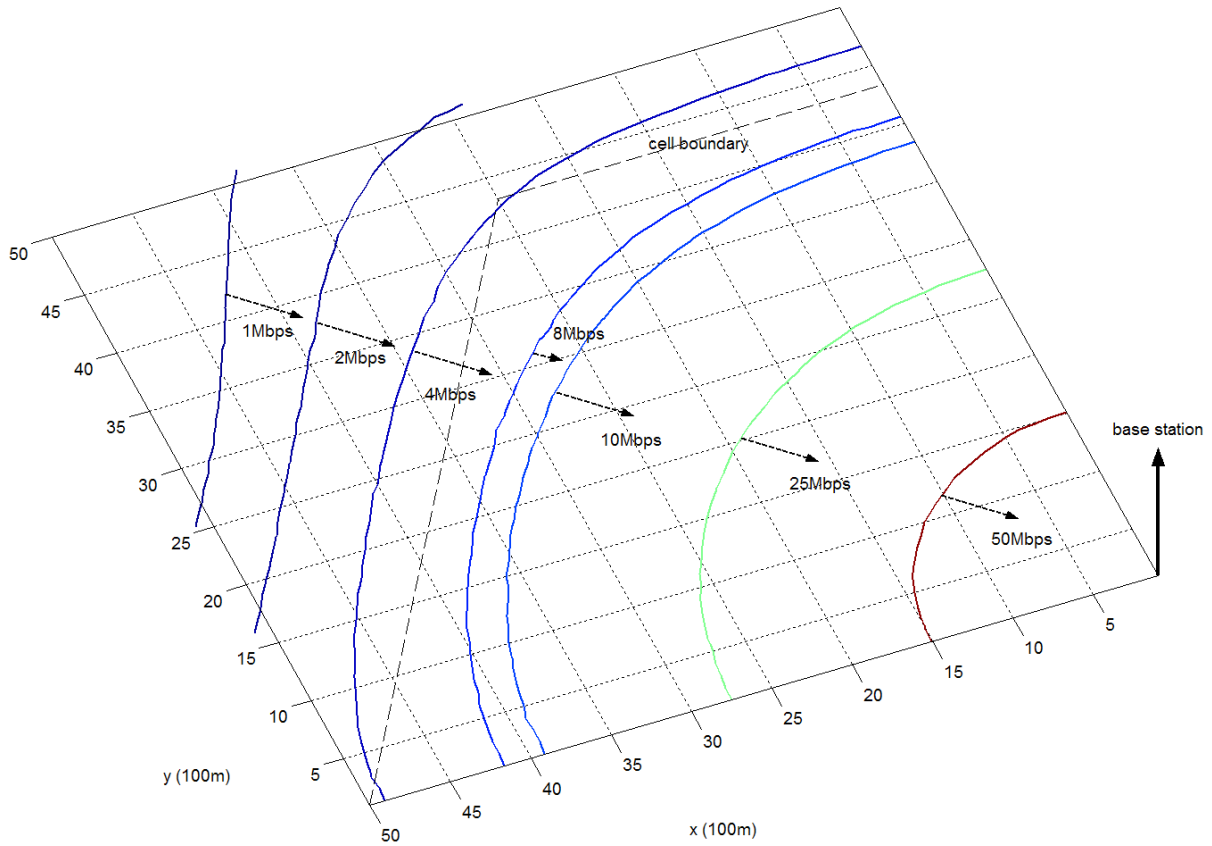
Figure 5.3: Downlink coverage map for a data user operating under ITU-R M.1225 vehicular channel model, $n_t = 1, n_r = 2$, user is assigned with M/M multicode channels
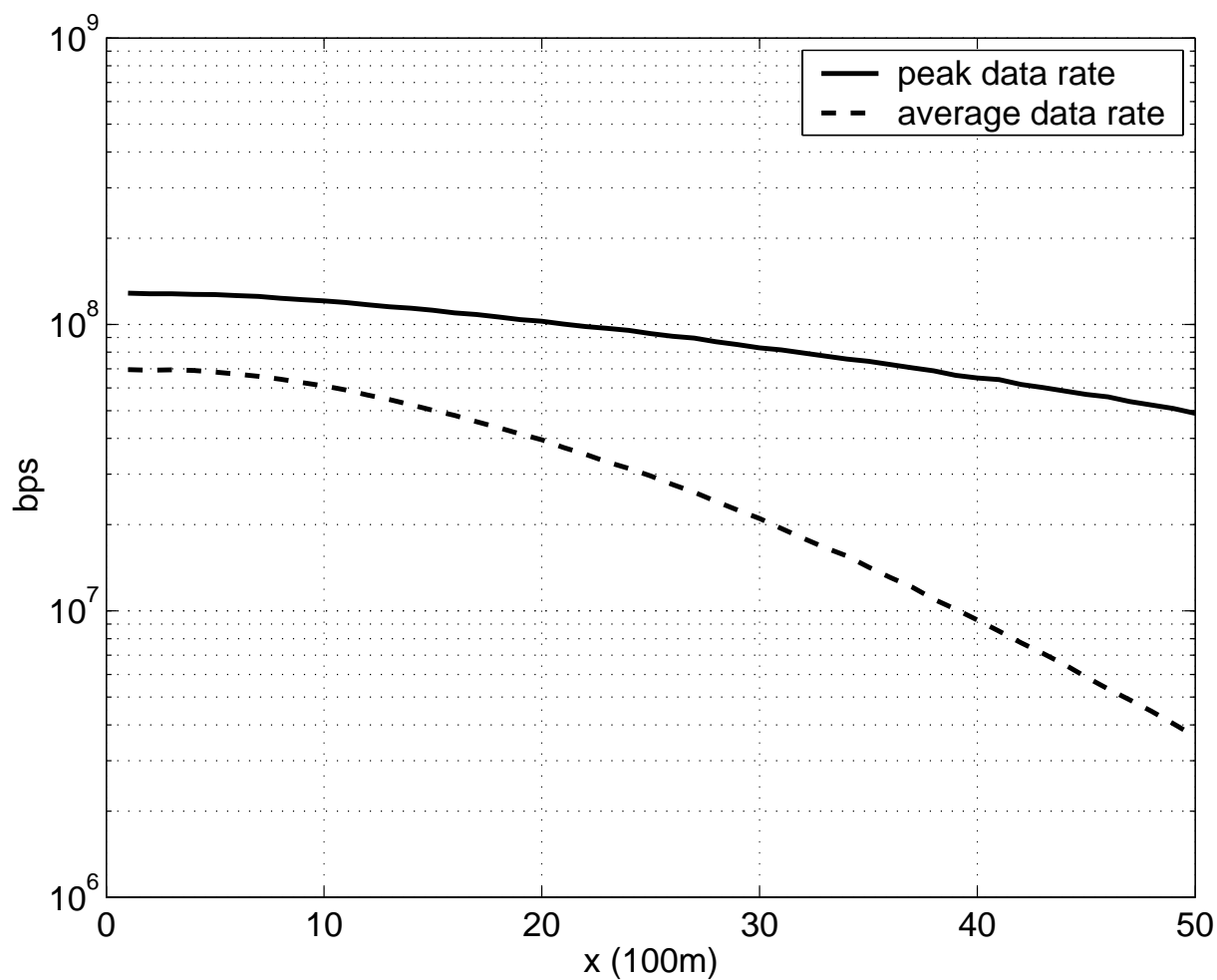
Figure 5.4: Downlink peak and average data rates of a data user operating under ITU-R M.1225 vehicular channel model along the x-axis, $n_t = 1, n_r = 2$, user is assigned with M/M multicode channels

Outdoor to Indoor and Pedestrian Channel

Figure 5.5 shows the peak and average data rates along the x-axis for the outdoor to indoor and pedestrian channel. Table 5.2 summarizes several key parameters for that channel. The operating frequency is assumed to be 2GHz.

Table 5.2: Downlink performance of a high-speed wireless data system supporting data user only operating under the ITU-R M.1225 outdoor to indoor and pedestrian channel model, $n_t = 1, n_r = 2$

Peak data rate (Mbps)	Peak throughput (Mbps)	Average throughput (Mbps)	Peak spectral efficiency (bps/Hz)	Average spectral efficiency (bps/Hz)
11.357	8.5228	2.6100	6.444 - 9.0859	0.6411 - 6.4453

Indoor Channel

Figure 5.6 shows the peak and average data rates along the x-axis for the indoor channel. Table 5.3 summarizes several key parameters for that channel. Since the operating environment is indoor, the radius of a cell is assumed to be 50m. It is also assumed that there are 2 floors in the propagation path between the transmitter and receiver.

Table 5.3: Downlink performance of a high-speed wireless data system supporting data user only operating under the ITU-R M.1225 indoor channel model, $n_t = 1, n_r = 2$

Peak data rate (Mbps)	Peak throughput (Mbps)	Average throughput (Mbps)	Peak spectral efficiency (bps/Hz)	Average spectral efficiency (bps/Hz)
125.13	83.065	17.712	55.704 - 100.108	3.8976 - 50.2908

5.2.1   Discussions

Results presented in Tables 5.1 - 5.3 may surprise some readers. The peak data rate, peak throughput and peak spectral efficiency are surprisingly good when the system is devoting
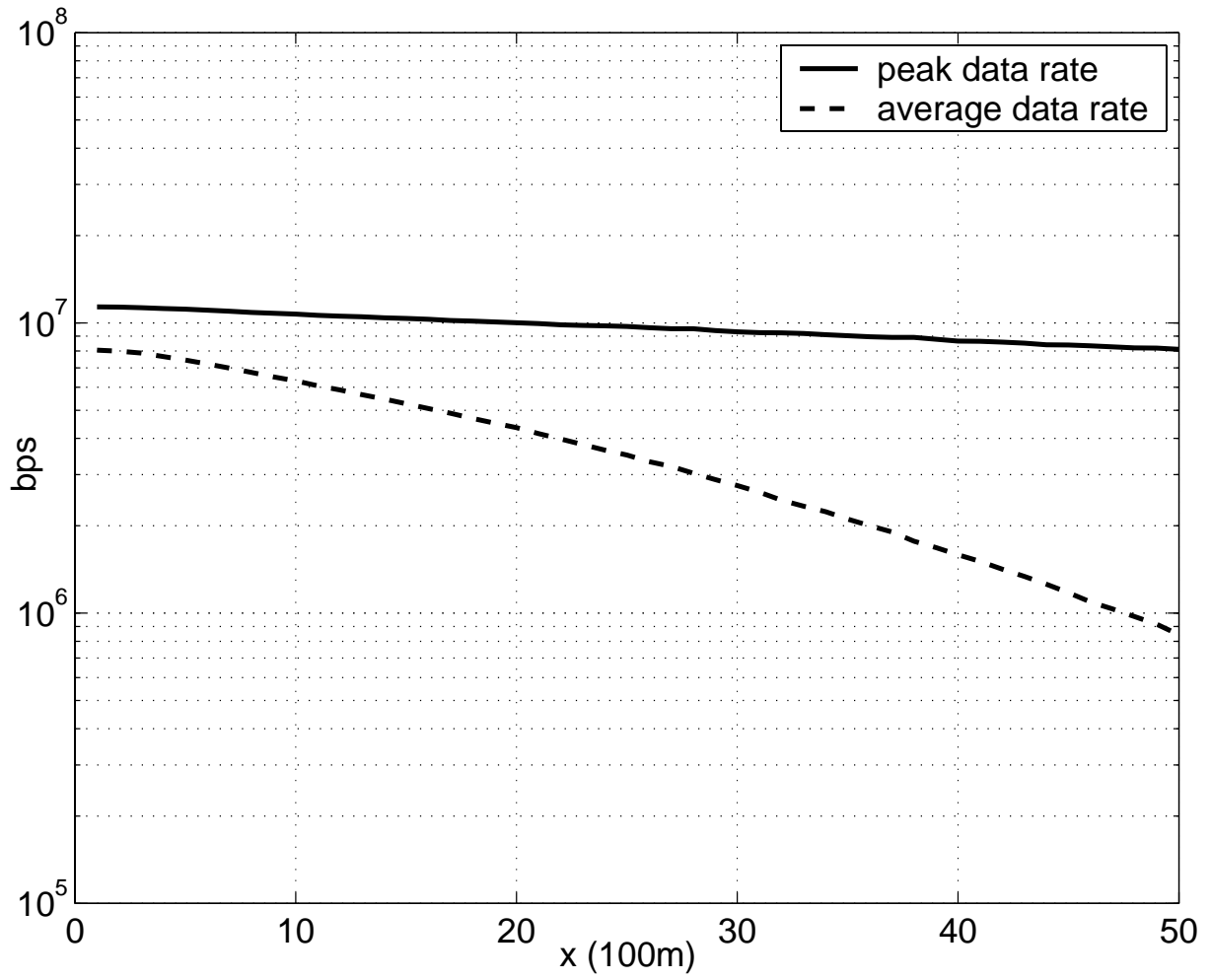
Figure 5.5: Downlink peak and average data rates of a data user operating under ITU-R M.1225 outdoor to indoor and pedestrian channel model along the x-axis, $n_t = 1, n_r = 2$, user is assigned with M/M multicode channels
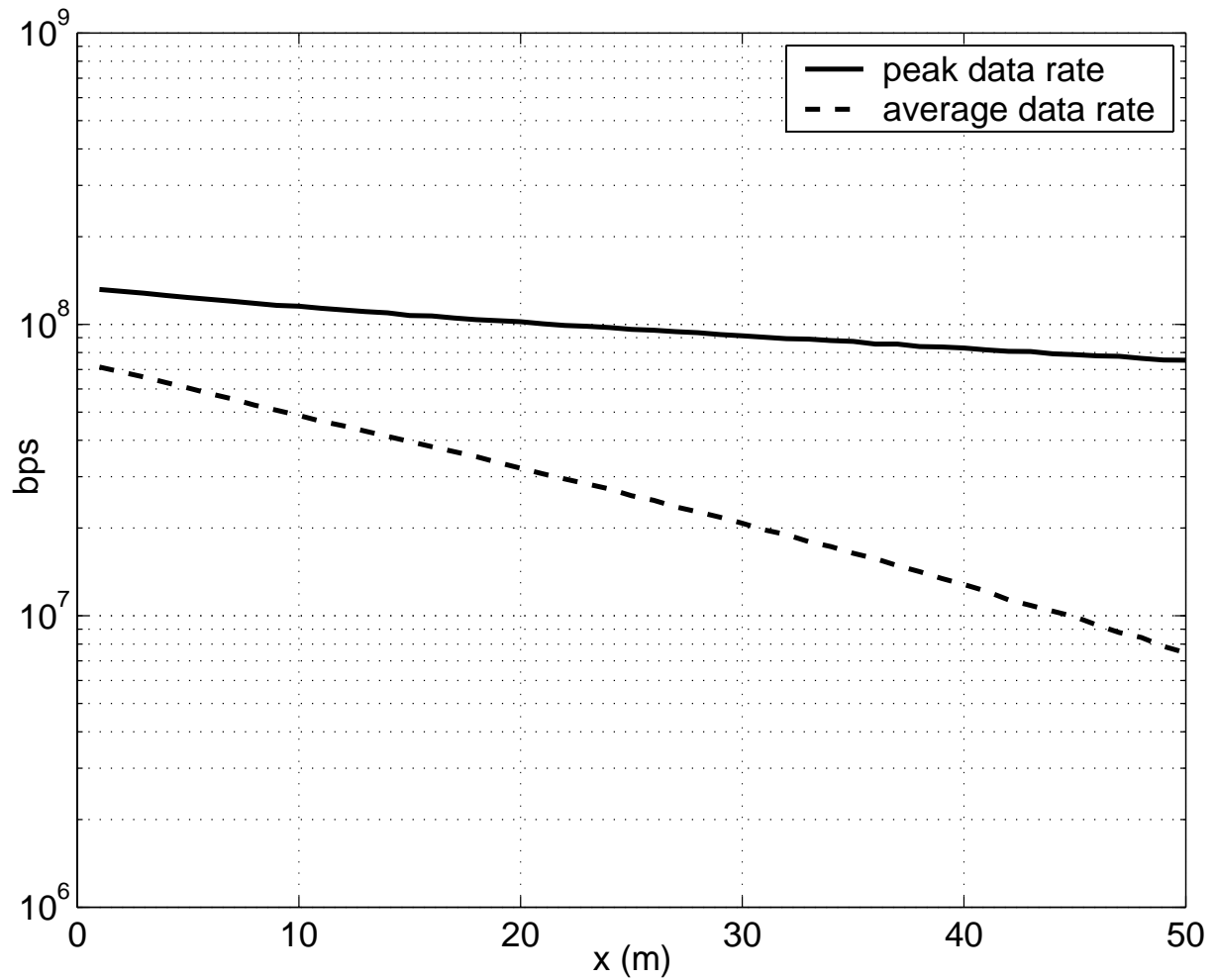
Figure 5.6: Downlink peak and average data rates of a data user operating under ITU-R M.1225 indoor channel model along the x-axis, $n_t = 1, n_r = 2$, user is assigned with M/M multicode channels

its full resources to a particular user. It should be noted that the peak values shown are theoretical maximum values. In most of the cases, these values cannot be realized in a real world system.

Since the system is devoting full system resources to only one user, the user will achieve very good SNR, especially for the case when the user is located very near to the base station. A very good SNR will deliver very good data rates, as shown in Tables 5.1 - 5.3.

Wireless system engineers should pay more attention to the average values, especially to the lower bound of the average spectral efficiency. For example, the lower bound of the average spectral efficiency for the outdoor to indoor pedestrian channel is just 0.6411bps/Hz. A 1.25MHz bandwidth can only deliver a data rate of 801.375kbps. User who requests a data rate higher than 801.375kbps cannot be guaranteed services all the time.

From Figure 5.4 - 5.6, it is interesting to note that there can be more than 10 times difference between the average data rates near the base station and the cell boundary. In other words, the data rates supported by the wireless channel drop dramatically as the user moves away from the base station.

System supporting data users in a TDM fashion is best mimicked by an IS-856 based high-speed wireless data system. In [34], an IS-856 airlink overview is presented. Table 5.4 shows several important figures extracted from that document. Note that the figures presented in Table 5.4 were obtained with 3-sector cells, which differs from the cell configuration used in this thesis. All cells are assumed not sectorized in this research.

Since [34] does not describe how the figures are obtained, it is unwise to make direct value-to-value comparisons with the results presented in this section. However, one interesting point is observed. From Table 5.1 and Table 5.2, it is shown that vehicular channel performs better than outdoor to indoor pedestrian channel. It coincides with the simulation results presented in Table 5.4 where a high-speed mobile user has a higher throughput than a low-speed mobile user.

Table 5.4: Forward link performance of an IS-856 based system (non transmit diversity) [34].

	Environment	Reported value	Receive antenna configurations
Peak throughput	not reported	7.4Mbps/cell	not reported
Average throughput	pedestrian	3.1Mbps/cell	single
Average throughput	pedestrian	4.0Mbps/cell	dual
Average throughput	low speed mobile	1.3Mbps/cell	single
Average throughput	low speed mobile	2.5Mbps/cell	dual
Average throughput	high speed mobile	2.0Mbps/cell	single
Average throughput	high speed mobile	3.1Mbps/cell	dual
Spectral efficiency	not reported	1.92bps/Hz	not reported

5.3   Result 2: System Supporting Maximum Number of Users

The second numerical result presented here is for systems which are designed to support maximum number of users. The system does so by only allocating one multicode channel to a particular user at a time. Users will suffer from intracell interference. Such configuration is aimed to support voice users and low data rate users. Numerical results obtained under such configuration is good for finding the worst case performance of a wireless systems optimized for data. Worst case performance data are important. For example, wireless operators will need to know if a user devoted with minimal resources located at the cell edge is still guaranteed with a certain grade of service.

Vehicular Channel

Let $n_t = 1$ and $n_r = 2$, Figure 5.7 is the coverage map for a voice user assigned with 1/28 multicode channel. Figure 5.8 shows the peak and average data rates along the x-axis for the vehicular channel. Table 5.5 summarizes several key parameters for the vehicular channel. The operating frequency is assumed to be 2GHz and the base station antenna is
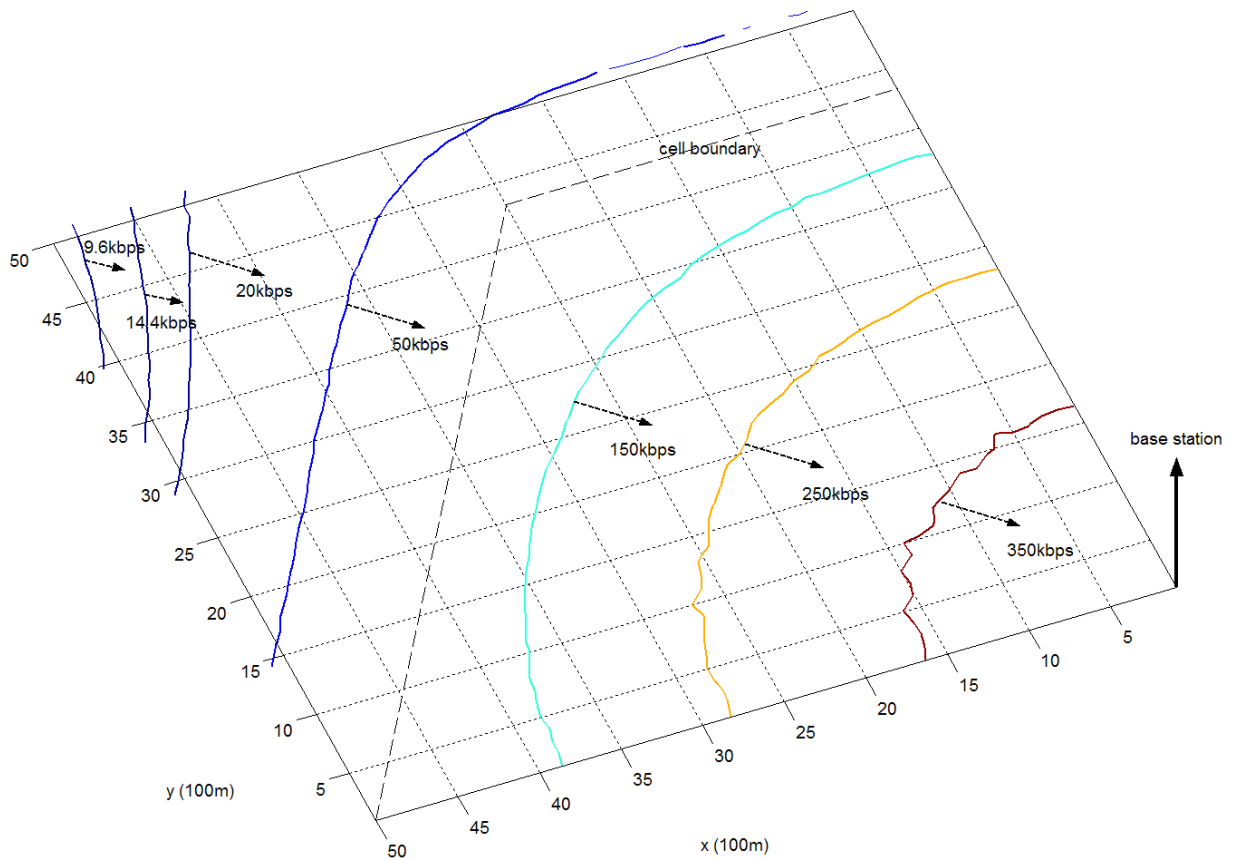
Figure 5.7: Downlink coverage map for a voice user operating under ITU-R M.1225 vehicular channel model, $n_t = 1, n_r = 2$, user is assigned with $1/28$ multicode channel

assumed to have a height of 15m.

Outdoor to Indoor and Pedestrian Channel

Figure 5.9 shows the peak and average data rates along the x-axis for the outdoor to indoor and pedestrian channel. Table 5.6 summarizes several key parameters for that channel. The operating frequency is assumed to be 2GHz.
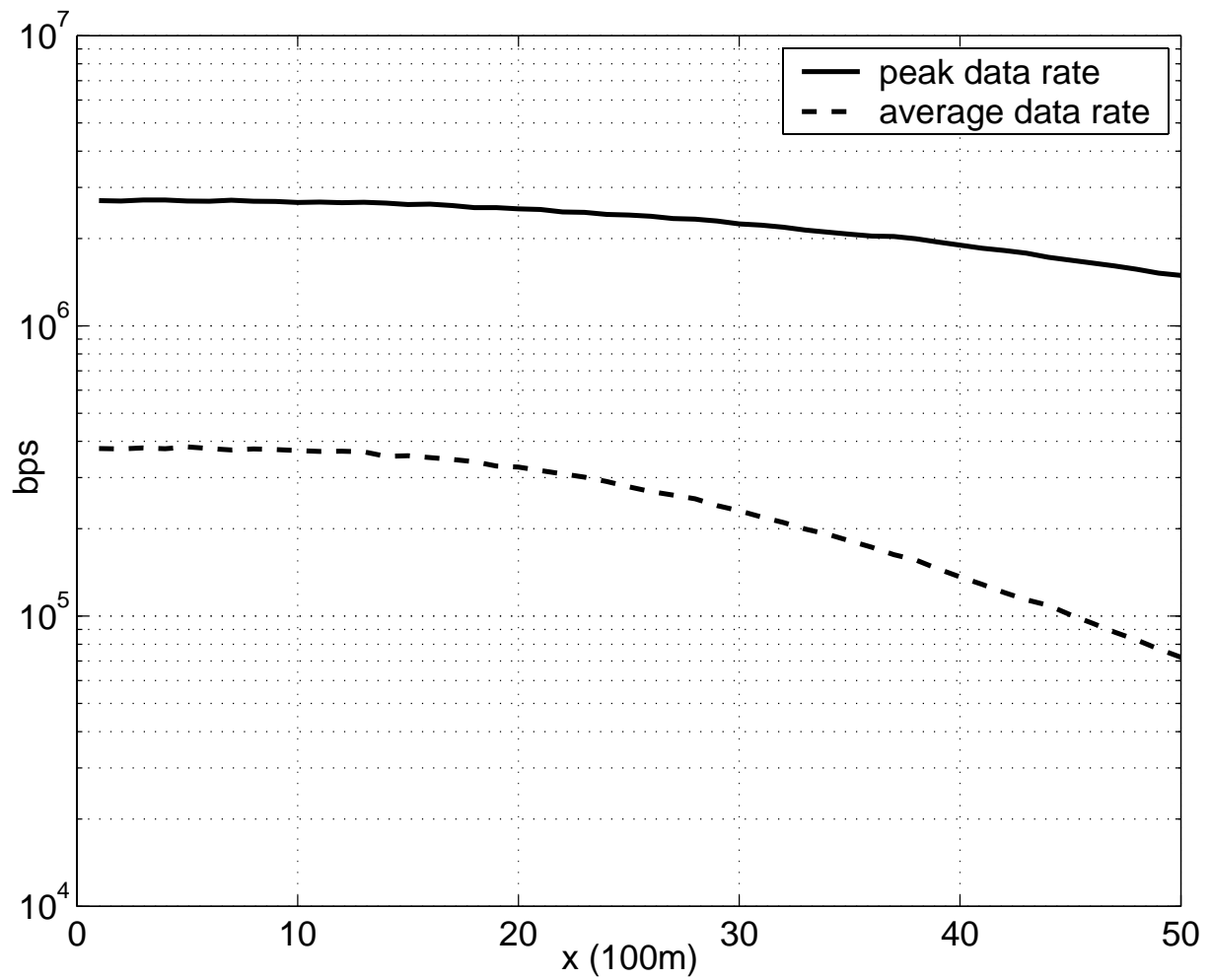
Figure 5.8: Downlink peak and average data rates of a voice user operating under ITU-R M.1225 vehicular channel model along the x-axis, $n_t = 1, n_r = 2$, user is assigned with 1/28 multicode channel
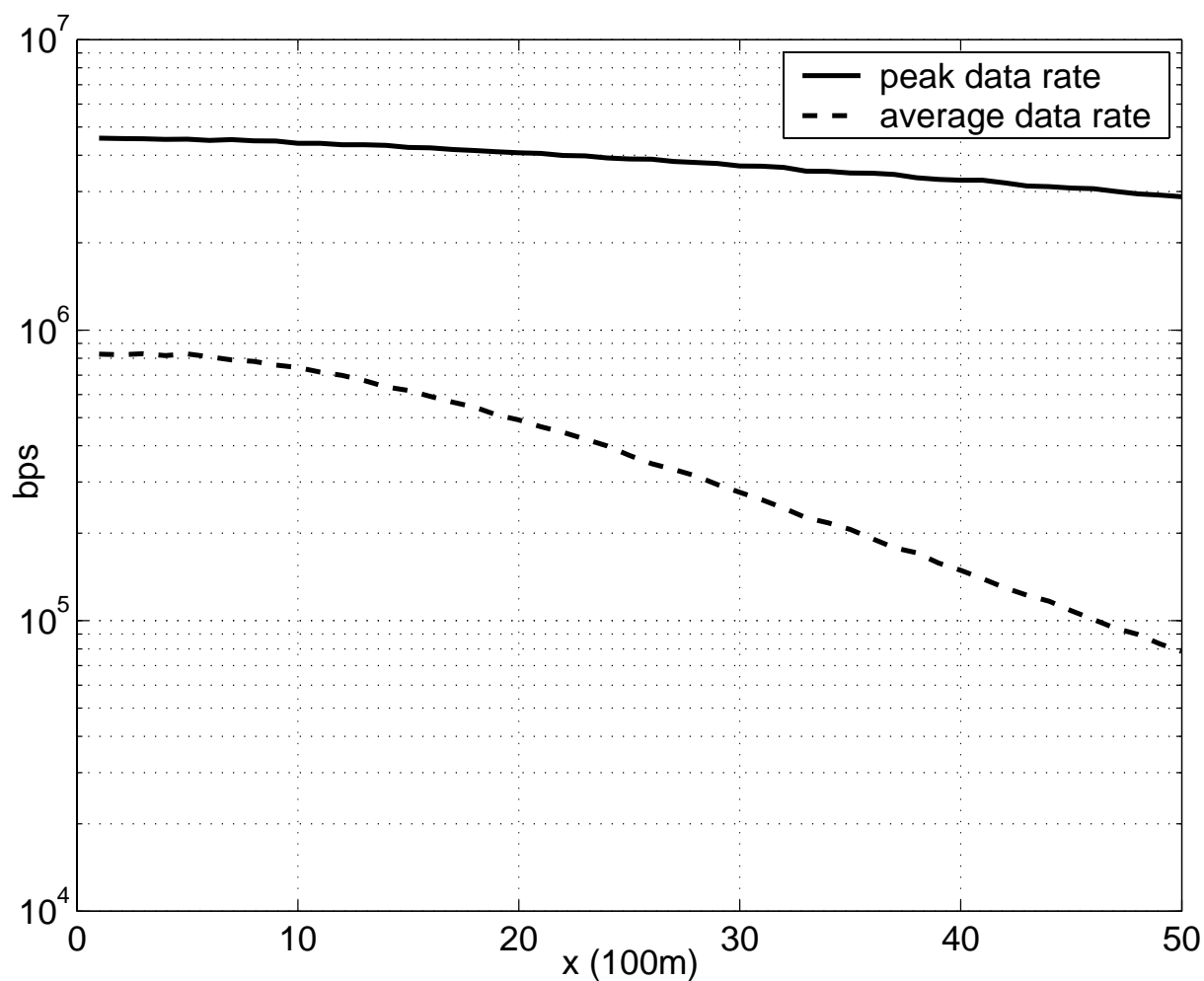
Figure 5.9: Downlink peak and average data rates of a voice user operating under ITU-R M.1225 outdoor to indoor and pedestrian channel model along the x-axis, $n_t = 1, n_r = 2$, user is assigned with 1/28 multicode channel

Table 5.5: Downlink performance of a high-speed wireless data system supporting a voice user operating under the ITU-R M.1225 vehicular channel model along the x-axis, $n_t = 1, n_r = 2$, user is assigned with 1/28 multicode channel

Peak data rate (Mbps)	User peak throughput (Mbps)	User average throughput (Mbps)	Peak spectral efficiency (bps/Hz)	Average spectral efficiency (bps/Hz)
2.7029	1.9858	0.1994	1.0960 - 2.1623	0.0471 - 0.3023

Table 5.6: Downlink performance of a high-speed wireless data system supporting a voice user only operating under the ITU-R M.1225 outdoor to indoor and pedestrian channel model, $n_t = 1, n_r = 2$, user is assigned with 1/28 multicode channel

Peak data rate (Mbps)	User peak throughput (Mbps)	User average throughput (Mbps)	Peak spectral efficiency (bps/Hz)	Average spectral efficiency (bps/Hz)
4.5789	3.3364	0.2768	2.2483 - 3.6631	0.0582 - 0.6612

Indoor Channel

Figure 5.10 shows the peak and average data rates along the x-axis for the indoor channel. Table 5.7 summarizes several key parameters for that channel. Since the operating environment is indoor, the radius of a cell is assumed to be 50m. It is also assumed that there are 2 floors in the propagation path between the transmitter and receiver.

Table 5.7: Downlink performance of a high-speed wireless data system supporting a voice user only operating under the ITU-R M.1225 indoor channel model, $n_t = 1, n_r = 2$, user is assigned with 1/28 multicode channel

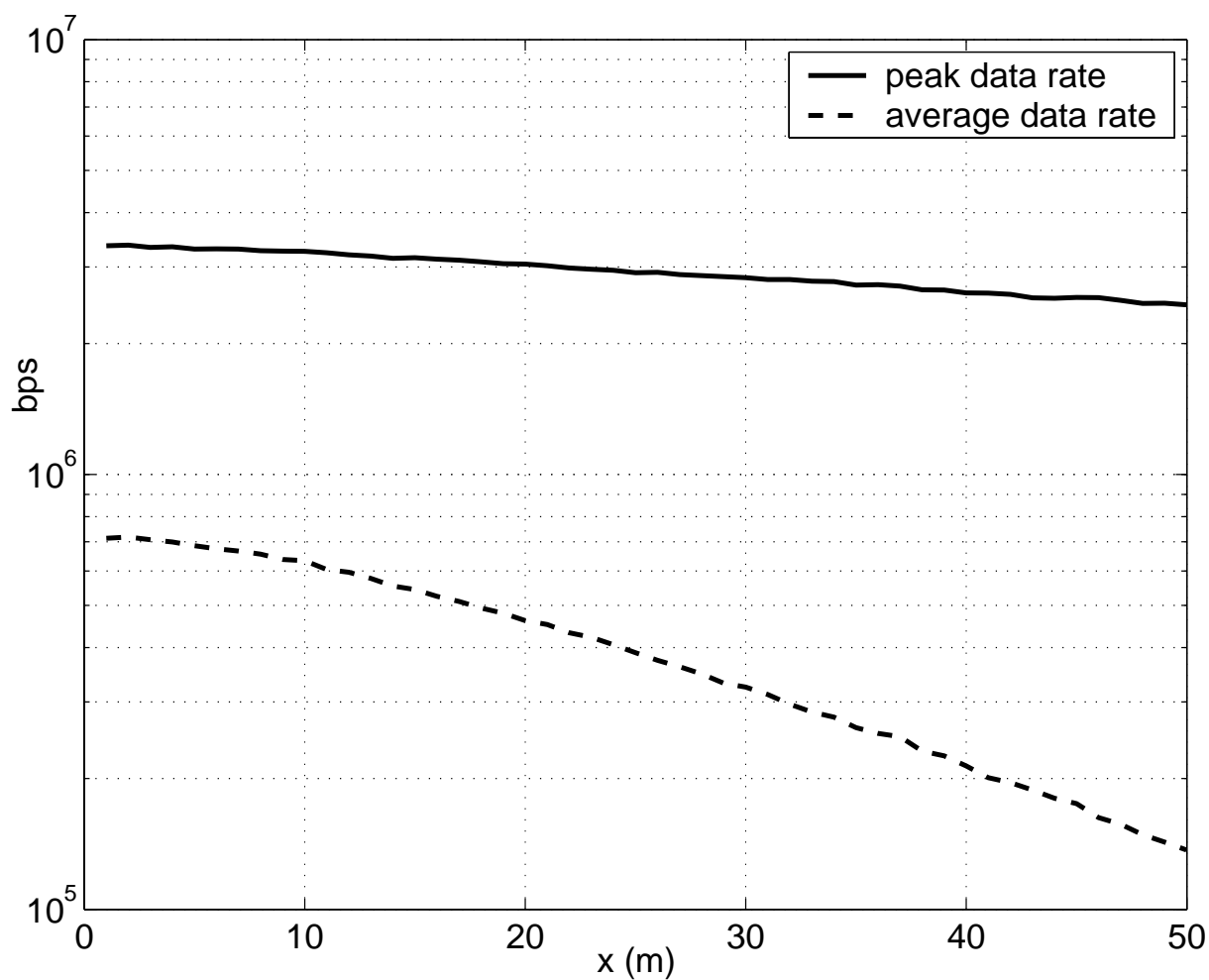| Peak data rate (Mbps)	Peak throughput (Mbps)	Average throughput (Mbps)	Peak spectral efficiency (bps/Hz)	Average spectral efficiency (bps/Hz)
3.3298	2.5858	0.2724	1.8420 - 2.6638	0.0785 - 0.5562

Figure 5.10: Downlink peak and average data rates of a voice user operating under ITU-R M.1225 indoor channel model along the x-axis, $n_t = 1, n_r = 2$, user is assigned with 1/28 multicode channel

5.3.1   Discussions

From the coverage map, it is shown that good data rates can still be delivered for users located at cell boundaries. As shown in Figure 5.8 - 5.10, different wireless channels are able to deliver an average data rate of about 70kbps to users located at cell boundaries. Since a typical vocoder has a code rate of about 9.6kbps to 14.4kbps, a multicode channel can literally support about 5 users in a TDM fashion. Since the simulation results are obtained with a total of 28 multicode channels, up to 140 voice users can be supported simultaneously under the assumed configurations.

5.4   Result 3: Multicode Allocation and its Improvement on Average Data Rate

It is an interesting topic to investigate the performance improvement as more multicodes are allocated to a particular user. Figure 5.11 shows the average data rate for a user operating under the ITU-R M.1225 vehicular channel along the x-axis with various multicode allocations out of a total of 28 multicodes.

5.4.1   Discussions

It is shown in Figure 5.11 that the more multicode channels is allocated to a user, the better the average data rate is available to the user. Doubling the number of multicodes allocated to a user will result into more than double the available average data rate. It is because doubling the number of multicodes allocated to a user does not just allow the user to receive data in parallel, it reduces intracell interferences as well. As a result, significant improvement on achievable data rates is observed. This is probably the reason why IS-856 system chose to have its forward link in a TDM fashion.
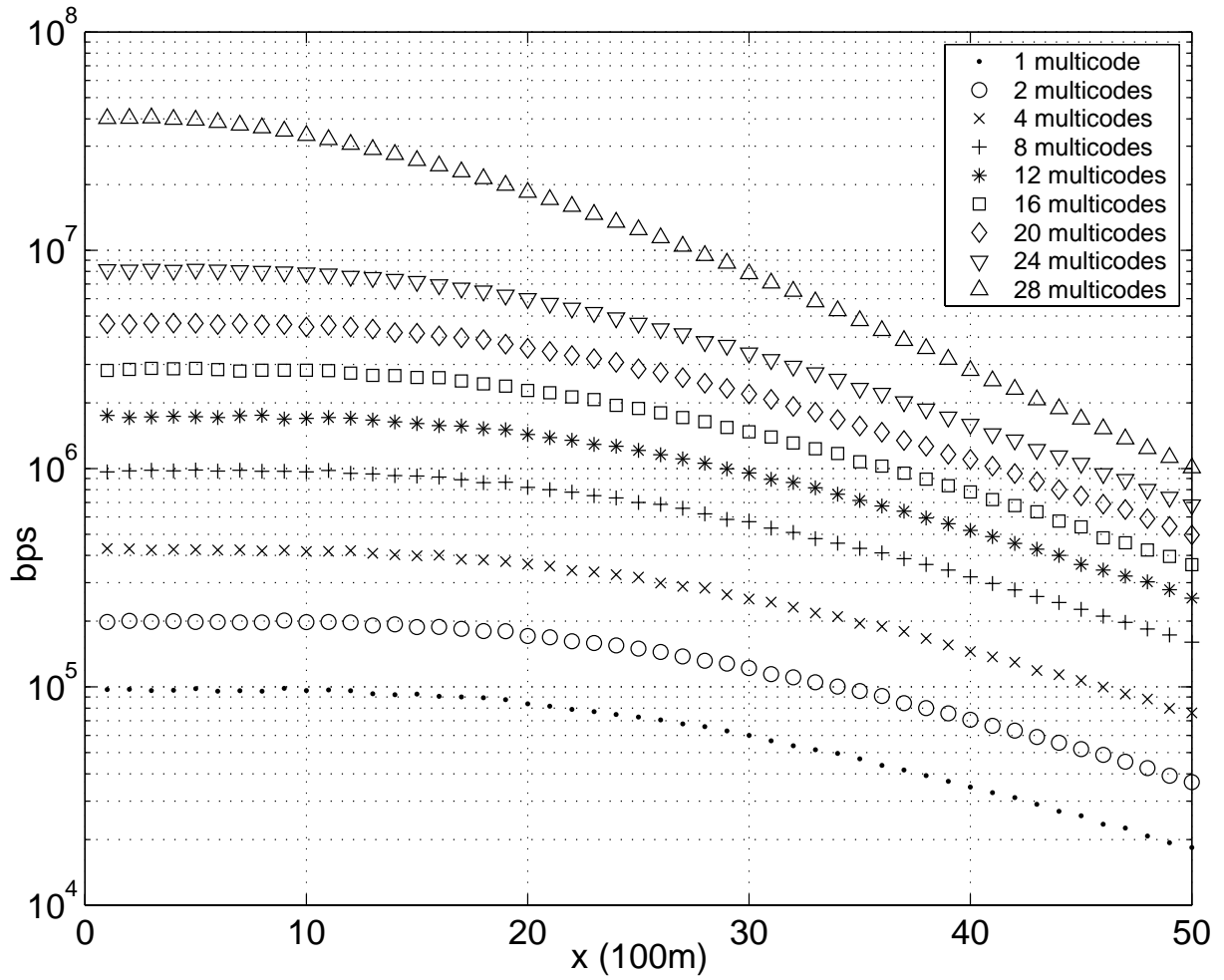
Figure 5.11: Downlink average data rate of a user with various multicode allocations out of a total of 28 multicodes operating under the ITU-R M.1225 vehicular channel along the x-axis, $n_t = 1, n_r = 1$

5.5   Result 4: System with Multiple Transmit and Receive Antennas

This section explores different transmit and receive antenna configurations and their impact on capacity. Before numerical results are presented, it is worthwhile to present results obtained in open literatures.

5.5.1   Results in Open Literatures

Before the discussion begins, few terms are needed to be defined. *M*ultiple *I*nput *M*ultiple *Output* (MIMO) system refers to the communication system in which multiple transmit and receive antennas are deployed. *M*ultiple *I*nput *S*ingle *Output* (MISO) system refers to the communication system in which multiple transmit antennas and one receive antenna are deployed. A *S*ingle *I*nput *S*ingle *O*utput (SISO) system refers to the conventional one transmit antenna and one receive antenna system.

There are two key results for a MIMO system. In [23], for a system with n transmit antennas and n receive antennas, it has been reported that the MIMO capacity grows at a rate of n bps/Hz for every 3dB of SNR increase. In addition, in [24], it has been shown that for a MIMO system with n transmit antennas and n receive antennas, the capacity grows linearly with n, assuming independent Rayleigh fading between antenna pairs, fixed total power and bandwidth. It is often referred to as the capacity scaling effect for a MIMO system. These are the two key results which drive the interest of deploying multiple antennas at the transmitter and receiver.

In addition, much of the research interests focus on the characterization of the effect of correlation between different MEA subchannels on the capacity scaling effect and the allocation of transmitter power among transmit antennas subjecting to a total power constraint. For example, it has been shown in [18] that the capacity scaling for a MIMO system with n transmit and n receive antennas is 10-20% smaller in the presence of correlated fadings when compared to the case of uncorrelated fadings. In addition, it has also been shown that the *waterfilling* algorithm for allocating transmit power among transmit antennas outperforms equal power distributions [31, 63, 18].

Few papers have investigated the MISO capacity. In [70], it has been argued that the

performance of a MISO system can be even worse than a conventional SISO system due to the fact that intracell interference and intercell interference can be enhanced by multi-antenna transmission and multipath channel. A *MISO precoder* is introduced in [70] to attack this problem. In [29], it has been argued that deploying more transmit antennas than necessary will not enhance capacity. It is due to the fact that with the total power constraint, deploying more transmitter will weaken the signal strengths. The "appropriate" number of transmitters to be used depends on the number of receive antennas and the *rank* of the wireless channel when the channel is represented in a matrix like the one shown in Equation (3.5).

Most of the results listed above were obtained by applying the generalized Shannon capacity equation shown in Equation (3.19). Several common characteristics are observed among these analyses. First of all, only one SNR value is used in the application of the capacity equation and it is assumed to be constant throughout the analysis. With the fast power control scheme described in Section 3.3.6, it is not a bad assumption since the receiver can request the transmitter to adjust its power level so that a constant SNR can be maintained. Secondly, the effect of log-normal fading and distance path loss are ignored. Only the effect of Rayleigh fading is considered. Thirdly, the analyses are done with a total power constraint. In summary, analyses available in open literatures focus on the capacity expression, the channel transfer matrix and the problem of allocating power among transmit antennas.

This research attempts to put the capacity expression described in Equation (3.19) to work in a real system context. In a real-world system, the SNR at the receiver is affected by the distance path loss, long-term and short term fadings. The system model used in this research assumes maximum allowable power is being transmitted by the transmitter always. It is a valid assumption because in a high-speed wireless system delivering data of bursty nature, transmitting maximum allowable power is of advantageous from a throughput point of view, as it is the case as in the IS-856 airlink. As a result, the SNR at the receiver will vary over time due to fadings. In addition, with the assumption that the receive antennas are placed at least half wavelength from each other or any other distance that makes them uncorrelated, each receive antenna will experience a different channel. Therefore, different SNR values will appear at different receive antennas. The numerical results presented in

this section will explore the capacities for various MIMO, MISO and SISO systems working under the system model described throughout this thesis. Comparison will be made with respect to results available in open literatures. The ITU-R M.1225 vehicular channel is used and results are presented along the x-axis. The user is assumed to possess all multicode channels.

5.5.2 Both the Transmitter and Receiver have the Same Number of Antennas (MIMO System)

This section tries to explore the capacity scaling effect when more antennas are deployed at both transmit and receive sides. It is assumed that the number of antennas at both the transmit and receive sides are equal. Let $n_t = n_r = n$, Figure 5.12 shows the 50 percentile capacity for $n, n = 1 \ldots 4$.

Observations

It is shown that the capacity does not grow linearly with n. However, the capacity does grow when more transmit and receive antennas are deployed.

5.5.3 Receive Diversity Only (SIMO System)

Figure 5.13 shows the average data rates for a receive diversity only system.

Observations

It is shown that deploying more receive antennas enhances the average data rate. Diminishing return is observed: the more receive antenna is deployed, the less gain in data rate results.

5.5.4 Transmit Diversity Only (MISO System)

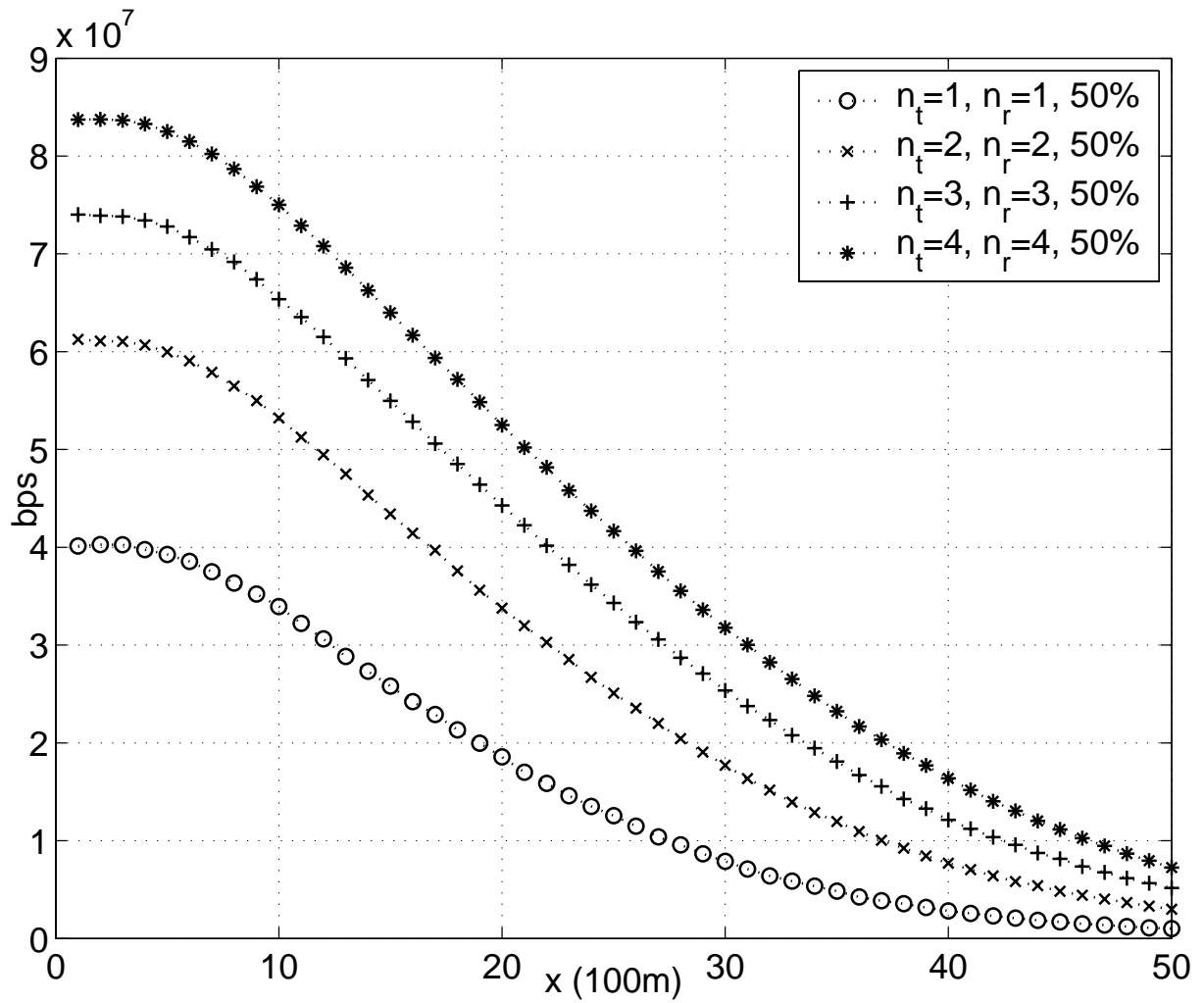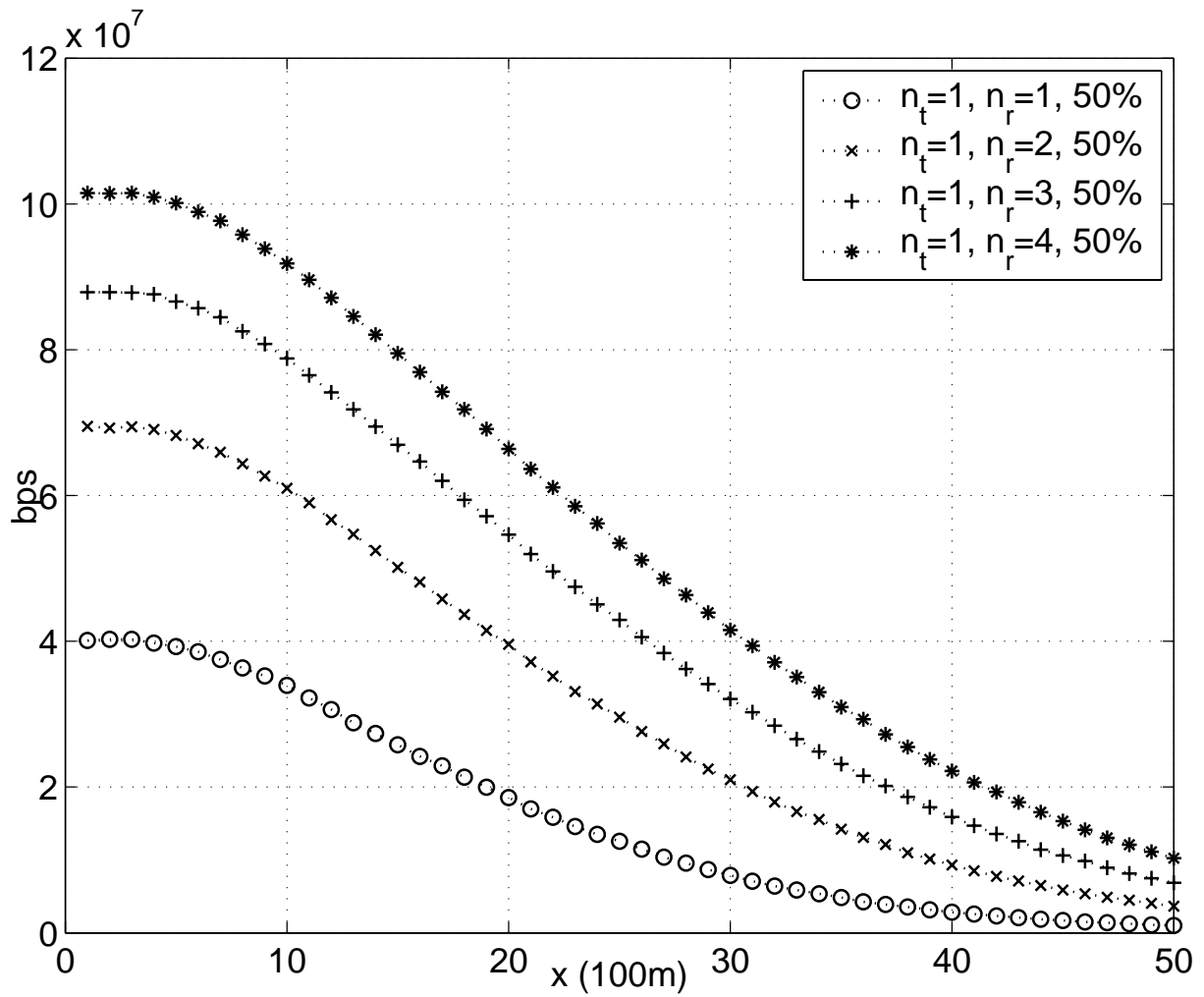Figures 5.14 shows the average data rates for a transmit diversity only system.

Figure 5.12: Downlink average data rate of a MEA system with the same number of transmit and receive antennas along the x-axis

Figure 5.13: Downlink average data rate of a receive diversity only system along the x-axis
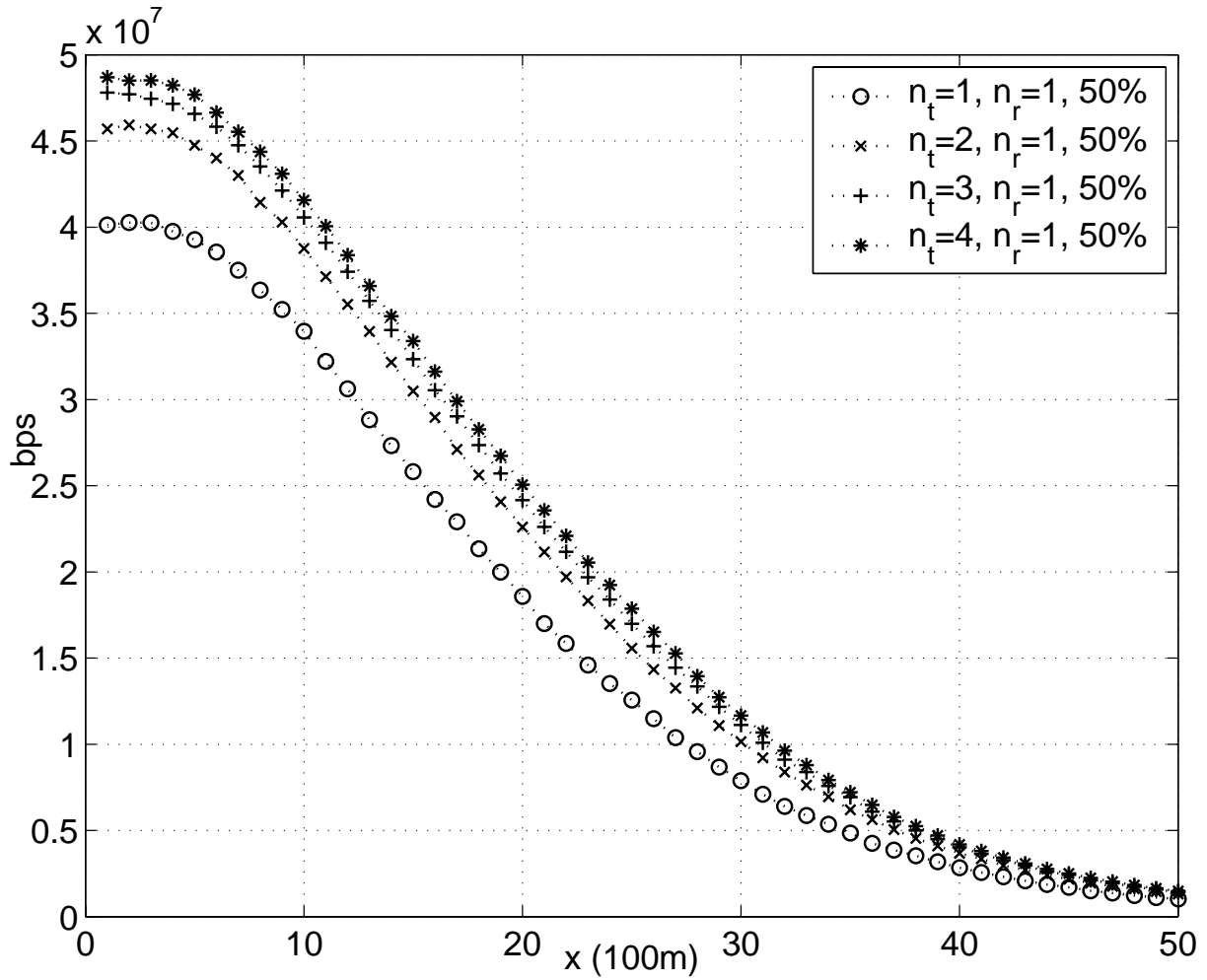
Figure 5.14: Downlink average data rate of a transmit diversity only system along the x-axis

Observations

It is shown that deploying multiple transmit antennas enhances the average data rate. However, the return of deploying multiple transmit antennas is not as good as deploying multiple receive antennas. These can be explained as follows: since it is assumed that the total power is kept constant regardless of the number of transmit antennas, MEA subchannels created by the multiple transmit antennas will have less power allocated to them, as shown by the n_t factor in Equation (3.21). Although the degree of diversity of each subchannel increases with the number of transmit antennas, since the signal quality ultimately determines the channel capacity, the overall benefit of deploying multiple transmit antennas is not as great as deploying multiple receive antennas.

5.5.5   Transmit and Receive Diversity

Figure 5.15 to Figure 5.17 show the average data rate for various transmit and receive diversity configurations.

Observations

Figure 5.15 to Figure 5.17 show that for a system which deploys receive diversity, deploying only one transmit antenna will result into the best average data rates most of the cases. This can be explained as follows: since there is already receive diversity which exploits the rich nature of a multipath channel, there is no need to deploy multiple transmit antennas. It is because with the constant total power assumption, transmit diversity will only weaken the signal quality of MEA subchannels, resulting into lower data rates. However, as discussed in Section 5.5.4, transmit diversity can still improve the average data rate for a system which does not employ receive diversity.

5.5.6   Allocation of Antennas among Transmitter and Receiver Sides

This section is devoted to the discussion on how to allocate a fixed number of antennas among transmitter and receiver sides to achieve the best data rates.
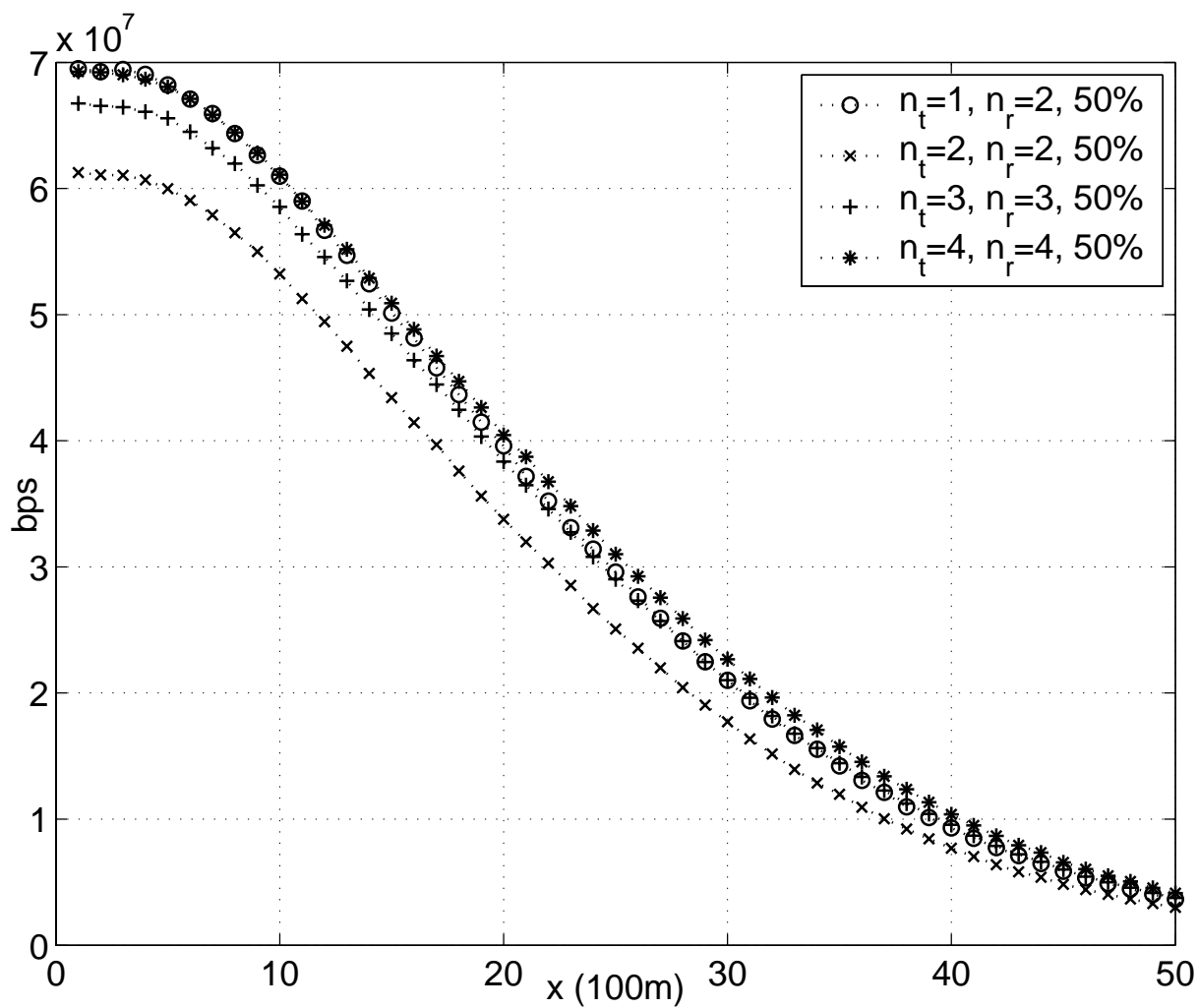
Figure 5.15: Downlink average data rate of a transmit diversity system with two receive antenna diversity along the x-axis
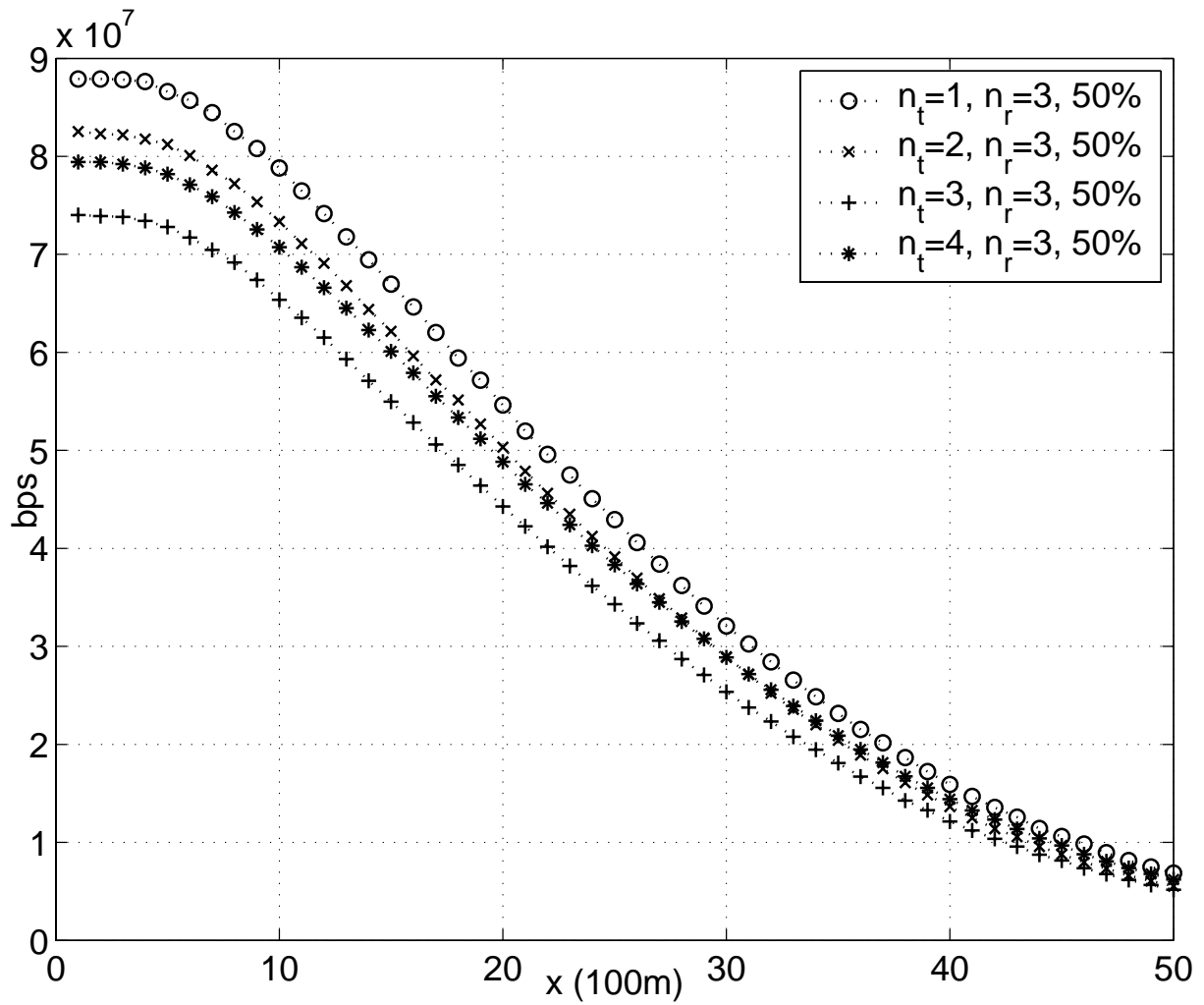
Figure 5.16: Downlink average data rate of a transmit diversity system with three receive antenna diversity along the x-axis
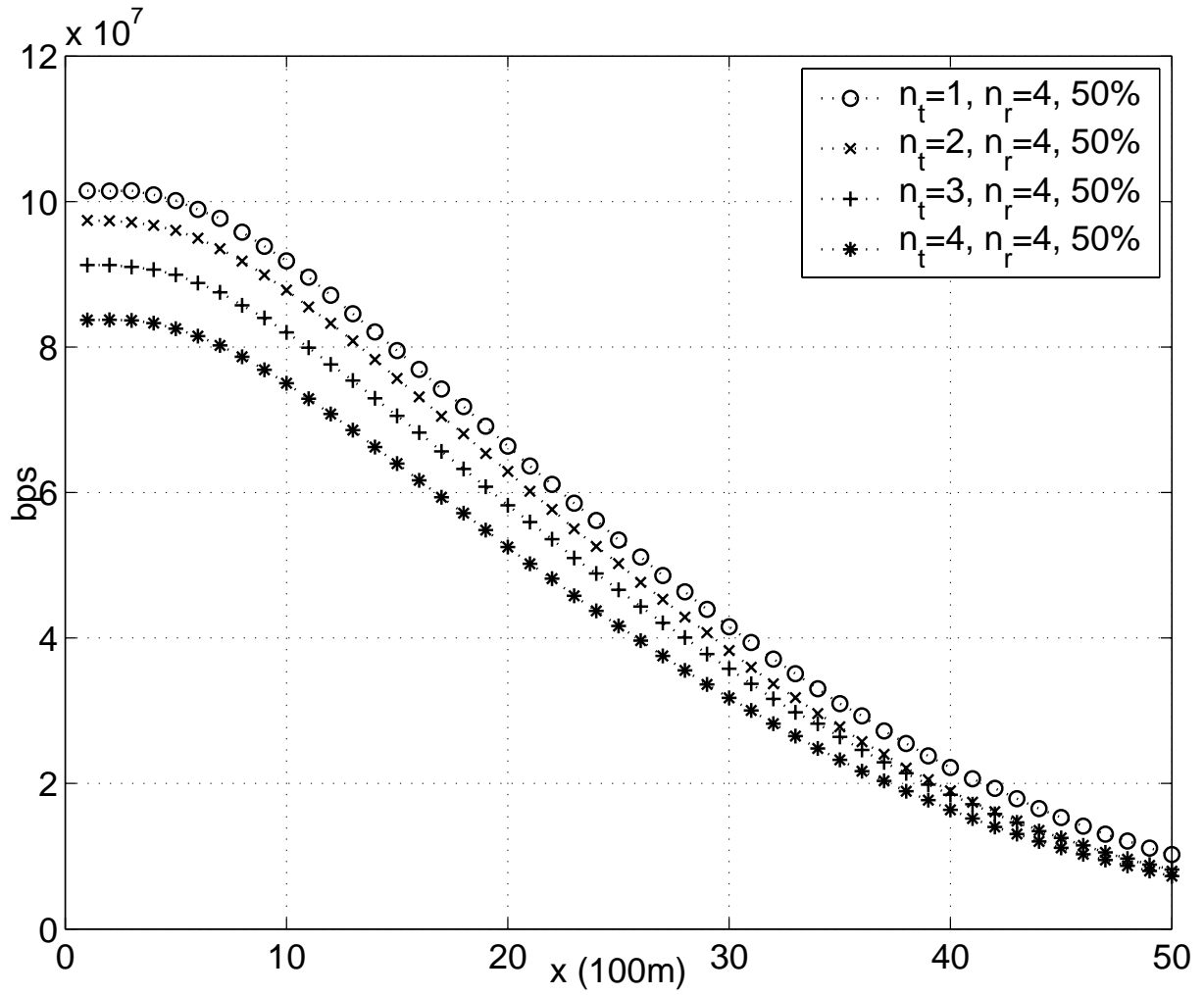
Figure 5.17: Downlink average data rate of a transmit diversity system with four receive antenna diversity along the x-axis

Figure 5.18 to Figure 5.21 show the average data rates for systems with 3, 4, 5 and 6 antennas.

Observations

It is shown that deploying as less transmit antennas as possible will result into the best average data rates. The simplest way to do so is to put only one antenna at the transmitter side and the rest at the receiver side.

5.5.7 Transmit and Receive Diversity System with Total Transmitter Power Scales with the Number of Transmit Antennas

It has already been shown in previous sections that with the constant total power assumption, deploying multiple transmit antennas does not provide as much gain as deploying multiple receive antennas. A logical investigation is to explore the performance improvement when the transmitter power scales with the number of transmit antennas.

To capture the fact that the total transmitter power scales with the number of transmit antennas, Equation (3.21) has to be modified. For the simplest case that the transmitter power scales linearly with the number of transmit antennas, removal of the factor $1/n_t$ in Equation (3.21) will do. Figure 5.22 shows the average data rate of a transmit diversity system with three receive antennas with scaling total transmitter power.

Observations

It is shown that deploying multiple transmit antennas with scaling total transmitter power enhances the average data rates. It is in contrary with what is shown in Figure 5.16 where the total transmitter power is kept constant regardless of the number of transmit antennas. In addition, diminishing return is observed here: the more transmit antenna is deployed, the less gain in data rate results. The practicability of deploying such configuration is in doubt because government regulations may have a limit on how much power can be transmitted from a close proximity.

Figure 5.18: Downlink average data rate of a transmit-receive diversity system with 3 antennas along the *x*-axis

Figure 5.19: Downlink average data rate of a transmit-receive diversity system with 4 antennas along the x-axis
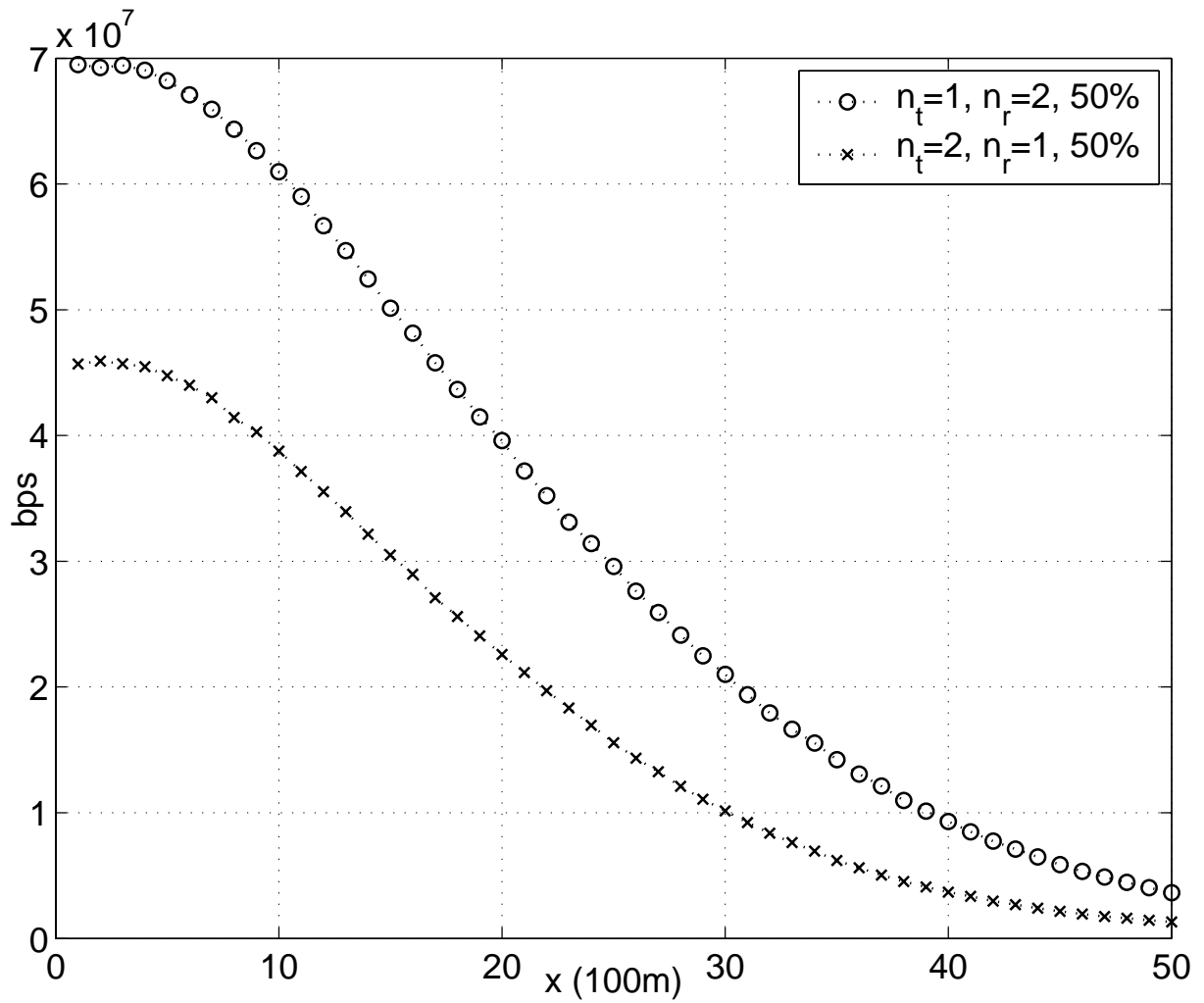
Figure 5.20: Downlink average data rate of a transmit-receive diversity system with 5 antennas along the x-axis
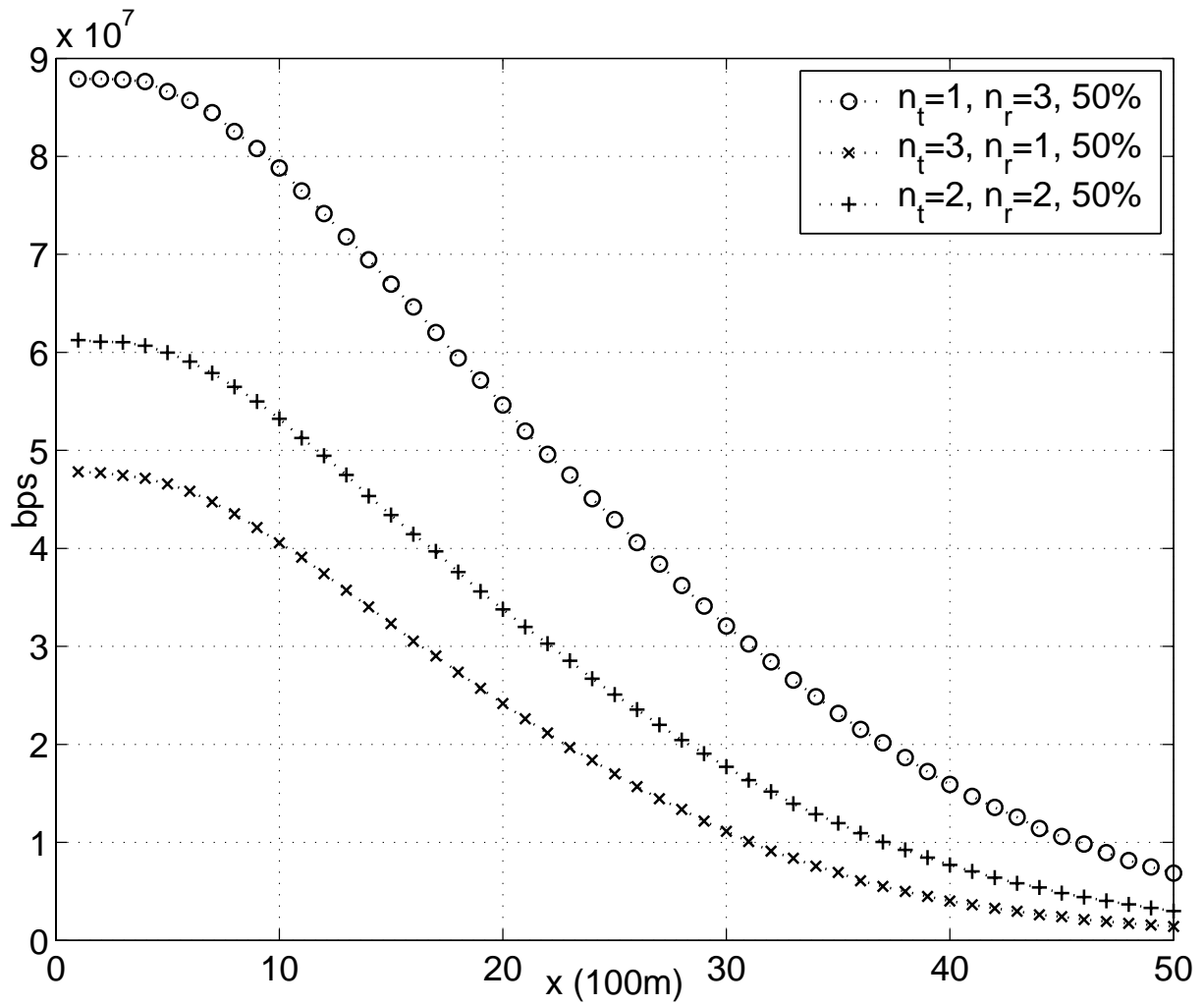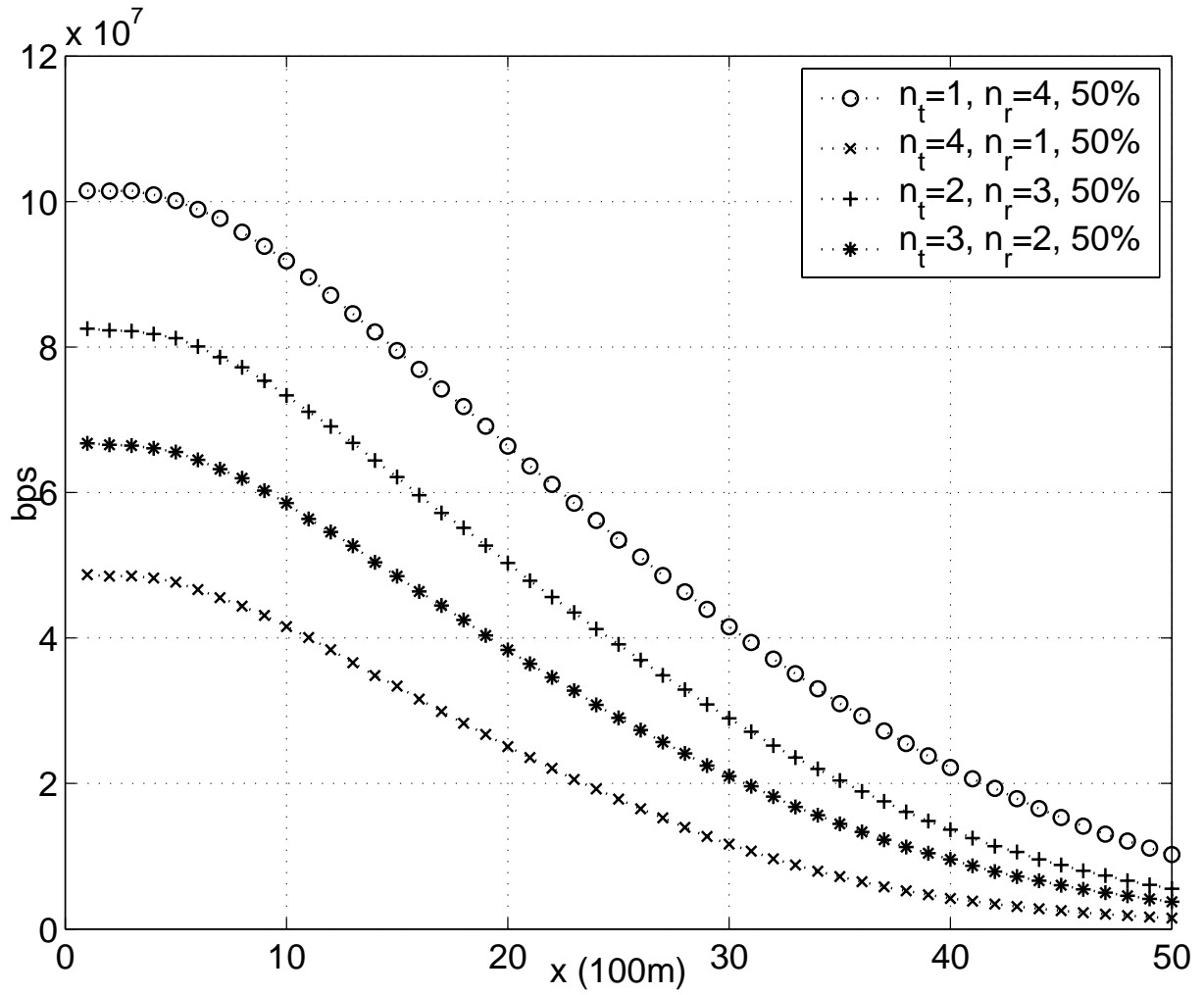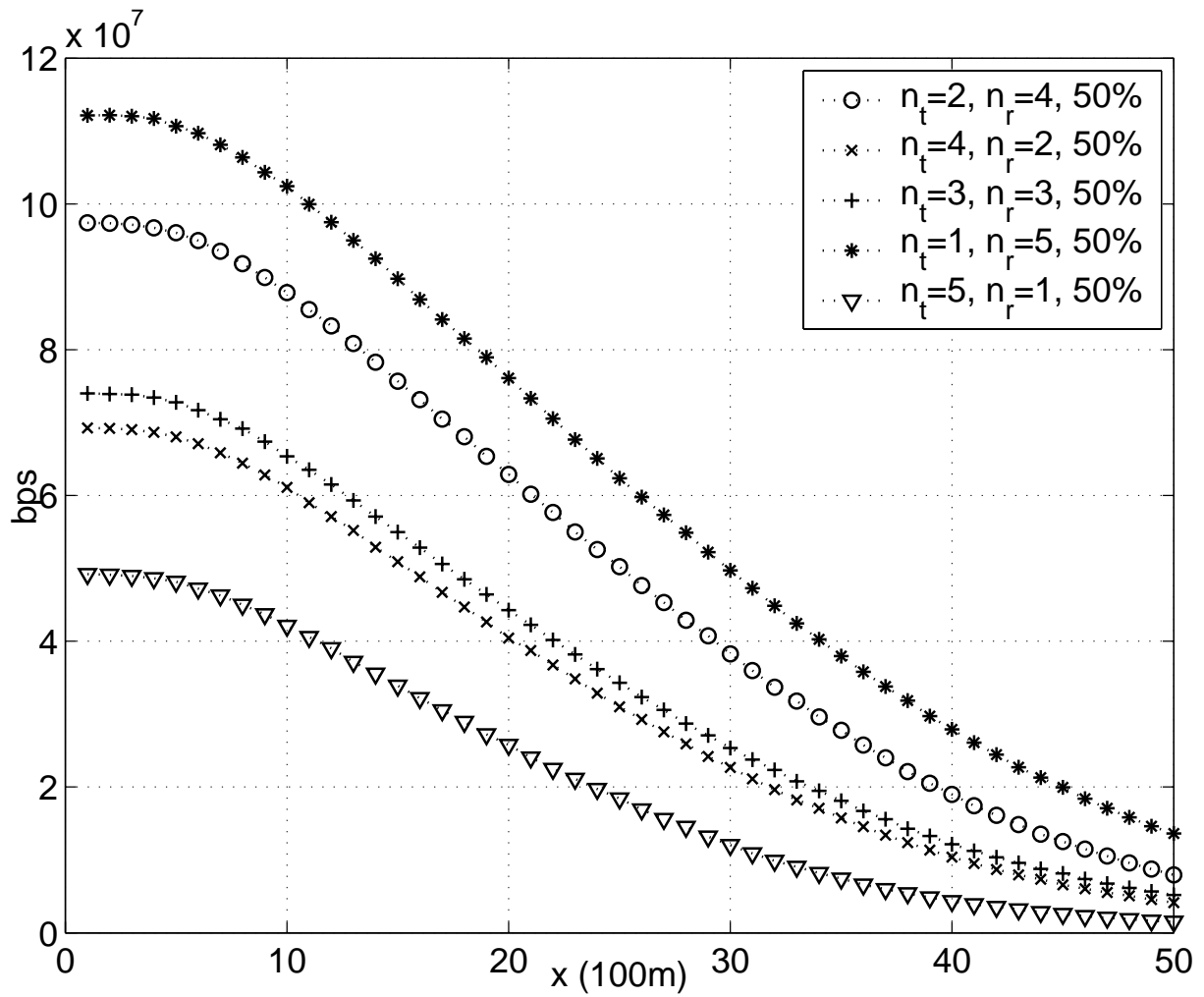
Figure 5.21: Downlink average data rate of a transmit-receive diversity system with 6 antennas along the x-axis
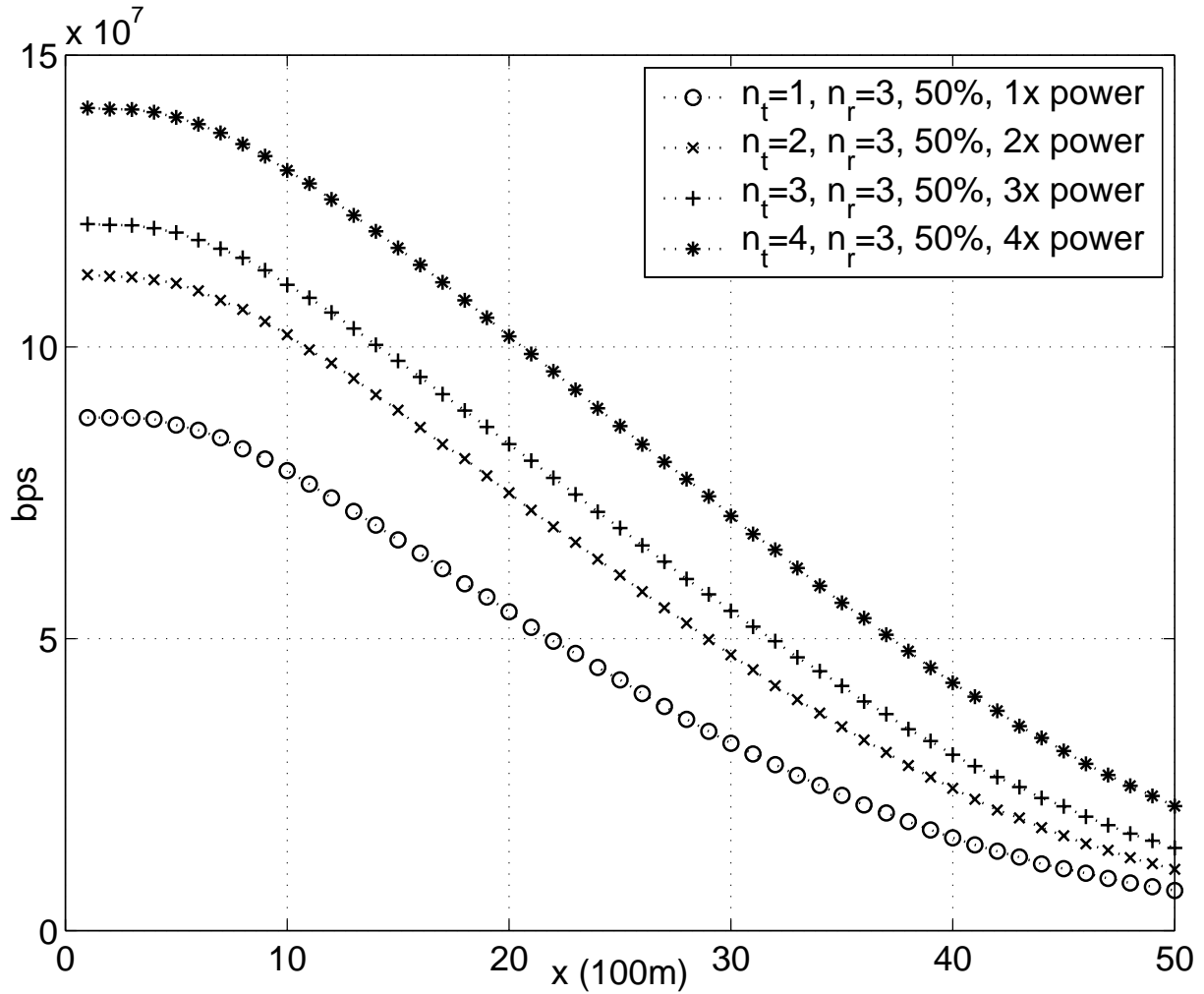
Figure 5.22: Downlink average data rate of a transmit diversity system with three receive antenna diversity along the x-axis, total transmitter power scales linearly with the number of transmit antennas

Summary

The simulation results obtained in this section differ from the results in open literatures in the following ways: First of all, the capacity scaling effect of a MIMO system is not as high as predicted in open literatures, when log-normal fading and distance path loss are taken into account and SNRs at different receivers are not of the same value. Secondly, when the total transmitter power scales with the number of transmit antennas, significant average data rate improvement is observed.

Numerical results for different resource allocations and different antenna configurations were presented. Conclusions will be drawn in the next section.

Chapter 6

Conclusions

This thesis presents an analysis of wireless high-speed data services for cellular CDMA systems. Such a system is characterized by asymmetric uplink and downlink data rates and very high downlink data rate. A lot of changes are required in order to implement such a system when compared to second generation voice oriented systems. These changes can be categorized into two major categories: advances in technologies and changes in design philosophy.

Advances in technologies include the application of antenna diversity at both the transmitter and receiver sides and the application of concatenated codes as the channel codec scheme. Design philosophy changes include the application of adaptive modulation and coding, hybrid automatic repeat request, incremental redundancy and opportunistic scheduling. In addition, noticeable changes in multiple access scheme, modulation scheme, handoff scheme and power control scheme are observed when comparing high-speed wireless data systems with second generation voice oriented systems. All the above contribute to the success in delivering high-speed data on the downlink.

Standards for high-speed wireless data access for 3G cellular CDMA systems have already been adopted as of end of 2002. As there are so many changes in the new systems when compared to second generation systems, a new mathematical model which allows wireless operators to independently evaluate the peak and average data rates, throughput and coverage of deploying such systems in their networks is immediately needed. In addition, wireless operators need a tool which can aid them in frequency planning, understand

the cost advantages / disadvantages and technical viabilities of various technologies, and deploy the proper amount of equipments at the right places. This thesis addresses the needs of wireless operators. This thesis presents a method which takes into account the major aspects of a typical high-speed wireless data systems' physical layer and applies the generalized Shannon capacity formula for multi-element antenna (MEA) systems. The method allows wireless operators to find out the peak and average data rates, throughput and coverage of deploying any CDMA based high-speed wireless data systems in their networks. In addition, the proposed method is flexible enough to be used in any propagation environments, antenna configurations, resources allocations, user distribution and cell site configurations, but yet mathematically trackable in which numerical results can be obtained in a matter of hours. By substituting different parameters into the proposed method and let the simulation runs for several hours, one can immediately obtain several key results which are of great importance.

Sample numerical results presented in this thesis use a system model with two-tier interfering cells. There is one transmit antenna and two receive antennas. Uniform user distribution is assumed. Users are allocated with either full system resources or minimal system resources (all multicode channels or one multicode channel). Coverage maps, peak data rate, peak throughput, average throughput, peak spectral efficiency and average spectral efficiency are obtained for various ITU-R M.1225 test environments. It has been shown that a data user with full system resources performs better under the vehicular channel than under the outdoor to indoor pedestrian channel.

Different antenna configurations are investigated. It is shown that the benefit of deploying transmit diversity is not as good as deploying receiver diversity. In most of the cases, simple one transmit antenna configuration will achieve the best data rate provided by the wireless channel.

Multicode allocation and its impact on average data rate is also investigated. It is shown that doubling the number of multicodes allocated to a user will result into more than double the achievable average data rate.

Appendix A

Abbreviations

GPRS General Packet Radio Service

EDGE Enhanced Data rate for Global Evolution enhancement over GPRS

cdma2000 1x cdma2000 one carrier

cdma2000 1xEV-DO cdma2000 one carrier radio transmission technology EVolution Data Optimized

HDR High Data Rate

cdma2000 1xEV-DV cdma2000 one carrier radio transmission technology EVolution integrated Data and Voice

L3NQS LG, Lucent, LSI Logic, Nortel, Qualcomm and Samsung

WCDMA Wideband CDMA

HSDPA High Speed Downlink Packet Access

MEA Multi-Element Antenna

TDM Time Division Multiplexing

MIMO Multiple Input Multiple Output

MISO Multiple Input Single Output

SISO Single Input Single Output

Bibliography

[1] China Wireless Telecommunication Standard (CWTS) Working Group 1 and Linkair. *Physical Layer Specification for LAS-2000*, July 13, 2000.

[2] 3rd Generation Partnership Project 2. *Physical Layer Standard for cdma2000 Spread Spectrum Systems*, March 2000. TIA/EIA/IS-2000.2-A-1.

[3] 3rd Generation Partnership Project 2. *cdma2000 High Rate Packet Data Air Interface Specification*, September 12, 2001. 3GPP2 C.S0024.

[4] Sirikiat Lek Ariyavisitakul. Turbo space-time processing to improve wireless channel capacity. *IEEE Transactions on Communications*, 48(8):1347–1359, Aug 2000.

[5] Deepak Ayyagari and Anthony Ephremides. Cellular multicode CDMA capacity for integrated (voice and data) services. *IEEE Transactions on Selected Areas in Communication*, 17(5):928–938, May 1999.

[6] Gerhard Bauch. Concatenation of space-time block codes and turbo-tcm. In *Proceedings of ICC'99*, volume 2, pages 1202–1206, 1999.

[7] P. A. Bello and B. D. Nelin. The influence of fading spectrum on the binary error probabilities of incoherent and differentially coherent matched filter receivers. *IRE Trans. Commun. Sys.*, CS-10:160–168, June 1962.

[8] P. Bender, P. Black, M. Grob, R. Padovani, N. Sindhushayana, and A. Viterbi. CDMA/HDR: A bandwidth-efficient high-speed wireless data service for nomadic users. *IEEE Communications Magazine*, pages 70 – 77, July 2000.

[9] S. Benedetto, D. Divsalar, G. Monorsi, and F. Pollara. Serial concatenation of inter-leaved codes: performance analysis, design and iterative decoding. *IEEE Transactions on Information Theory*, 44(3):909–926, May 1998.

[10] S. Benedetto and G. Monorsi. Iterative decoding of serially concatenated convolutional codes. *Electro. Letters*, 32(13):1186–1187, 20th June, 1996.

[11] C. Berrou. Near optimum error correcting coding and decoding: turbo-codes. *IEEE Transactions on Communications*, 44(10):1261–1271, Oct 1996.

[12] C. Berrou, A. Glavieux, and P. Thitimajshima. Near shannon limit error-correcting coding and decoding: Turbo-codes. In *Proceedings of ICC'93*, pages 1064–1070, Geneva, Switerland, May 1993.

[13] E. Biglieri, J. Proakis, and S. Shamai (Shitz). Fading channels: Information-theoretic and communications aspects. *IEEE Transactions on Information Theory*, 44(6):2619–2692, October 1998.

[14] Paulo Cardieri and Theodore S. Rappaport. Statistics of the sum of lognormal variables in wireless communications. In *Proceedings of 2000 IEEE Vehicular Technology Conference*, pages 1823–1827. IEEE, 2000.

[15] N. Chandran and M. C. Valenti. Three generations of cellular wireless systems. *IEEE Potentials*, 20:32– 35, Feb-March, 2001.

[16] D. Chase. Code combining. a maximum-likelihood decoding approach for combining an arbitrary number of noisy packets. *IEEE Transactions on Communications*, pages 385–393, May 1985.

[17] Wan Choi, Byung Shik Kang, Jun Cheol Lee, and Kuen Tae Lee. Forward link Erlang capacity of 3G CDMA system. In *Proceedings of 1st International Conference on 3G Mobile Communication Technologies*, pages 213–217, March 27-29, 2000.

[18] Chen-Nee Chuah, David N.C. Tse, Joseph M. Kahn, and Reinaldo A. Velenzuela. Capacity scaling in MIMO wireless systems under correlated fading. *IEEE Transactions on Information Theory*, 48(3):637–650, March 2002.

[19] K. G. Coffman and A. M. Odlyzko. Internet growth: Is there a "Moore's Law" for data traffic? In J. Abello, P. M. Pardalos, and M. G. C. Resende, editors, *Handbook of Massive Data Sets*. Kluwer, 2001. to appear.

[20] D. Divsalar and F. Pollara. On the design of turbo codes. *TDA Progress Report 42-123*, pages 99–121, Nov 15, 1995.

[21] LG Electronics, LSI Logic, Lucent Technologies, QUALCOMM Incorporated, and Samsung Electronics. *Updated Joint Physical Layer Proposal for 1xEV-DV*, June 11, 2001. 3GPP2-C50-20010611-009.

[22] G. D. Forney. *Concatenated Codes*. MIT Press, Cambridge, MA, 1966.

[23] G. J. Foschini and M. J. Gans. On limits of wireless communications in a fading environment when using multiple antennas. *Wireless Personal Communications*, pages 311–355, 1998.

[24] Gerald J. Foschini. Layered space-time architecture for wireless communication in a fading environment when using multi-element antennas. *Bell Labs Technical Journal*, pages 41–59, Autumn 1996.

[25] Gerard J. Foschini, Glen D. Golden, Reinaldo A. Valenzuela, and Peter W. Wolniansky. Simplified processing for high spectral efficiency wireless communication employing multi-element arrays. *IEEE Journal on Selected Areas in Communications,*, 17(11):1841–1852, November 1999.

[26] Robert G. Galllager. *Information Theory and Reliable Communication*. John Wiley and Sons, 1968.

[27] Wen Gao, Joon Ho Cho, and James S. Lehnert. Chip waveform design for DS/SSMA systems with aperiodic random spreading sequences. *IEEE Transactions on Wireless Communication*, 1(1):37–45, Januray 2002.

[28] Klein S. Gilhousen, Irwin M. Jacobs, Roberto Padovani, Andrew J. Viterbi, Lindsay A. Weaver Jr., and Charles E. Wheatley III. On the capacity of a cellular CDMA system. *IEEE Transactions on Vehicular Technology*, 40(2):303–312, May 1991.

[29] D.A. Gore, R.U. Naber, and A. Paulraj. Selecting an optimal set of transmit antennas for a low rank matrix channel. In *Proceedings of 2000 IEEE International Conference on Acoustics, Speech, and Signal Processing*, pages 2785–2788. IEEE, 2000.

[30] M. Hata. Empirical formula for propagation loss in land mobile radio services. *IEEE Transactions on Vehicular Technology*, VT-29(3):317–325, Aug 1980.

[31] Jack M. Holtzman. CDMA forward link waterfilling power control. In *Proceedings of 2000 IEEE Vehicular Technology Conference*, pages 1663–1667. IEEE, 2000.

[32] Chih-Lin I and Richard D. Gitlin. Multi-code CDMA wireless personal communications networks. In *Proceedings of ICC'95*, volume 2, pages 1060–1064, Seattle, Washington, June 18-22, 1995.

[33] European Cooperation in the Field of Science and Technical Research EURO-COST 231. *Urban transmission loss models for mobile radio in 900 and 1800 MHz bands*, Sept 1991. The Hague.

[34] Qualcomm Inc. 1xEV: 1x evolution IS856 TIA/EIA standard airlink overview, November 7, 2001. http://www.qualcomm.com/main/whitepapers/ 1xEV_AirlinkOverview_110701.pdf.

[35] Qualcomm Incorporated. White paper: the economics of wireless mobile data, 2001. http://www.qualcomm.com/main/whitepapers/WirelessMobileData.pdf.

[36] QUALCOMM Incorporated. *QUALCOMM Incorporated 2001 Annual Report*, 2002.

[37] W.C. Jakes. *Microwave Mobile Communication*. Wiley, 1974.

[38] Ahmad Jalali and Alberto Gutierrez. Performance comparison of direct spread and multicarrier CDMA systems. In *Proceedings of 1998 IEEE Vehicular Technology Conference*, pages 2042–2046, April, 1998.

[39] L. Jalloul and K. Rohani. CDMA forward link capacity and coverage in a multipath fading channel. In *Proceedings of 47-th IEEE Vehicular Technology Conference*, pages 1440–1444. IEEE, 1997.

[40] Louay M. A. Jalloul, Kamyar Rohani, Kiran Kuchi, and Jiangnan (Jason) Chen. Performance analysis of CDMA transmit diversity methods. In *Proceedings of 50th VTC*, pages 1326–1330, Fall 1999.

[41] Samir Kallel and Davvid Haccoun. Generalized type II hybrid ARQ scheme using punctured convolutional coding. *IEEE Transactions on Communications*, 11(38):1938–1946, Nov 1990.

[42] F. Kelly. Charging and rate control for elastic traffic. *European Transactions on Telecommunications*, 8:33–37, 1997.

[43] Duk Kyung Kim and Dan Keun Sung. Characterization of soft handoff in CDMA systems. *IEEE Transactions on Vehicular Technology*, 48(4):1195–1201, July 1999.

[44] V. Kuhn. Evaluating the performance of turbo codes and turbo-coded modulation in a DS-CDMA environment. *IEEE Journals on Selected Areas in Communications*, 17(12):2138–2147, Dec 1999.

[45] E. A. Lee and D. G. Messerschmitt. *Digital Communication*. Kluwer, Norwell, MA, second edition, 1994.

[46] Jhong Sam Lee and Leonard E. Miller. *CDMA Systems Engineering Handbook*. Artech House, first edition, October 1998.

[47] Zhuyu Lei, David J. Goodman, and Narayan B. Mandayam. Location-dependent other-cell interference and its effect on the uplink capacity of a cellular CDMA system. In *Proceedings of 1999 IEEE Vehicular Technology Conference*, pages 2164–2168, May 16-20, 1999.

[48] T.H. Liew, J. Pliquett, B. L. Yeap, L-L. Yang, and L. Hanzo. Comparative study of space time block codes and various concatenated turbo coding schemes. In *Proceedings of IEEE PIMRC 2000*, pages 741–745, 2000.

[49] Xin Liu, Edwin K. P. Chong, and Ness B. Shroff. Transmission scheduling for efficient wireless utilization. In *Proceedings of INFOCOM 2001: Twentieth Annual Joint*

Conference of the IEEE Computer and Communications Societies, volume 2, pages 776 –785, 2000.

[50] Thomas L. Marzetta and Bertrand M. Hochwald. Capacity of a mobile multi-antenna communication link in Rayleigh flat fading. *IEEE Transactions on Information Theory*, 45(1):139–157, Jan 1999.

[51] Thomas L. Marzetta and Byertrand M. Hochwald. Unitary space-time modulation for multiple-antenna communications in Rayleigh flat fading. *IEEE Transactions on Information Theory*, 46(2):543–564, March 2000.

[52] Motorola, Nokia, LSI Logic, Texas Instruments, Dot Wireless, and Broadcom. *Proposed 1XTREME Physical Layer Delta Specification*, June 8, 2000. C00-1XTR-20000608-003.

[53] Sanjiv Nanda, Krishna Balachandran, and Sarath Kumar. Adaptation techniques in wireless packet data services. *IEEE Communications Magazine*, pages 54–64, Jan 2000.

[54] Stefan Parkvall, Erik Dahlman, Pal Frenger, Per Beming, and Magnus Persson. The evolution of WCDMA towards higher speed downlink packet data access. In *Proceedings of 2001 IEEE Vehicular Technology Conference*, pages 2287–2291. IEEE, 2001.

[55] M. Patzold, U. Killat, and Frank Laue. A deterministic digital simulation model for Suzuki processes with application to a shadowed Rayleigh land mobile radio channel. *IEEE Transactions on Vehicular Technology*, 45(2):318–331, May 1996.

[56] L. C. Perez, J. Seghers, and Jr. D. J. Costello. A distance spectrum interpretation of turbo codes. *IEEE Transactions on Information Theory*, 42:1698–1709, Nov 1996.

[57] Roger L. Peterson, Rodger E. Ziemer, and David E. Borth. *Introduction to Spread-Spectrum Communications*. Prentice Hall, third edition, 1995.

[58] J. G. Proakis. *Digital Communication*. Mcgraw-Hill, third edition, 1995.

[59] T. S. Rappaport. *Wireless Communications*. Prentice Hall, Upper Saddle River, NJ, 1996.

[60] Theodore S. Rappaport, A. Annamalai, R. M. Buehrer, and William H. Tranter. Wireless communications: past events and a future perspective. *IEEE Communication Magazine*, pages 148–161, May 2002 50th Anniversary Issue.

[61] M. Robinson. Life on the edge. *Wireless Review*, 17(18):36–40, Sept 15, 2000.

[62] International Telecommunication Union Radiocommunication Sector. *Recommendation ITU-R M.1225 Guidelines for evaluation of radio transmission technologies for IMT-2000*, 1998.

[63] Da-Shan Shiu, Gerard J. Forchini, Michael J. Gans, and Joseph M. Kahn. Fading correlation and its effect on the capacity of multielement antenna systems. *IEEE Transactions on Communications*, 48(3):502–513, March 2000.

[64] Bernard Sklar. Rayleigh fading channels in mobile digital communication systems part I: Characterization. *IEEE Communication Magazine*, pages 90–100, July 1997.

[65] Elvino S. Sousa, Vladan M. Jovanovic, and Christian Daigneault. Delay spread measurements for the digital cellular channel in Toronto. *IEEE Transactions on Vehicular Technology*, 43(4):837–847, Nov 1994.

[66] Motorola CDMA systems division. A technology and standards proposal for 1xEV-DV (data and voice), November 2000. http://www.motorola.com/aspira/pdfs/CDMA-1X-V2.pdf.

[67] O. Y. Takeshita and D. J. Costello. New deterministic interleaver designs for turbo codes. *IEEE Transactions on Information Theory*, 46(6):1988–2006, Sept 2000.

[68] Vahid Tarokh, Hamid Jafarkhani, and A. R. Calderbank. Space-time block codes from orthogonal designs. *IEEE Transactions on Information Theory*, 45(5):1456–1467, July 1999.

[69] I. Emre Telatar. Capacity of multi-antenna Gaussian channels. *European Transactions on Telecommunications*, 10(6):585–595, Nov/Dec 1999.

[70] Haifeng Wang, Zhiyong Bu, and Jorma Lilleberg. Multiple-input single-output precoder for WCDMA TDD downlink transmission. In *Proceedings of 54th IEEE Vehicular Technology Conference*, pages 581–585. IEEE, Fall 2001.

[71] Jack H. Winters, Jack Salz, and Richard D. Gitlin. The impact of antenna diversity on the capacity of wireless communication systems. *IEEE Transactions on Communications*, 42(2/3/4):1740–1751, Feb/Mar/Apr 1994.

[72] John M. Wozencraft and Irwin Mark Jacobs. *Principles of Communication Engineering*. John Wiley and Sons, 1965.

[73] www.mobileGPRS.com. White paper: YES to GPRS, February 2001. http://www.mobilewhitepapers.com/pdf/gprs.html.

[74] Young C. Yoon. An improved Gaussian approximation for probability of bit-error analysis of asynchronous bandlimited DS-CDMA systems with BPSK spreading. *IEEE Transactions on Wireless Communication*, 1(3):373–382, July 2002.

[75] Jie Zhou, Ushio Yamamoto, and Yoshikuni Onozato. On the feasibility of high data rate services in wireless system using code division multiple access. *IEICE Trans. Fundamentals*, E83-A(7):1347–1355, July 2000.